

Exploring the spatio-temporal dynamics of lipid rafts and their role in signal transduction

A Modeling and Simulation approach

Dissertation

zur

Erlangung des akademischen Grades

Doktor-Ingenieur (Dr.-Ing.)

der Fakultät für Informatik und Elektrotechnik
der Universität Rostock

vorgelegt von:

Fiete Haack

aus Rostock

Rostock, 2015/10/05

Gutachter:

1. Gutachterin:

Prof. Dr. Adelinde M. Uhrmacher,
Institut für Informatik und Elektrotechnik, Universität Rostock

2. Gutachter:

Prof. Dr. Kevin Burrage,
Computational Mathematics, QUT, Brisbane, Australia;
Department of Computer Science, University of Oxford, UK

3. Gutachterin:

Prof. Dr. Dr. h.c. Edda Klipp,
Institut für Biologie, Theoretische Biophysik,
Humboldt-Universität zu Berlin

Datum der Einreichung: 06. Oktober 2015

Datum der Verteidigung: 29. April 2016

Abstract

Modeling and simulation of signal transduction pathways facilitate the integration of experimental knowledge into a coherent picture and is increasingly regarded as a valuable complement to wet-lab experiments. However, despite its importance, the implications of space (e.g. diffusion, molecular crowding or active transport) have traditionally been neglected in common models of signal transduction. Seizing on this problem, the aim of this thesis is to elucidate the biological as well as methodological implications that arise from modeling the spatio-temporal dynamics of lipid rafts, particularly in the context of signal transduction. Lipid rafts are small, dynamic structures that are crucially involved in the spatial organization of the cell membrane, hence play a central role in signaling. Notably, lipid rafts are involved in almost all central physiology-related signaling pathways and are associated with a continuously growing list of diseases, including immune disorders, degenerative diseases and cancer. Though, the actual impact of lipid rafts on downstream signaling components and their exact role in the majority of signaling pathways is still largely unknown.

Therefore the effect of raft-dependent receptors dynamics on both, individual signaling events as well as an entire signaling transduction pathway, is explicitly analyzed here. First, a Cellular-Automata based membrane model is developed to explore the effect of lipid rafts on individual signaling events, such as the association of peripheral proteins to membrane-integral receptors and the subsequent formation of a ternary receptor complex. After that, the specific involvement of lipid rafts in Wnt/ β -catenin signaling during neural differentiation is explored by means of an integrated *in silico* and *in vitro* approach. Accordingly, based on experimental data retrieved from human neural progenitor cells an extended model of the canonical Wnt signaling pathway including membrane-related processes and lipid rafts is developed.

However, the level of abstraction, i.e. the spatial scale required to describe certain aspects of spatial membrane dynamics, strongly depends on the subject of interest, the concrete addressed scientific questions and eventually on the experimental data available. Therefore a particular focus is laid on the close interplay between the formal representation of cellular or subcellular dynamics and experimental investigation.

Zusammenfassung

Computergestützte Modellierung und Simulation von Signaltransduktionswegen erleichtert es experimentelle Daten in einen kohärenten Zusammenhang zu bringen und gilt zunehmend als wertvolle Alternative zu Laborexperimenten. Allerdings wird in den meisten Signaltransduktionsmodellen der Einfluss räumlicher Aspekte (wie bspw. Diffusion, Molecular Crowding, oder aktiver Transport) vernachlässigt, obwohl diese von großer Wichtigkeit sind. Dieses Problem wird in der vorliegenden Arbeit aufgegriffen. Ziel der Arbeit ist es, die biologischen als auch die methodischen Implikationen zu erfassen, die während der Erforschung von Raum/Zeit Dynamiken von Lipid Rafts und insbesondere im Kontext von Signaltransduktion auftreten. Lipid Rafts sind kleine, dynamische Strukturen, die einen wesentlichen Einfluss auf die räumliche Organisationsstruktur von Zellmembranen und dadurch eine wichtige Rolle in der Signaltransduktion spielen. Bemerkenswerterweise sind Lipid Rafts in den Signalwegen fast aller physiologischen Funktionen involviert und zudem werden sie mit einer wachsenden Vielzahl von Krankheiten assoziiert, wie bspw. Immundefekte, degenerative Krankheiten oder aber auch Krebs. Jedoch ist der tatsächliche Einfluss von Lipid Rafts auf die konkreten Signalwege oder einzelne Signaltransduktionsereignisse noch größtenteils unklar. Aus diesem Grund soll im Rahmen dieser Arbeit der Einfluss von Lipid-Raft abhängigen Rezeptordynamiken sowohl bezüglich einzelner Signaltransduktionsschritte, als auch bzgl. eines kompletten Signaltransduktionsweges analysiert werden. Zunächst wird ein Membranmodell basierend auf einem Zellulären Automaten implementiert. Dieses Membranmodell wird genutzt, um den Einfluss von Lipid Rafts auf einzelne Signaltransduktionsschritte, wie z.B. die Assoziation von peripheren Proteinen an Membranrezeptoren und die anschließende Bildung eines ternären Komplexes, zu untersuchen. Anschließend wird der spezifische Einfluss von Lipid Rafts auf den kanonischen WNT Signalweg während der Embryonalen Entwicklung untersucht. Dies geschieht im Rahmen einer kombinierten Labor- und Simulationsstudie. Basierend auf experimentellen Daten aus humanen, neuronalen Progenitorzellen wurde ein erweitertes Modell des kanonischen WNT Signalwegs entwickelt, welches räumliche Membrandynamiken und den Einfluss von Lipid Rafts beschreibt. Allerdings ist das Abstraktionsniveau, d.h. die verwendete räumliche Auflösung/Skalierung, die benötigt wird, um die entsprechenden Aspekte der räumlichen Membrandynamiken darzustellen, stark von den eigenen Forschungsinteressen, der wissenschaftlichen Fragestellung und letztlich auch von den verfügbaren experimentellen Daten abhängig. Aus diesem Grund wird ein besonderer Fokus der Arbeit auf das Zusammenspiel zwischen formaler Repräsentation von zellulären und subzellulären Dynamiken und experimentellen Versuchen gelegt.

Acknowledgements

First of all, my sincerest thanks go to my supervisor Lin Uhrmacher, who supported me throughout all stages of this work in so many different ways. This dissertation is the result of her endless confidence and trust in me and my research. Thank you. I am also grateful to Kevin Burrage, who draw my interest to the area of lipid rafts and spatial membrane dynamics. I greatly enjoyed the countless discussions during the very pleasant stay in Oxford. I would like to thank Edda Klipp, who spontaneously agreed on reviewing my thesis just a few weeks before the submission.

I also want to thank Sergei Kuznetsov and Dieter G. Weiss for providing me the opportunity to perform my own wet-lab experiments and to use the facilities at the Life Cell Imaging Center in Rostock. Special thanks go to Bärbel Redlich and my colleague Heiko Lemke for their excellent technical support, assistance and counsel in the lab, as well as their endless patience for all my questions. You have done a great job and were such a great help with the unfamiliar lab work. Also I want to thank Tareck Rharass, for so many vivid discussions and the wicked humor we could share along “the long way we did. Now, it’s for very real... ”

I am thankful to all my colleagues of the modeling and simulation group and the interdisciplinary research training school diEM oSiRiS for their support, fruitful discussion and the great time we spent together. Special thanks go to Stefan Rybacki, my long-time “office neighbor ” for countless discussions, chats and laughter, but also valuable technical support, Roland Ewald, Jan Himmelspace and Tobias Helms who bore a helping hand whenever needed. Many thanks to Dr. Susanne Beyer who always had open eyes and ears for “her” graduate students and to Jens Hildebrand for proof reading the manuscript.

Lastly, but not less importantly I am grateful to my parents for their support and trust in me. But above all, I thank my lovely wife for her support, trust and guidance, for fruitful discussions and helpful suggestions, and most importantly for her endless patience, and all her efforts in keeping me free of ties in the last stage of writing. This thesis would have not been finished without you.

Contents

Abstract	iii
Zusammenfassung	v
Acknowledgements	vii
Contents	ix
List of Figures	xiii
List of Tables	xv
1 Introduction	1
1.1 Motivation and Problem Statement	1
1.2 Biological Background - Initial events in signal transduction and the role of lipid rafts	3
1.2.1 Lipid Rafts as essential feature of spatial membrane dynamics . . .	5
1.2.2 Approaches to studying Lipid Rafts	5
1.3 Summary and aim of this work	9
2 Modeling the diffusion dynamics of plasma membrane receptors under the influence of lipid rafts	11
2.1 Modeling small scale lipid rafts dynamics	11
2.1.1 Model features of microscopic lipid rafts dynamics	12
2.1.2 Individual-based approaches to model microscopic raft/receptor dynamics in the context of signal transduction	12
2.2 A Plasma Membrane Model based on Cellular automata	15
2.2.1 Lattice-Gas Cellular Automata: Particle Movement for cellular automata	15
2.2.2 Modeling individual-based random motion in LGCA	22
2.2.3 Modeling Lipid Rafts - Multi-Scale modelling with Cellular Automata	26
2.3 Concluding remarks	35
3 Studying raft-dependent receptor distribution and binding kinetics	37
3.1 Model and Parameters	37
3.2 Characterizing lipid rafts and receptor interaction	39
3.2.1 Raft fluidity controls extend of receptor enrichment	40

3.2.2	Under physiological conditions, receptor enrichment is raft size dependent	41
3.3	The role of lipid rafts on Binding of peripheral proteins to membrane-bound receptors	42
3.3.1	Extending the model description	44
3.3.2	Lipid Rafts play ambivalent role in the protein-receptor binding . .	45
3.3.3	Lipid rafts promote slow binding kinetics	46
3.3.4	Raft properties have significant impact on binding kinetics	47
3.3.5	Characterizing the ambiguous effects of raft properties on protein receptor bindings	48
3.4	Concluding remarks	50
4	Modeling raft-dependent WNT signaling	53
4.1	Biological Background - Key regulatory aspects of WNT/ β -catenin pathway	54
4.2	Existing WNT/ β -catenin models	61
4.3	Modeling membrane-related processes in signal transduction	64
4.3.1	Modeling features required to capture membrane-related processes in signal transduction	65
4.3.2	Rule-based modeling approaches	68
4.3.3	Multi-level, rule-based modeling in ML-Rules	74
4.4	A rule-based model of raft-dependent WNT/ β -catenin signaling	78
4.4.1	Membrane WNT Model in ML-Rules	78
4.4.2	AXIN/ β -catenin model	85
4.4.3	Putting it together - a combined lipid raft and β -catenin WNT model	89
4.5	Concluding remarks	95
5	Studying Raft-dependent WNT signaling in Neural Differentiation using an integrative in-vitro and in-silico approach	99
5.1	Background (Early differentiation in human neural progenitor cells) . . .	99
5.2	In vitro Exploration	100
5.2.1	Materials and methods	100
5.2.2	Experimental Results	102
5.2.3	Discussion	104
5.3	In silico Exploration	105
5.3.1	Experiment specification and execution	105
5.3.2	Model Parametrization	108
5.3.3	Validation of the model	111
5.3.4	Simulation results	112
5.3.5	Discussion	114
5.4	Concluding remarks	116
6	Endogenous Reactive Oxygen Species induce early immediate beta-catenin activation in a WNT-independent manner	117
6.1	Involvement of Reactive Oxygen Species in WNT signaling	118
6.2	In silico exploration - extending the WNT model	120
6.2.1	Extending the existing WNT model by endogenous ROS signaling	120

6.2.2	Methods and Parametrization	129
6.2.3	Parameter Adjustment	129
6.2.4	Simulation results and Discussion	132
6.3	In vitro validation	135
6.3.1	Material and methods	135
6.3.2	Experimental results	136
6.4	Concluding remarks	138
7	Summary and Concluding Remarks	141
7.1	Methodology / Model development	141
7.2	Application / Biological insights	142
	Bibliography	145
	Erklärung	166

List of Figures

1.1	The ligand receptor pathway	4
2.1	Representation of (unoccupied) velocity channels	17
2.2	Collision handling according to HPP model	18
2.3	Collision and Propagation step according to HPP model	19
2.4	Cell configurations	20
2.5	Shuffling and Propagation step according to a probabilistic LGCA model	21
2.6	Two kinds of collisions	23
2.7	Two kinds of collisions	23
2.8	Neighborhood information in raft graph	31
3.1	A schematic view protein-receptor binding	39
3.2	The sweeping effect	41
3.3	Equilibrium receptor concentrations inside lipid rafts	42
3.4	Trajectory of receptor concentrations inside lipid rafts	43
3.5	Successful protein-receptor bindings	45
3.6	Protein-receptor binding ratios	50
4.1	The <i>destruction complex</i>	56
4.2	Formation of Signalosome	57
4.3	Inactive vs. Active state of canonical Wnt signaling	58
4.4	Membrane WNT model	80
4.5	Intracellular Wnt model	86
4.6	Combined intracellular and membrane WNT model	90
5.1	LRP6 staining	102
5.2	Impact of Raft disruption on nuclear β -catenin levels	103
5.3	106
5.4	107
5.5	Raft/Receptor dynamics.	109
5.6	Model validation	113
5.7	Nuclear β -catenin concentration fold of WNT/ β -catenin model	115
6.1	Extended WNT/ β -catenin model	124
6.2	Simulation results for the redox model	130
6.3	Nuclear β -catenin concentration fold changes of extended WNT/ β -catenin model	133
6.4	Upstream β -catenin inhibition	136
6.5	Mitochondrial mito-ROS levels	139

List of Tables

3.1	Parameters of Membrane Model	40
3.2	PRCC values for input parameters significantly correlated with model outcome (binding ratio)	48
5.1	Parameter Table of the WNT/ β -catenin model.	110
5.2	Table of varying WNT stimuli	112
6.1	Parameter Table of the ROS/DVL model component.	131
6.2	Parameter Table of the extended ROS/ β -catenin model component.	132

Chapter 1

Introduction

Cellular signal transduction enables cells to sense changes in their environment and to initiate the cellular response by regulating gene expression, target protein modifications, or metabolism. The proper functioning of these pathways is crucial for adaptation and survival under varying conditions, but also for differentiation and cell fate. However, the exploration of signal transduction pathways by classical biochemistry and molecular biology techniques is often problematic, due to limited spatial and temporal resolution, unspecific side effects of chemical or genetic treatments or the inability to deal with emergent properties [24]. Bottom-up systems biology approaches, i.e. kinetic modeling, could fetch up these limitations by complementing the available experimental data with model-based quantitative analyses. Thereby modeling and simulation provide additional insights about the mechanisms and dynamics of signal transduction and helps to integrate experimental knowledge into a coherent picture [20]. Indeed, with a detailed kinetic model one can perform time-course simulations, derive, support, or falsify hypotheses about underlying mechanisms of the signal transduction and predict the cellular response to varying stimuli. Therefore, *in silico* experiments are increasingly regarded as a valuable complement to wet-lab experiments. Accordingly, computational modeling and simulation of signal transduction pathways is obtaining growing attention from researchers with experimental or theoretical background [49, 105].

1.1 Motivation and Problem Statement

To understand the complex behavior of signaling networks, numerous computational modeling approaches have been developed, typically with a specific application in mind.

Each of these approaches employs a different level of detail, ranging from abstract models that emphasize some key features of signaling pathways [82, 156] over detailed models that represent the dynamics of specific pathways in specific organisms, e.g. [38, 102, 106, 116], down to micro-scale models that describe the molecular interactions, trying to approximate the exact physical processes [146, 157, 198].

Thereby model reusability and readability should be considered as key features when developing and specifying models. This is where modeling languages come in, i.e. formalized approaches for writing model components and interactions. The model is detached from the simulation and it may even be possible to use the same model description with different simulation approaches, e.g. ordinary differential equations (deterministic) as well as the Stochastic Simulation Algorithm. [13, 66]. This separation of concerns is of great importance, as it allows to annotate, store, exchange and combine models, independently of the simulation algorithm and its configuration used execute the model [26, 40, 93, 100, 178, 179, 209]. Within the last decade sophisticated modeling formalisms were established that are capable of describing complex properties of proteins, their interactions within the signal transduction networks and the corresponding kinetics. Thereby means for describing attribute species, hierarchical nesting (multi-level) including dynamics structures as well as constrains and arbitrary functions are currently considered as the most important modeling features required to represent any process involved in signal transduction. Attributed species allow for the definition of multi-state components. Multi-level approaches describe causal relationships, i.e. upward- and downward causation between different hierarchical layers and dynamic structures. Lastly constraints and arbitrary functions make it possible to formulate reaction kinetics other than mass action.

Despite these advances in computational modeling methodology, research efforts have traditionally been concentrated on exploring signal transduction networks and focus on the involved proteins and their reaction kinetics. Though, yet too little attention has been paid to the actual spatial properties of the surrounding environment, that contribute to overall signaling characteristics of the system by introducing non-linear signal delays [197]. However, spatial processes are difficult to capture with standard experimental techniques, because neither qualitative nor quantitative data can provide sufficient insight to capture the spatial dynamics of processes like receptor clustering, molecular crowding, endocytosis. For that reason spatial processes can particularly benefit from insights obtained by computational modeling.

To seize on the issues of considering spatial processes in cellular as well as computational biology, this thesis focusses on the lipid rafts/receptor interaction and its impact on signal transduction. Lipid rafts are small, dynamic structures that are crucially involved in the spatial organization of the cell membrane, hence play a central role in signal transduction. The small-scale, dynamic nature of lipid rafts hampers their exploration in

vitro, but also leads to severe difficulties when it comes to modeling their dynamics in the context of signal transduction. With lipid rafts dynamics and their involvement in signal transduction being the central scope of this thesis, this work provides ample evidence why neglecting spatial aspects of signal transduction is problematic and addresses the challenges that arise from the need of spatial representations in computational modeling.

1.2 Biological Background - Initial events in signal transduction and the role of lipid rafts

Ligand binding and receptor activation are the initial steps in cellular signal transduction and provide the opportunity to capture extracellular signals and transduce them inward to control target proteins or gene expression [114]. To actually induce an intracellular signaling cascade the ligand has to be successfully bound by the receptor established and the resulting ligand-receptor complex has to be maintained for a certain amount of time. This means the strength/effectiveness of the signal transduction depends on how many ligand can be bound by receptors and how stable the complex is, i.e. how long the interaction between receptor and ligand lasts.

However, the formation as well as the stability of the receptor complex is not only affected by the ligand-receptor affinity, but also by the interaction with other membrane-associated proteins, such as G-proteins, coated pit adaptors, cytoskeletal elements or other receptors. Thereby the interaction may eventually lead to the formation of a ternary complex, consisting of ligand, receptor and peripheral protein. As a result the binary ligand-receptor complex additionally binds to the peripheral protein yielding a ternary complex. The impact of such receptor coupling interactions and the formation of a ternary complex is two-fold. On the one hand, the association and dissociation rates for receptor-ligand binding can vary significantly between binary and ternary complexes - a fact that has to be taken into close consideration when analyzing experimental data. Renown examples for this effect are receptor/G-protein coupling and EGF receptor/adaptor coupling [45, 84, 115, 117]. On the other hand, the interaction with membrane-associated proteins induces further signaling events, like internalization (endocytosis) and recycling processes or receptor accumulation (see Fig. 1.1).

Note, that the kinetics of these cellular regulation mechanisms are determined by the signal transduction reactions on the one hand and the molecules' mobility (e.g., diffusion and active transport) on the other. According to the classic fluid mosaic model of the cell membrane, introduced by Singer and Nicolson in 1972, the lipid bilayer is a neutral two-dimensional solvent in which proteins diffuse freely [187]. Therefore it has long been

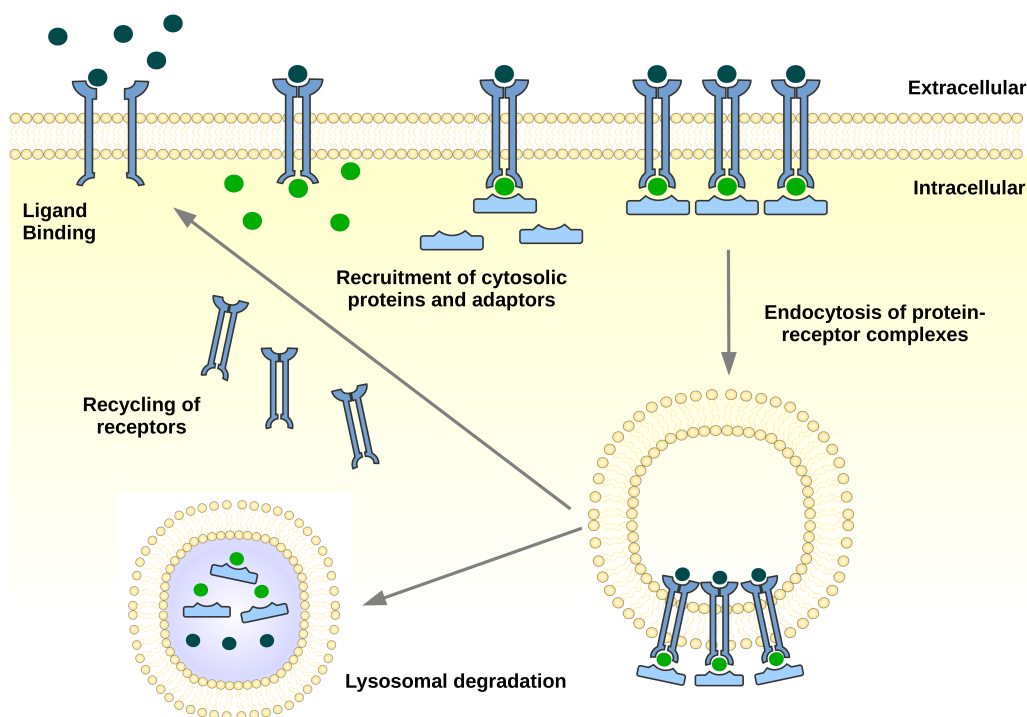


FIGURE 1.1: The ligand receptor pathway.

common sense, that membrane-associated proteins have a similar lateral diffusion coefficient and are homogeneously distributed throughout the membrane. This leads to the general assumption that the impact of molecular mobility on the signal transduction and in particular on receptor dynamics can be neglected when studying signal transduction pathways. Within the last two decades, however, it became apparent, that the membrane comprises a complex and highly compartmentalized structure, characterized by large stable multi-receptor-complexes (often termed *signalosome*), actin-mediated cytoskeleton fences, and mobile lipid rafts [207]. The ascribed static and dynamic organization of the membrane significantly alters the diffusional properties of membrane-bound particles thus leads to highly inhomogeneous spatial distribution, having major implications for the dynamics of receptor interactions. Indeed an increasing number of studies manifest the understanding, that the impact of the molecules' mobility on signal transduction is much larger than originally assumed. Meanwhile it has become well accepted, that the assumption of homogeneity does not apply in the cytoplasm and particularly not in the plasma membrane. This work aims to contribute to the understanding of how spatial membrane dynamics influence signal transduction processes. Thereby the primary focus is set on lipid rafts and the question why they have such a significant effect on receptor signaling.

1.2.1 Lipid Rafts as essential feature of spatial membrane dynamics

Lipid rafts are small, mobile local assemblies in the cell membrane composed of highly concentrated saturated sphingolipids, cholesterol and proteins [122, 153]. They are mobile entities, most likely performing lateral diffusion within the membrane. Moreover lipid rafts possess a very dynamic life cycle, i.e. depending on the local lipid composition as well as protein density, lipid rafts may spontaneously emerge, disappear or be internalized and recycled; further they are also subject to growth, shrinkage or merging processes [205]. In fact, the lipid composition of the membrane determines the amount and the characteristics of lipid rafts, i.e. the average size, life span and concentration of lipid rafts. Therefore lipid rafts are the most dynamic feature of spatial membrane dynamics and therefore extremely difficult to study *in vitro*.

However, the spatial dynamics of lipid rafts are of particular interest for a number of reasons. Due to their specific composition, they exhibit a reduced fluidity. This means, the movement of receptors inside rafts is significantly slowed down, which in turn influences the general diffusion and localization of transmembrane receptors [19, 122]. The slow down of the protein's diffusion by rafts is considered as moderate on the short time scale but strong on the long time scale [151]. Thereby receptors and other membrane-bound molecules are temporarily localized and enriched inside rafts, which heavily influences the signal transduction, as demonstrated in several *in vitro* and *in silico* studies [58, 139, 150, 163].

Likewise, lipid rafts are involved in the regulation of various signaling pathways and have been related to a continuously growing list of diseases, including immune disorders, Alzheimer's and Parkinson's diseases as well as viral and bacterial infections (for a comprehensive review, see [185]). Another important property is their ability to specifically include and exclude proteins. Thereby lipid rafts are capable of selectively concentrating proteins in order to facilitate the assembly of signaling complexes [74]. However, not only the interaction between membrane-bound molecules may be facilitated by lipid rafts, but also the binding of cytosolic molecules to transmembrane receptors and the subsequent formation of a ternary complex [29, 67].

1.2.2 Approaches to studying Lipid Rafts

The previously described static and dynamic characteristics of lipid rafts illustrated the impact of the membrane's spatial organization on receptor dynamics and prove that a thorough consideration of space is required when studying signal transduction pathways [164].

While the structural organization of the membrane and the heterogeneous distribution of membrane proteins is undisputed, researchers have long been and still are struggling to determine lipid rafts characteristics and to evaluate their actual impact on receptor interactions and signal transduction [2]. Even though a number of complementary approaches has been available to study lipid rafts and their potential involvement in signal transduction, the resulting experimental data are often unambiguous [149]. Moreover the size of lipid rafts in unstimulated, resting cells is smaller than the optical diffraction limit ($\sim 300\text{nm}$) rafts can and have only been visualized either after crosslinking/ligating raft molecules or at low temperatures [112]. Therefore the very existence of lipid rafts has long been questioned and controversially discussed. Eventually, recent advances particularly in the field of microscopy have confirmed the existence of nanoscale liquid-ordered and liquid-disordered microdomains predicted by the raft hypothesis and allowed to determine essential characteristics, like life span and size of lipid rafts in vitro [16, 74].

In vitro approaches

Notably, a number of important insights about lipid rafts are the result of computational studies. Modeling and simulation offers the opportunity to test, support, or falsify hypotheses about underlying mechanisms of lipid rafts mediated signaling. Therefore in-silico experiments provide a valuable alternative to wet-lab experiments. In the following we shortly evaluate what experimental approaches are available to analyze lipid rafts, what data they yield and why modeling indeed proves a complementary approach, in particular when studying the impact of lipid rafts on signal transduction.

Detergent resistant membranes (DRM)

There are various experimental techniques to study lipid rafts in vitro, each with different scope, advantages and pitfalls. One of the most common approach is to identify proteins that are located within detergent resistant membranes (DRM). Thereby lipid rafts are set equal with membrane domains, that cannot be extracted by non-ionic detergents. Accordingly proteins found within DRMs are considered as raft-associated. Undoubtedly this method is very usefulness and easy to apply, however it also has several pitfalls, as it strongly depends on the experimental conditions and often leads to controversial results [2, 186].

Lipid rafts disruption

Another effective and commonly used approach is the disruption of lipid rafts by manipulating the cholesterol content of the membrane. Thereby pharmacological agents, like nystatin and methyl- β -cyclodextrin are applied to either attenuate cholesterol production or directly deplete cholesterol from the membrane. This method is primarily used to study the physiological relevance of certain raft-associated proteins or the general role of lipid rafts in signal transduction pathways. However, as with any pharmacological agent, the cholesterol manipulation may have severe side effects, resulting in altered cellular physiology and biased experimental results [132].

Biophysical and Imaging techniques

Lastly, imaging and biophysical techniques have provided valuable data regarding lipid rafts characteristics in dependence of the cellular state (active or inactive) and the lipid composition of the membrane [47, 194, 195]. In fact, lipid rafts diameters in the wide range of 10nm - 700nm have been reported using different techniques including fluorescence resonance energy transfer (FRET) [70, 74], electron microscopy [109, 163], fluorescence correlation spectroscopy [120], to name only a few. The same variability has been observed for the life time of lipid rafts spanning from milliseconds [52], to seconds [16] and even minutes, as e.g. seen in the case of T-cell microclusters [23, 25].

Even though these methods are powerful approaches with the major advantage of not relying on cell disruptions, they are not free of pitfalls. Notably, most of the visualization techniques require fixatives, protein labels or crosslinkers like antibodies and cholera toxin. Each of these compounds influence lipid rafts constitution and typically induce or at least promote the clustering of raft molecules. After all, there is still a need for an improved methodology to further elucidate the nature of these nanoscale, dynamic membrane structures [2]

In silico approaches

Similar to the experimental techniques there exists various modeling and simulation approaches that have been applied to study lipid rafts. Each method employs a different level of abstraction and typically the level of detail scales with the computational complexity, i.e. one has to trade speed for accuracy.

Molecular Dynamics

The most detailed in silico approach is based on molecular dynamics simulations. Such high-detailed simulation approaches consider individual membrane-integral proteins and the surrounding lipid bilayer on atomistic scale. This provides not only means for the isolated investigation of the molecular mechanisms underlying the formation of lipid rafts and their association with membrane proteins, but also to analyze the consequences of individual environmental factors, like varying lipid composition and local protein concentrations [47, 157]. Recent simulation studies explored the effects of protein clustering on diffusive behavior of lipids and membrane proteins and on the formation of raft-like assemblies (e.g. [27–31]). Dissecting the individual impact of the diverse environmental factors that influence raft protein interaction contributes in resolving conflicting behavior observed in some experiments [157].

Grid-based approaches

To explore the impact of lipid rafts on the diffusion and distribution of receptors on longer time scales (like milliseconds or seconds) a more coarse-grained approach is required. Studies addressing this question typically employ particles based approaches, where proteins are characterized by a position, a center of mass and their random movement being modelled as Brownian motion within a two-dimensional grid (the membrane). Most often the two dimensional grid resembles is scaled, such that the size of an individual grid cell approximates the diameter of a protein and only one protein may reside on a grid cell. Lipid rafts are considered as confined areas within the grid that [wield-/comprise] slightly different environmental characteristics, such as a reduced diffusion coefficient. This means particles located within a raft-associated grid cell are e.g. subject to a reduced mobility. With this approach a nonlinear impact of varying lipid rafts characteristics, like density, size and fluidity on protein diffusion and accumulation was revealed and anomalous diffusion coefficients for different lipid rafts regimes were determined [150, 151].

Mathematical Modelling

While mathematical approaches, typically based on ordinary differential equations (ODE), are most commonly used to study signal transduction networks, there are only a few studies, that more or less fall in this category. Turner et. al. used a sophisticated mathematical model to determine the life time of lipid rafts in dependence of lipid rafts

growth and recycling processes. Whereas *Saitou et. al.* performed a combined analysis that included mathematical modeling and in vitro experiments, to analyze the involvement of lipid raft in the regulation c-Src activation. Interestingly their results provided evidence that c-Src function is dependent on the lipid-raft volume [171] Lastly, ODE models that describe subsequent signaling events in EGF signaling have been coupled with stochastic MC approaches, like the one described before [58]. Intriguingly, the results of this study suggest an ambivalent role of lipid rafts in G-protein coupled receptor signaling (GPCR), i.e. rafts can either enhance or attenuate GPCR signaling. This hybrid approach was apparently the first to embed receptor-raft dynamics in an actual model of receptor signaling, hence analyzing the effect of raft-mediated receptor organization on a signal transduction pathway.

Pathway-related studies

In fact models that consider lipid rafts dynamics in the context of signal transduction are surprisingly rare. There exists numerous computational and mathematical studies analyzing the impact of receptor co-localization and clustering on signaling, whereas, to our knowledge, there exist only the two studies that explicitly include the effect of lipid rafts on the actual level of signal transduction [58, 171]. Intriguingly both studies revealed a crucial, but nonlinear impact of lipid rafts on the signal transduction pathway under study.

Apparently there is a great discrepancy between the ambiguous role that lipid rafts play in signal transduction and the nominal attention it currently receives in systems biology.

1.3 Summary and aim of this work

Lipid raft-dependent receptor dynamics have been well characterized by small scale computational as well as biophysical and imaging-based approaches. As a result, it is meanwhile well accepted that the spatial organization of membrane bound proteins in terms of diffusion, localization and protein-specific aggregation is tightly regulated by lipid rafts. These effects crucially depend on environmental factors like lipid composition and local protein density within the membrane.

At the same time, lipid rafts have been reported to be involved in a large number of central signaling pathways, such as differentiation (Wnt), proliferation (EGFR) and immune response (T-cell signaling). This means, the regulation of lipid rafts actually affects numerous physiological processes. However, the actual impact of lipid rafts on subsequent signaling events is poorly explored compared to the knowledge gained about

receptor-raft interaction. Only a handful of experimental and even less computational studies actually consider the effects of receptor-lipid rafts interaction on signal transduction.

This apparent discrepancy is the primary motivation for this thesis. Here we aim to explicitly analyze how raft-dependent receptors dynamics affect on both, individual signaling events as well as an entire signaling transduction pathway. In other words, we aim to study lipid rafts-dependent signaling on the micro- and on the macroscopic scale.

Chapter 2

Modeling the diffusion dynamics of plasma membrane receptors under the influence of lipid rafts

In this chapter a detailed, spatial model of the plasma membrane is developed to capture lipid rafts and receptor diffusion dynamics, as well as the spatial effects resulting from their interaction. The goal is to arrive at a model that represents varying lipid rafts characteristics, such as density, size, mobility and fluidity and the interdependent diffusion of lipid rafts and receptors. This allows to analyze the impact of the aforementioned lipid rafts characteristics on the spatial organization of receptors and on subsequent signaling events, like the formation of a ternary complex between activated receptors and peripheral proteins.

2.1 Modeling small scale lipid rafts dynamics

As described in Section 1.2, the cell membrane plays a significant role in signal transduction, as it directly interacts with the extracellular space by transmembrane receptors. The static and dynamic organization of plasma membranes leads to highly inhomogeneous spatial distributions, demanding a thorough consideration of space when modeling and simulating such systems [38]. Thereby one of the key player in spatial membrane dynamics are lipid rafts. They impeded the diffusion of membrane-bound molecules, such as membrane integral receptors. As a result lipid rafts promote the dimerization, activation and aggregation (clustering) of receptors [37, 44, 58]. To study lipid rafts dynamics, its impact on receptor diffusion and the arising consequences for subsequent signaling

events, a detailed spatial model of the plasma membrane is required.

When modeling receptor and lipid rafts dynamics it is generally important to take the availability of the reaction volume, i.e. excluded volume effects into account. *Excluded volume* effects can only be captured by individual based approaches that track the movement of individual particles and their size in space [12]. There exists a plethora of individual-based approaches and each method employs a different level of abstraction. Typically the level of detail scales with the computational complexity, i.e. one has to trade speed for accuracy. However, the level of abstraction required to describe spatial dynamics strongly depends on the subject of interest and the addressed scientific questions. Therefore we will first carefully consider, what level of detail, i.e. spatial resolution and what model features are required to capture the interdependent spatial dynamics of lipid rafts and receptors, before we actually describe the plasma membrane model that has been implemented.

2.1.1 Model features of microscopic lipid rafts dynamics

However, in addition to the excluded volume effect, the interaction between receptor and lipid rafts is characterized by complex spatial interdependencies that have to be described properly in an individual-based model. First, a representation is required for the localization of particles *inside* a lipid raft. Second, due to their composition, lipid rafts reduce the diffusion coefficient of raft-associated particles. Accordingly the diffusion coefficient depends on the location of the particle. Third, we consider rafts as moving entities. This has two major consequences. First the movement of lipid rafts has to be represented in the model; and second, particles that are contained within lipid rafts are not only subject to their own movement, but also to the movement of the raft they are located in. This means, the modeling and simulation approach has to provide means to 1. describe a nesting of particles as well as for the shuttling of the receptors into and out of the lipid rafts 2. account for the reduced diffusion coefficient of raft-associated particles 3. incorporate combined movement of raft and receptor.

2.1.2 Individual-based approaches to model microscopic raft/receptor dynamics in the context of signal transduction

Individual-based approaches employ the highest level of detail by considering each individual molecule, i.e. its shape, its position (coordinates) and motion (trajectory) in continuous space. The spatial and temporal scale strongly vary between different approaches, reaching from nanometers to centimeters or millimeters and femto- or picosecond to simulated seconds or minutes. Highly realistic simulation approaches incorporate

explicit representations of the position and energy of every atom in the system and consider detailed chemical reactions, like formation and breaking of bonds between single atoms. Such fundamental approaches mainly operate on very low spatial and temporal scales (pico- or nanometer/seconds) yielding a very accurate and realistic representation of the molecular processes under study. Of particular interest for this work are recent studies that analyze the mobility, dimerization and clustering of individual membrane proteins with regard to the physical properties of the surrounding lipid environment, i.e. considering lipid packing, lipid rafts or protein crowding), like [69, 140, 157]. However, due to their computational complexity, these high-resolution approaches are infeasible to simulate the interaction of a larger amount of receptors and lipid rafts over time scales of seconds to minutes, like it is required for the scope of this work.

On the other hand, individual-based simulation approaches can also employ a very simplistic particle-based representation, in which all molecular properties, despite the position, the size and diffusive motion of the involved molecules are disregarded and chemical reactions, if considered at all, are solely diffusion-limited. Therefore particle-based approaches seem equally suited regarding their temporal and spatial scale.

Corresponding modeling and simulation methods can be narrowed down to approaches that fall into one of the two categories: continuous and discrete/grid-based.

Individual continuous-based approaches

In continuous approaches particles are associated with real-valued coordinates, a shape and a manner of movement (most often diffusion in terms of Brownian Dynamics (BD)). However, in continuous space it is challenging to implement the localization of particles within lipid rafts and in particular the shuttling process, i.e. consumption of a particle by the larger lipid rafts. For particles having a distinct shape and a real valued position in continuous-based approaches, the transition of a particle into or out the lipid raft requires two crucial steps. First the collision has to be detected between particle and lipid raft; second the particle has to be placed at some location at the in- or outside of the raft in terms of a well defined *jump procedure*. Accordingly for crowded environments the involved steps, like collision detection, are computationally exhausting, since the frequency of collision events will be significantly increased yielding exceedingly small time steps between individual collisions and very high computational costs. This is a general drawback of BD simulation with explicit particle representation in space, i.e. with position, momentum and shape. With a physiological concentration of receptors within the plasma membrane of about 30 %, we are indeed faced with a large number

of particles in a crowded environment, which renders a continuous individual-based solution impractical for a combined lipid raft/receptor model.

Individual grid-based approaches

In grid-based approaches, i.e. Cellular Automata (CA), each grid-site is characterized by a finite number of states, that evolve in discrete time according to a set of local transition rules (state automata) depending on its own state and the state of its neighbors. Thereby spatial information can only be provided in terms of lattice coordinates. Accordingly, any information about the molecule's shape and exact size is disregarded. However, a coarse representation of the molecular size can be retained, if the exclusion principle applies, i.e. if lattice cells may be occupied by at most one particle at a time and if the lattice cell size is set to the approximate diameter of the (smallest) molecule in the system. Thereby volume exclusion and anomalous diffusion effects are still accurately represented, which allows for detailed micro-scale simulations of diffusion processes. As a consequence grid-based approaches are typically more efficient than continuous-based dynamics. Furthermore due to the lattice-based discretization of space, the boundaries of particle and rafts can be directly assessed in terms of neighborhood. Also the transition of a particle into or out of rafts simply refers to the transition of one grid to a neighboring one according to the transition rules equally defined for all grid-sites. As a result both steps involved in the localization and shuttling of particles and lipid rafts, i.e. collision detection and particle placement are clearly defined, hence easy to handle in grid-based approaches.

Summary

After all, Cellular Automata/grid-based approaches are apparently best suited to describe the combined spatial dynamics of receptor and lipid rafts. Indeed, this is in line with the numerous amount of studies, that apply individual, grid-based approaches to study non-linear diffusion effects on the membrane, like sub-diffusion and raft-association, and their impact on receptor localization, cell polarization and eventually signal transduction [37, 38, 148, 150].

However, the large majority of these studies did not implement their models according to the CA-formalism, but with an almost identical approach termed lattice-based Monte Carlo (MC). The main difference between these individual grid-based approaches is that in lattice-based MC approaches particles are considered individually from a global view. This means, the state of a grid cell is changed according to global rules, instead of local

transition rules that apply for all individual cells, as done in CA. Also, the update of the lattice is performed asynchronously, i.e. state changes are not applied synchronously for all grid cells, but one after another. Moreover, in most of the implementations model and simulator are closely intertwined, which makes it difficult to distinguish and compare between individual models, and to reproduce simulation results.

In this work however, we stick to the CA formalism and provide a model that represents all model features we identified to model and simulate the micro-scale lipid rafts dynamics. In the following the concept and the main components of the CA-based membrane model will be described in detail.

2.2 A Plasma Membrane Model based on Cellular automata

The main requirements to model spatial membrane dynamics in terms of the CA formalism are rule schemata that allow the specification of random movement and collision handling as well as group behavior to represent the lateral diffusion of particles and lipid rafts dynamics, respectively. Due to synchronous update scheme of the CA formalism, dependencies may arise from concurrent collisions in neighboring cells. Common way to circumvent this problem, is to introduce a multi step evaluation of the CA, i.e. to distinguish between collision and movement step. Thereby potential conflicts are avoided.

2.2.1 Lattice-Gas Cellular Automata: Particle Movement for cellular automata

Modeling microscopic particle movement is not straightforward in traditional CA. Typically, each cell in the CA lattice possesses one of the two possible states: occupied or empty, i.e. each cell can contain at most one individual particle at a time. As a result, random movement and particularly collisions can hardly be resolved with the traditional (synchronous) update scheme of CA without additional information. There exist a number of cellular automata models that represent individual particle movement [30]. However, the Lattice Gas Cellular Automata (LGCA) provides the most natural representation of lateral diffusion, as it considers the discrete dynamics of gas particles moving and colliding on a two-dimensional lattice conserving mass and momentum. We thus adopt the basic idea of LGCA to model the lateral movement of membrane-integral proteins (e.g. receptors). In the following the concepts of LGCA are briefly

introduced and followed by a discussion of how these concepts can be used to model spatial membrane dynamics.

Basic Introduction of Lattice Gas Cellular Automata

LGCA were introduced in 1973 by Hardy, Pomeau and dePazzis (also known as HPP model) to study classical particle dynamics and transport phenomena in fluids [77]. The idea was to model motion and interaction of individual particles with a simple, discrete approach that conserves mass and momentum and eventually follows the Navier-Stokes equation of hydrodynamics. However, only the subsequent extension of the model by Frisch, Hasslacher, Pomeau (FHP model) was sufficient to yield the Navier-Stokes equation in the macroscopic limit [62]. Fritsch et. al. (1986) revealed that besides mass and momentum conservation another third condition is crucial for the correct simulation of the Navier-Stokes equation in terms of LGCA: The lattice has to possess a certain symmetry. While the quadratic lattice employed by the HPP model failed to reproduce the Navier-Stokes equation due to the inadequate symmetry, the hexagonal lattice employed by the FHP model is sufficient for simulations in 2D. Notably, for (random) diffusional processes, on the other hand, it is sufficient to consider the HPP [30]. The LGCA is an extension of the classical CA approach with specific state space and transition rules. A CA can be described as a tuple $\mathcal{C} = \{\mathcal{L}, \mathcal{S}, \mathcal{N}, \mathcal{B}, \Phi\}$ [48], consisting of a regular lattice \mathcal{L} of autonomous cells, and a transition rule Φ defining the state change of an individual cell $\mathbf{c} \in \mathcal{L}$ during an update step according to the cell's state $s \in \mathcal{S}$ and the local neighborhood \mathcal{N} . CAs allow to mimic complex system dynamics in terms of simple transition and interaction rules (e.g., [81, 133, 158]). However, as explained above, modeling particle movement as done in LGCA, is not straightforward in traditional CA.

The LGCA approach circumvents the limitations of traditional CA approaches by extending each cell $\mathbf{c} \in \mathcal{L}$ by a number of velocity channels $(\mathbf{c}, \mathbf{v}_i), i = 1, \dots, b$, that specify the direction and the momentum of a particle. Typically, there is one velocity channel for each adjacent cell and a number of additional resting channels (β) with zero velocity. In general, a variable number of rest-channels may be introduced, yielding a total number of $\tilde{b} = b + \beta$ velocity channels per cell. However, we restrict our approach to exactly one zero-velocity channel per cell $\beta = 1$. That means for any cell in a quadratic lattice, as employed in the HPP model, there are five velocity channels, whereas cells in the hexagonal lattice of the FHP model comprise six velocity channels (cf. Figure 2.1B). In general, for two-dimensional lattices, as considered here, the set of velocity channel can be represented as 2D vectors indicating the direction of moving particles. In case of

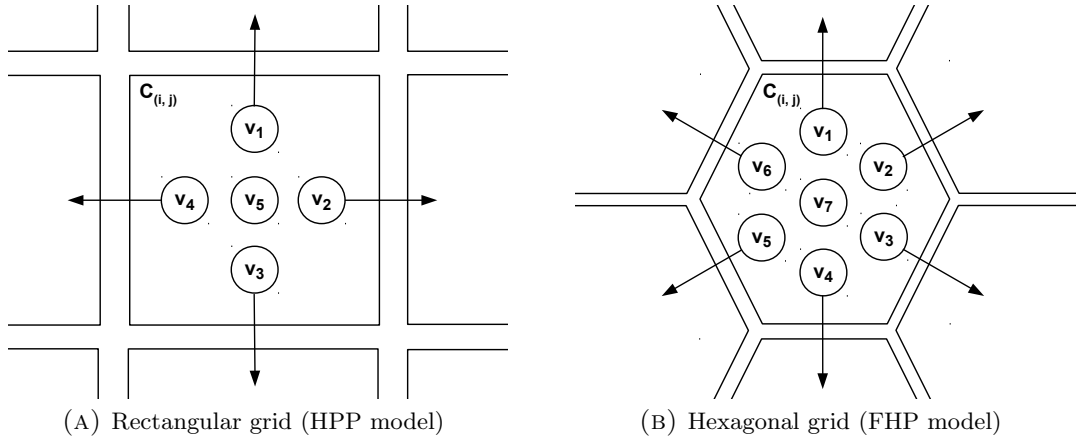


FIGURE 2.1: Representation of (unoccupied) velocity channels of an individual cell according to the (a) HPP and (b) FHP model, i.e. LGCA with quadratic and hexagonal lattice.

the HPP model, the velocity channels are defined as follows:

$$\mathbf{v}_0 = \begin{pmatrix} 0 \\ 0 \end{pmatrix}, \quad \mathbf{v}_1 = \begin{pmatrix} -1 \\ 0 \end{pmatrix}, \quad \mathbf{v}_2 = \begin{pmatrix} 0 \\ 1 \end{pmatrix}, \quad \mathbf{v}_3 = \begin{pmatrix} 1 \\ 0 \end{pmatrix}, \quad \mathbf{v}_4 = \begin{pmatrix} 0 \\ -1 \end{pmatrix}$$

(see Figure 2.1A). Further, the state of an arbitrary cell at time t , $s(\mathbf{c}, t)$, can be described by the cell configuration $\boldsymbol{\eta}(\mathbf{c}, t)$, which relates to the occupation of the velocity channels:

$$s(\mathbf{c}, t) = \boldsymbol{\eta}(\mathbf{c}, t) \quad (2.1)$$

$$\boldsymbol{\eta}(\mathbf{c}, t) := (\eta_1(\mathbf{c}, t), \dots, \eta_{\tilde{b}}(\mathbf{c}, t)) \quad (2.2)$$

with $\eta_i(\mathbf{c}, t) \in \{0, 1\}$, $i = 1, \dots, \tilde{b}$ being the occupation numbers of the velocity channels (\mathbf{c}, v_i) indicating the presence ($\eta_i(\mathbf{c}, t) = 1$) or absence ($\eta_i(\mathbf{c}, t) = 0$) of a particle. The total number of particles present at cell \mathbf{c} , also referred to as *particle density*, is defined as

$$n(\mathbf{c}, t) = \sum_{i=1}^{\tilde{b}} \eta_i(\mathbf{c}, t). \quad (2.3)$$

Further, in contrast to classical CA, the transition rule of LGCA is split into two distinct parts: a local interaction, or collision step and a neighborhood-dependent propagation step. Accordingly the transition operator is defined as the composition of interaction/collision and propagation:

$$\boldsymbol{\eta}(\mathbf{c}, t+1) = \Phi^P (\Phi^C (\boldsymbol{\eta}(\mathbf{c}, t))) \quad (2.4)$$

This allows the propagation of particles between individual cells with due regard to mass and momentum conservation while keeping the corresponding update rules as simple as

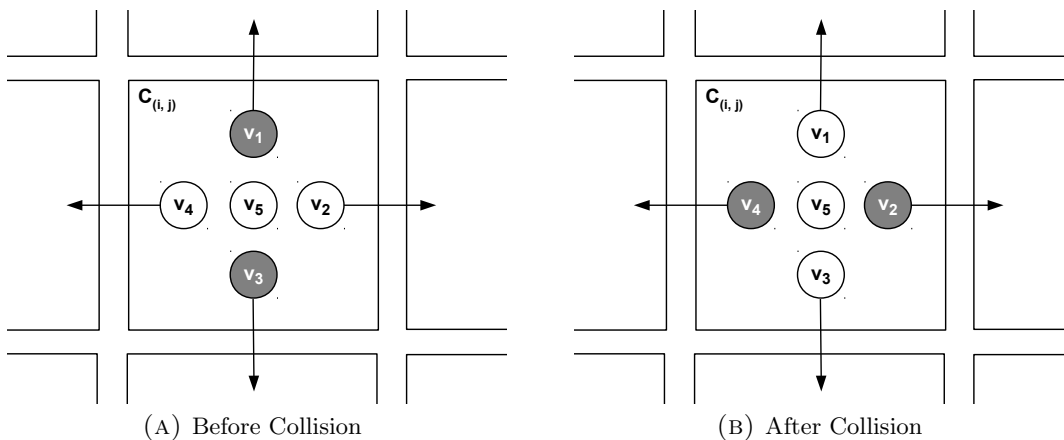


FIGURE 2.2: Collision handling according to HPP model. Velocity channels occupied by particles are gray-colored.

possible, as explained in the following.

During the interaction/collision step the configuration of the velocity channels of all $\mathbf{c} \in \mathcal{L}$ are changed according to a model-specific interaction/collision rule Φ^C , i.e.

$$\eta_i^C(\mathbf{c}, t) = \Phi_i^C(\boldsymbol{\eta}(\mathbf{c}, t)), \quad i = 1, \dots, \tilde{b},$$

In LGCA the interaction/collision rule is used to resolve potential particle collisions according to the collision handling scheme of the current model. In the HPP model, for instance, there is only one collision configuration, i.e. if two particles occupy opposite velocity channels of the same cell. In this case the collision handling is straight forward as the directions of the involved particles are swapped by 90 degrees (Figure 2.2). In contrast, the collision handling of the FHP model is much more complex. When considering one rest channel per cell as well as all collisions that conserve mass and momentum at each site, one obtains a total number of 76 possible collisions. A complete list of the collision rules of the FHP model can be found in [22].

During the deterministic propagation step, the state of each cell is propagated to a neighboring cell $\Phi_i^P(\mathbf{c}, t) : \eta_i^C(\mathbf{c}, t) \rightarrow \eta_i(\mathbf{c} + \mathbf{v}_i, t + \tau)$, i.e. each particle is *moved* according to its direction, which is described by the propagation operator. Hence all particles are transferred simultaneously to the corresponding neighboring node and, following momentum conservation, placed on the same cell/velocity channel again (cf. Figure 2.3). Combining both interaction and propagation rule the changes of a cell's configuration during one time step τ is described as:

$$\eta_i(\mathbf{c} + \mathbf{v}_i, t + \tau) = \eta_i^C(\mathbf{c}, t), \quad i = 1, \dots, \tilde{b}. \quad (2.5)$$

Note, that in this approach particles can only alter the direction of their movement by

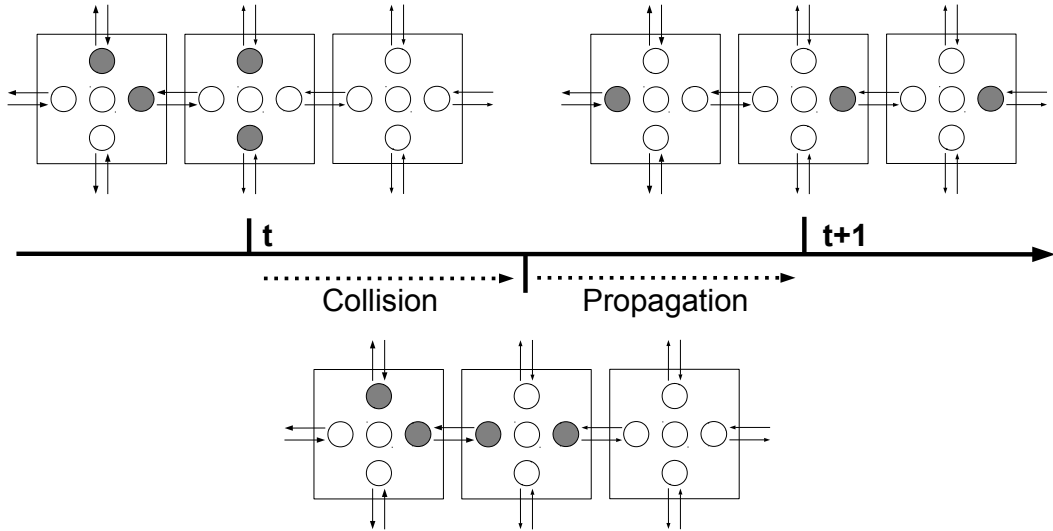


FIGURE 2.3: Collision and Propagation step according to HPP model during one time step on an arbitrary section of a square lattice. Occupied velocity channels are indicated by gray color. Note, that particles may be transferred to neighboring cells, that are outside of the displayed section and hence excluded from the illustration. Due to this, the number of particles displayed may vary between different time steps

means of collisions and otherwise perform ballistic motion. However, there also exist stochastic implementations of the LGCA that allow the simulation of random movement.

A probabilistic LGCA model for random movement

The previously described deterministic dynamics of lattice gas cellular automata allow the modelling of ballistic movement, i.e. particles change their direction only after colliding with another particle. However, movement of membrane-associated proteins is characterized by brownian motion, i.e. particles change direction in a probabilistic way. Therefore we have to consider probabilistic LGCA approaches that model random motion instead, such as [48, 81] In probabilistic LGCA the deterministic collision/interaction operator Φ^C is typically replaced by a probabilistic reorientation (shuffling) rule Φ^S , while the subsequent propagation (Φ^P) remains unchanged. This means, before particles are transferred to the neighboring cells as explained in the previous section, the configuration of each cell, i.e. the occupation of the velocity channels is permuted randomly (see Fig. 2.5). The cell configuration after shuffling is defined by:

$$\eta'(\mathbf{c}, t) = (\Phi_i^S(\eta(\mathbf{c}, t)))_{i=1}^b, \quad \text{with } \mathbb{P}(\eta \rightarrow \eta')(\mathbf{c}, t) \quad (2.6)$$

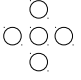



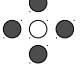
$n(\mathbf{c}, t)$	$\boldsymbol{\eta}'(\mathbf{c}, t)$	$(\mathbb{P}(\boldsymbol{\eta} \rightarrow \boldsymbol{\eta}'))$
0 channel		(1)
1 channel		(1/4)
2 channel		(1/6)
3 channel		(1/4)
4 channel		(1)

FIGURE 2.4: Possible cell configurations depending on the number of channels occupied

where \mathbb{P} is the state- and time dependent transition probability that transforms the given channel configuration $\boldsymbol{\eta}$ into a certain permutation $\boldsymbol{\eta}'$ [30, 48]. For random walk models, the corresponding transition probabilities are defined as:

$$\mathbb{P}(\boldsymbol{\eta} \rightarrow \boldsymbol{\eta}')(\mathbf{c}, t) = \frac{1}{Z} \delta(n(\mathbf{c}, t), n'(\mathbf{c}, t)),$$

where the normalization factor Z corresponds to the number of all possible configurations that retain the particle density $n(\mathbf{c}, t)$ of the given cell \mathbf{c} with due regard to mass conservation (cf. Fig. 2.4) [80]:

$$\begin{aligned} Z &= \sum_{\boldsymbol{\eta}'(\mathbf{c}, t)} \delta(n(\mathbf{c}, t), n'(\mathbf{c}, t)) \\ &= \binom{b}{n(\mathbf{c}, t)}. \end{aligned}$$

LGCA incorporating random movement are promising models for studying and analyzing transport and interaction processes in biological systems [30, 48]. In particular these model have been extensively used in the context of cell migration [80], tumor growth [144, 158] and tumor invasion [81]. Further, in contrast to cellular automata based fluid models, it is sufficient to consider square lattices here, since diffusional processes do not require a fourth-order tensor for their description [30, 81].

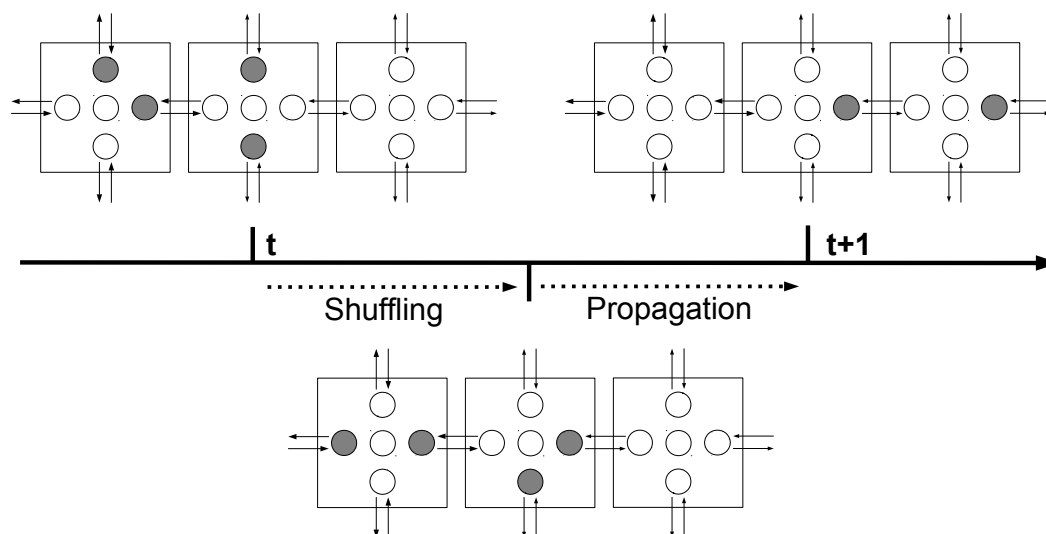


FIGURE 2.5: Shuffling and Propagation step according to a probabilistic LGCA model during one time step on an arbitrary section of a square lattice. Occupied velocity channels are indicated by gray color. Note, that particles may be transferred to neighboring cells, that are outside of the displayed section and are hence excluded from the illustration. Due to this, the number of particles displayed may vary between different time steps

Why common LGCA models are not sufficient to represent spatial membrane dynamics

LGCA indeed form a promising basis for the modeling of lateral diffusion in spatial membrane dynamics as they provide a concise way of representing (random) movement in the context of CA. However, deterministic and probabilistic LGCA models operate on a mesoscopic scale, as they consider only one particle type¹ and no individual-based collision handling. This is a major shortcoming when modeling detailed receptor and lipid rafts dynamics. To illustrate this issue, let's refer to a situation, where two individual particles are located in neighboring cells at directly adjacent velocity channels. In common LGCA models, both particles would simply switch positions (cells) during the propagation step, instead of being reflected due to a collision. Such collision handling is unproblematic, as long as the system only refers to uniform particles that are not further attributed or specified. In our approach, however, we aim to distinguish between different types of membrane proteins and receptors and therefore require an individual based representation of particles. In this case common LGCA models cannot be applied one-on-one for simulating spatial membrane dynamics, because they contradict the exclusion condition of individual-based approaches. Nevertheless, the general concept of

¹Note, that multi-component LGCA are capable of representing different types of particles, which, however, reside on separate lattices and therefore the exclusion principle is not implied/applied between different types of particles

probabilistic LGCA provides a sound basis that we adopt to create a 2D lattice-based membrane model that is specifically tailored to our needs.

2.2.2 Modeling individual-based random motion in LGCA

To construct a spatial membrane model incorporating individual receptor movement, we need to distinguish between the individual (particle) entities. To stick to the notation used to this point, the term particle is further used to refer to any individual membrane entity with the approximate size of a protein (2nm). To represent the two-dimensional membrane layer, we employ a two-dimensional lattice and, following the notation of the 2 dimensional HPP model, attribute each cell with five velocity channels, each for one direction and a resting channel. Any channel can be occupied by exactly one individual entity.

Individual-based collision handling

When modeling the particles' dynamics, however, one has to account for the exclusion principle of individual based approaches. Therefore, instead of one collision, we need to consider two different types of collisions: either when two individual particles approach the same cell (cf. Fig. 2.6a), or when neighboring particles move in opposite direction (c.f. Fig. 2.6b). In the following we denote the first type as field collision and the latter as direct collision. While the first type of collision (field collision) resembles the collision propagator of common deterministic LGCA models, the second type (direct collision) is neglected in the common LGCA models, because neighboring particles that move in opposite directions as depicted in Figure 2.6b do not collide, but rather jump over each other, literally spoken. For our model, however, we assume, that particles are always reflected when colliding with one another, i.e. after the collision the involved particles return to their previous cell. This means, for direct collisions the particles' movement is directly rejected, and particles are located at the same cell at the end of the **current** update step, see Figure 2.7a. In contrast, during field collisions, the particles are actually transferred to the neighboring cell, but immediately assigned to the velocity channel of the opposite direction. Hence only when the **next** update step has been successfully executed, the particles return to their original position/cell (see Fig. 2.7b for clarification). This approach resolves both collision types on an individual-based level and further ensures that the traveled distance during collisions is kept equal for direct and field collision events. However, as a consequence, the proposed individual-based collision scheme has major implications not only for the collision handling, but for the transition operator in general.

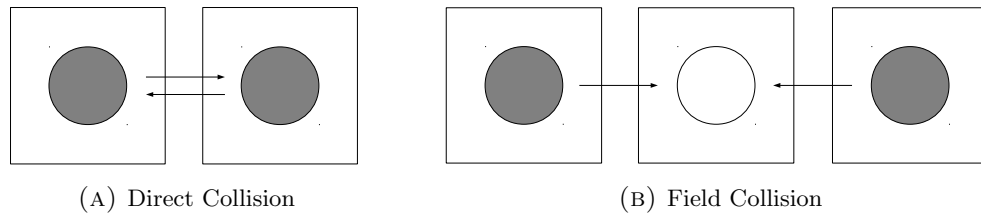


FIGURE 2.6: The two different kinds of collisions that may occur in the implemented synchronous CA approach under due regard of exclusion effects

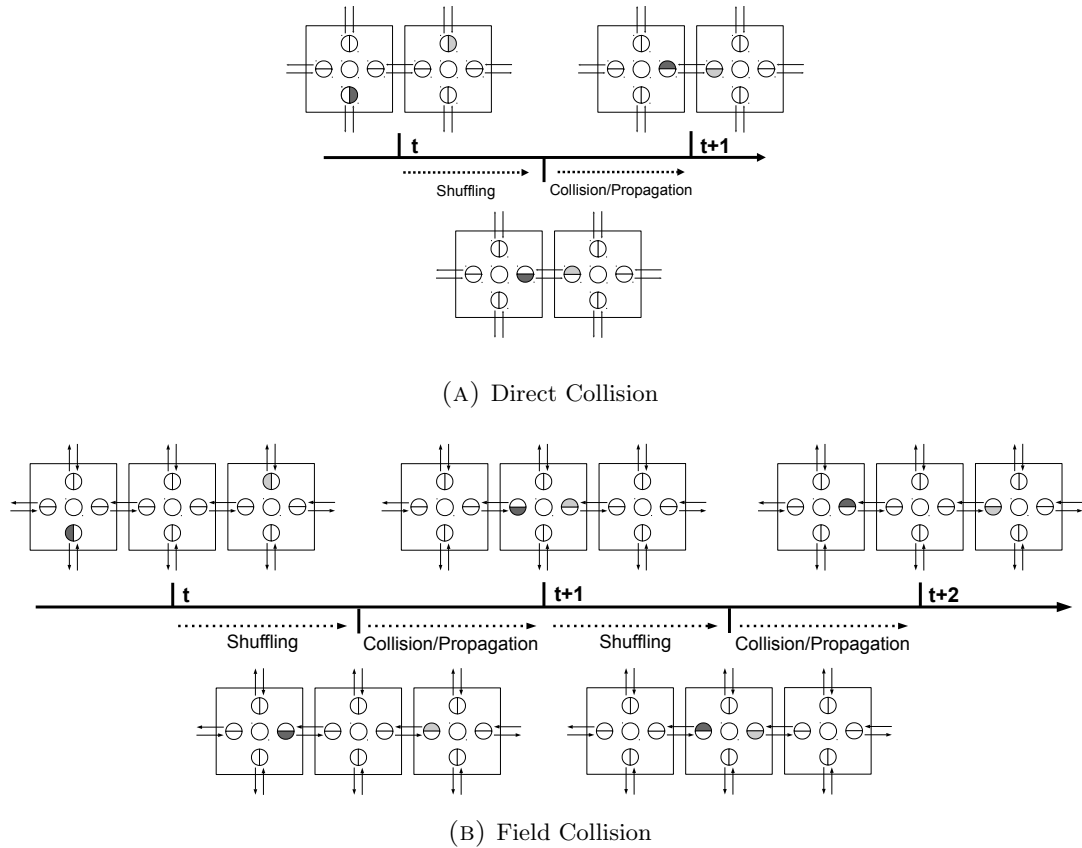


FIGURE 2.7: The two different kinds of collisions that may occur in the implemented synchronous CA approach under due regard of exclusion effects

Transition Operator for random movement of individual particles

To realize the individual-based collision handling as outlined above, we adopt the basic ideas of the previously described deterministic and probabilistic LGCA approaches. In doing so, we combine the collision handling of the deterministic HPP model with the random motion approach of probabilistic LGCA and apply some modifications.

Basically the update rule of the presented membrane CA consists of a propagation and a combined collision and shuffling operator. For the detailed description of the update rule and the individual propagators, it is useful to extend the state of the velocity channels in terms of *incoming* and *outgoing* slots, $\boldsymbol{\eta}^{\text{in}}(\mathbf{c}, t)$ and $\boldsymbol{\eta}^{\text{out}}(\mathbf{c}, t)$ to better distinguish

between incoming and outgoing information [31]. To account for the restriction that channels can take up exactly one particle, only one slot per velocity channel may be occupied by a particle at a time. In the following the individual steps of the update rule, and particularly the individual-based collision handling of our approach are explained in detail.

As described above, and in accordance with the HPP model, the update routine starts with the shuffling/collision step. At the initial situation, all particles are either placed on a resting channel or on an incoming slot of a velocity channel. Based on the random motion approach of probabilistic LGCA, during the shuffling/collision step all particles are assigned to the outgoing slot of a randomly chosen velocity channel. However, if several particles (up to the number of velocity channels) occupy a single cell concurrently, a field collision is caused in the respective cell. In this case, the distribution of the particles, i.e. the shuffling of the particles, is not random, but deterministic. Consequently, instead of randomly placing each particle on an unoccupied velocity channel, particles are now switched from their current incoming slot to the outgoing slot of the same velocity channel:

$$\boldsymbol{\eta}^{\text{out}}(\mathbf{c}, t) = \begin{cases} (\Phi_i^S(\boldsymbol{\eta}^{\text{in}}(\mathbf{c}, t)))_{i=1}^b, & n(\mathbf{c}, t) = 1 \\ \boldsymbol{\eta}^{\text{in}}(\mathbf{c}, t), & \text{else} \end{cases} \quad (2.7)$$

Thereby particles are scheduled to move in reverse direction during the subsequent propagation (c.f. Fig 2.7B), which accounts for the reflecting collision behavior. Note, that the shuffling operator Φ^S is only applied, when the cell \mathbf{c} contains exactly one particle. Consequently the corresponding transition probability \mathbb{P} has a fixed value of 1/4 (cf. 2.6):

$$\mathbb{P}(\boldsymbol{\eta}^{\text{in}} \rightarrow \boldsymbol{\eta}^{\text{out}})(\mathbf{c}, t) = 1/4. \quad (2.8)$$

The movement of individual particles thus only follows the random walk of Brownian motion, when it is not subject to a (field) collision. In this case, the particle's movement is determined by a shuffling operator that resembles the orientation operator of probabilistic LGCA. In the other case, i.e. for multi-particle movement in terms of a field collision, a variant of the collision propagator of the HPP model is applied, with a modified collision rule to account for the reflective collision behaviour. Accordingly, in contrast to the 90° rotation applied in the HPP model, in our approach the particle's direction is always changed by a 180° rotation upon (field) collisions.

Similar to deterministic LGCA, the subsequent propagation operator transfers all particles from one cell to the neighboring one according to the particle's direction. However,

in our model the propagation operator does not only perform the actual transition of particles, but it is also responsible for detecting and resolving direct collisions. We thereby incorporate the particle transitions and the handling of direct collisions in one operator. What might seem unusual from first view, becomes evident, when regarding the dynamics in terms of outgoing and incoming slots. For this consider a pair of [neighboring/contiguous] cells with $(\mathbf{c}, \mathbf{v}_i)$ and $(\mathbf{c} + \mathbf{v}_i, \mathbf{v}_k)$ being adjacent velocity channels in \mathbf{c} and $\mathbf{c} + \mathbf{v}_i$ respectively. Given one of the velocity channels is occupied by a particle, i.e. $\eta_i^{\text{out}}(\mathbf{c}) = 1$ and $\eta_k^{\text{out}}(\mathbf{c} + \mathbf{v}_i) = 0$, the propagation operator simply transfers this particle to the incoming slot of $(\mathbf{c} + \mathbf{v}_i, \mathbf{v}_k)$:

$$\Phi_i^{Pr}(\mathbf{c}, t) : \eta_i^{\text{out}}(\mathbf{c}, t) \rightarrow \eta_k^{\text{in}}(\mathbf{c} + \mathbf{v}_i, t + \tau) \quad (2.9)$$

$$k = i + 2 \cdot \sum_{l=0}^{d=2} v_{il} ,$$

Note, that this propagation rule slightly differs from that of common LGCA models (cf. 2.2.1).

However, in the case when both outgoing slots of the adjacent velocity channels are occupied, i.e. $\eta_i^{\text{out}}(\mathbf{c}) = \eta_k^{\text{out}}(\mathbf{c} + \mathbf{v}_i) = 1$, the movement of both particles causes a direct (head-on) collision and ought to be rejected (c.f. Fig 2.7a). Accordingly, instead of transferring both particles, the colliding particles are reassigned from the outgoing slot to the corresponding incoming slot of the same velocity channel:

$$\Phi_i^{Pc}(\mathbf{c}, t) : \eta_i^{\text{out}}(\mathbf{c}, t) \rightarrow \eta_i^{\text{in}}(\mathbf{c}, t + \tau). \quad (2.10)$$

The same applies to $\eta_k^{\text{out}}(\mathbf{c} + \mathbf{v}_i)$. In this way the reflecting effect of a direct collision is represented.

During propagation, particles are now either transferred to the neighboring cells or reflected in terms of a direct collision, depending on the occupation of the local velocity channel and its adjacent neighbor. The change in the occupation of a cell's velocity channel after propagation reads as:

$$\eta_k^{\text{in}}(\mathbf{c} + \mathbf{v}_i, t + \tau) = \begin{cases} \eta_i^{\text{out}}(\mathbf{c}, t) & : \delta(\eta_i^{\text{out}}(\mathbf{c}, t), \eta_k^{\text{out}}(\mathbf{c} + \mathbf{v}_i, t)) = 0 \\ \eta_k^{\text{out}}(\mathbf{c} + \mathbf{v}_i, t) & : \text{else} \end{cases} \quad (2.11)$$

After propagation, the time advances by the given time step τ and the particles are immediately rescheduled for the next movement/update step.

In summary, to model the lateral diffusion of individual receptors in cell plasma membranes, we combine basic concepts of common LGCA models. Thereby the transition

operator Φ is composed of the two steps shuffling/collision and propagation. The shuffling routine schedules the direction of the subsequent movement and thereby processes field collisions, while the propagation step is used to detect and handle direct collisions as well as to execute particle transitions.

2.2.3 Modeling Lipid Rafts - Multi-Scale modelling with Cellular Automata

The previously described approach allows the representation of random motion of individual particles associated or bound to plasma membranes. However, the lateral diffusion of membrane-bound proteins is significantly influenced by lipid rafts with major implications on their localization, activation and eventually on the subsequent signal transduction (cf. 1.2). To characterize the impact of lipid rafts on these processes, the current membrane CA model needs to be extended with an explicit representation of lipid rafts including raft diffusion and raft/receptor interaction. Though, when modeling lipid rafts and in particular their diffusion in the framework of CA we are faced with severe difficulties for a number of reasons.

Rafts are moving entities that are significantly larger than common membrane particles, like receptors. Accordingly rafts span a number of lattice cells, that have to change their state in a coordinated and concurrent manner to account for arbitrary state changes of rafts, in particular regarding motion. In addition, lipid rafts follow the same exclusion principle as membrane particles, i.e. one cell cannot be occupied by more than one raft at the same time. Obeying the exclusion principle for rafts requires sophisticated local update rules, that are capable of handling the motion and collision of rafts properly. However, the exclusion principle does not apply to the interaction of membrane particles and rafts, i.e. receptors may be located within rafts (termed raft-associated receptor), hence rafts and receptors can occupy the same lattice cell at the same time. In consequence, the effects that rafts exert on raft-associated particles have to be incorporated in the model as well.

Basically there exist plenty (multi-level) CA approaches that are capable of handling objects larger than common lattice cell size and interacting objects on different spatial levels. However, the huge majority of the approaches either applies asynchronous update schemes that resemble agent-based systems [151, 204] or an hybrid approach, where the diffusion of smaller particles like ions is modeled implicitly [30, 48]. Whereas none of the given approaches obeys the interaction and collision scheme outlined above while being based on a clear CA formalism with synchronous update scheme. Therefore, following the ideas of multi-scale Complex Cellular Automata (CxA) [88] we develop an new implementation that is tailored to the simulation and analysis of receptor/raft

interaction in the context of signalling transduction. In the following the basic definition of Complex Cellular Automata will be shortly introduced before describing the developed receptor/raft model.

Complex Cellular Automata (CxA)

The basic idea of complex Cellular Automata (CxA) is to decompose a multi-scale model into several (n) CA-based submodels, such that each submodel contains solely processes that operate on the same or on a similar spatio-temporal scale. The individual submodels are coupled through communication channels and may dynamically exchange information, while being executed separately. All submodels are executed sequentially and exchange information after each individual update. A CxA can thus be considered as a set of coupled, self-contained cellular automata $\mathcal{C} = \{C_1, \dots, C_n\}$, whose individual dynamics depend on the input-output relations between the coupled/connected CA. Accordingly the original definition of CA has to be extended, to allow an exchange and processing of external information. Notably, for the sake of consistency, the definition of CxA presented here follow the notation of *Hoekstra et. al. (2010)* [88]:

$$C = \{A(\delta, \mathcal{L}, \tau, T), \mathcal{S}, \Phi, \mathbf{s}_{init} \in \mathcal{S}, \mathbf{u}, \mathbf{O}\} \quad (2.12)$$

where A is a more general description of the temporal and spatial domain of the CA. The domain A is further specified by the formerly defined lattice \mathcal{L} , the cell size δ as well as the temporal scale T and the time step τ . Also, the initial state of each CA can be explicitly defined by \mathcal{S}_{init} . In addition a field \mathbf{u} and the functional \mathbf{O} are included in the definition. The field \mathbf{u} provides additional information that has been passed from other coupled CA or the environment in the course of each iteration, whereas the functional $\mathbf{O} : \mathcal{S} \rightarrow \mathbb{R}^d$ defines an observable, that specifies the quantity that shall be observed during the execution of the CxA.

Based on the general description of the state of a CA at a certain time point $\mathbf{s}(t) \in \mathcal{S}$, all CA submodels of a CxA evolve according to

$$\mathbf{s}(0) = \mathbf{s}_{init}[\mathbf{u}_0] \quad (2.13)$$

$$\mathbf{s}(t + \tau) = \Phi[\mathbf{u}; \mathbf{s}(t)]. \quad (2.14)$$

The implementation of the submodel specific transition operator Φ basically resembles the previously introduced collision-propagation update rule of LGCA, where:

$$\Phi[\mathbf{u}; \mathbf{s}(t)] = (\Phi^B[\mathbf{u}_B] \circ \Phi^P \circ \Phi^C[\mathbf{u}_C])[\mathbf{s}(t)]. \quad (2.15)$$

Accordingly the collision operator Φ^C and the newly introduced boundary condition Φ^B depend on external field parameters \mathbf{u}_C and \mathbf{u}_B . The additional operator Φ^B allows to modify the boundaries, hence the topology of the domain, with regard to the external field parameter \mathbf{u}_B . This means, the domain of an individual CA $C_i \in \mathcal{C}$ is not fixed, but may be changed through the interaction with other coupled CA. Thereby two fully coupled, single-scale CA-submodels, that evolve according to the transition operator defined in (2.15) have the following form:

$$\begin{aligned} \mathbf{s}_1(0) &= \mathbf{s}_{\text{init},1}[\mathbf{s}_2] \\ \mathbf{s}_1(t + \tau) &= (\Phi_1^B[\mathbf{s}_2] \circ \Phi_1^P \circ \Phi_1^C[\mathbf{s}_2])[\mathbf{s}_1(t)]. \end{aligned} \quad (2.16)$$

$$\begin{aligned} \mathbf{s}_2(0) &= \mathbf{s}_{\text{init},2}[\mathbf{s}_1] \\ \mathbf{s}_2(t + \tau) &= (\Phi_2^B[\mathbf{s}_1] \circ \Phi_2^P \circ \Phi_2^C[\mathbf{s}_1])[\mathbf{s}_2(t)]. \end{aligned}$$

In the given example both CAs are coupled in all the components and the external field parameters contain the corresponding state of the coupled CA, i.e. the initial condition as well as the boundary and collision operator of C_1 depend on the state of the C_2 and vice versa. In a concrete implementation, the depicted general coupling concept might lead to cyclic interaction between the submodels. Thus, the execution scheme has to be carefully adapted to avoid a possible deadlock situation, which could e.g. occur when each model depends on the initialization of the other.

However, the concept of CxA provides a suitable theoretical framework to represent the ascribed raft/receptor dynamics. Thereby we aim to couple the cellular automata model of individual receptor diffusion outlined above with one or more additional CA-submodels that represent the raft dynamics. Though before we can introduce a submodel describing lipid rafts dynamics, it has to be clear, what scales and processes can be considered in a separate CA model. Therefore, we first recapitulate the dynamic interaction between lipid rafts and membrane-bound particles, in particular with regard to the different spatio-temporal scales involved, before introducing the basic ideas of the coupled receptor/raft model.

Spatio-temporal scales in a combined receptor/raft model

Lipid rafts and receptor dynamics are closely intertwined and most processes occur on a similar, if not the same temporal and spatial scale. For a start, even though rafts are significantly larger than receptors and span an arbitrary number of lattice cells, they have the same step size (one cell) with regard to diffusion. Accordingly, in a coupled receptor/raft model, both submodels have to be executed on the same temporal scale. At the same time, raft-associated particles are hampered in their diffusion, which is reflected by a reduced diffusion coefficient. Further the movement of raft-associated particles is also coupled to the rafts' motion. This means in addition to their own, reduced movement, raft-associated particles are *dragged* along with the diffusing raft. This effect is termed *sweeping effect*.

As a consequence, information about the spatial expansion and the (movement) direction of rafts has to be available for each individual lattice cell. Apparently, this is best incorporated in a separate lattice-based submodel, with groups of lattice cells being associated to an individual raft entity according to its expansion (diameter) and under consideration of the exclusion principle. Thereby the spatial information of rafts, like position and expansion of each individual raft is implicitly stored/represented in the *raft lattice*. The raft and receptor lattices have equivalent spatial domains, allowing a simple, cell-wise coupling between both lattices. According to the CxA framework the raft and particle submodels may continuously exchange information during the stepwise execution of the update rule. Thereby the raft lattice may provide the information to the particle model required to realize the impeded movement of raft-associated particles described above. These two models are well suited to express the raft-receptor interaction, but insufficient for representing individual rafts dynamics. However, to express state-related raft properties, like neighborhood, direction of movement and collision status, a further mechanism for the global coordination of raft-associated cells is required. As a consequence a third, more abstract CA-submodel is introduced that describes the global properties of rafts and their neighborhood, which is particularly required for modelling lipid rafts movement and collision handling. This model is closely coupled with the raft lattice, but also interacts with the particle lattice as we will see later.

Lipid Rafts Submodel(s)

To describe raft-specific properties and dynamics we introduce two additional CA-models, C^{rl} and C^{rg} , that are closely coupled in terms of Complex Cellular Automata (CxA). Both models [function] on the same temporal, but on a different spatial scale. While the first submodel (C^{rl}) relates to the spatial properties of the lipid rafts, like

position, spatial extension and also the handling of movement updates, the second sub-model (C^{rg}) considers global, state-related parameters like neighborhood, direction of movement and collision status. Accordingly we term both models local and global raft model, respectively.

As mentioned in the previous paragraph, the local raft model is based on a lattice domain, closely related to the lattice of the particle model. This means, the raft lattice (C^{rl}) has the same spatial domain, i.e. expansion and cell size, as the particle lattice. Each individual cell of the raft lattice comprises five velocity channels and the state of an arbitrary cell at time t can be described in terms of the cell configuration $\boldsymbol{\eta}(\mathbf{c}^{rl}, t)$ that relates to the occupation of the velocity channels, c.f. 2.4. For the raft lattice, however, we modify the definition of the cell configuration. Instead of specifying a general occupation of the velocity channel, we use an identifier to address the individual raft (entity) that is associated to the current cell:

$$\eta_i(\mathbf{c}^{rl}, t) = \nu, \nu \in \{0, \dots, n^{rg}\}, i = 1, \dots, \tilde{b}, \quad (2.17)$$

where n^{rg} is the total number of rafts available in the system. We thus combine the information of which raft occupies the velocity channel \mathbf{v}_i of the current cell and what is the direction of the raft's movement. For this, the definition particle density $n(\mathbf{c}^{rl})$, that refers to the total number of rafts present at cell \mathbf{c}^{rl} , has to be adapted accordingly:

$$n_i(\mathbf{c}^{rl}) = \begin{cases} 1 & \text{if } \eta_i(\mathbf{c}^{rl}) \neq 0 \\ 0 & \text{else} \end{cases} \quad (2.18)$$

$$n(\mathbf{c}^{rl}) = \sum_{i=1}^{\tilde{b}} n_i(\mathbf{c}^{rl}) \quad (2.19)$$

In contrast, the global raft CA-model (C^{rg}) is not lattice based, but [uses] a more abstract representation of the interaction between rafts. That is, the domain of the global raft CA-model is loosely defined as directed graph (V, E) , where V corresponds to a set of cells, that are connected by a set of edges E . Thereby each cell $\mathbf{c}^{rg} \in V$ relates to an individual raft entity. To specify the direction of the next movement, a *global raft cell* \mathbf{c}^{rg} constitutes five velocity channels. An edge $e_i \in E$ between two *global raft cells* \mathbf{c}_1^{rg} and \mathbf{c}_2^{rg} indicates a pair of contiguous rafts and is specified as a tuple:

$$e_j = \{\mathbf{v}_i(\mathbf{c}_1^{rg}), \mathbf{v}_k(\mathbf{c}_2^{rg})\} \quad (2.20)$$

where \mathbf{v}_i and \mathbf{v}_k determines the relative position of the neighborhood in raft 1 and raft 2 respectively. In general rafts are considered as contiguous, if they occupy two or more

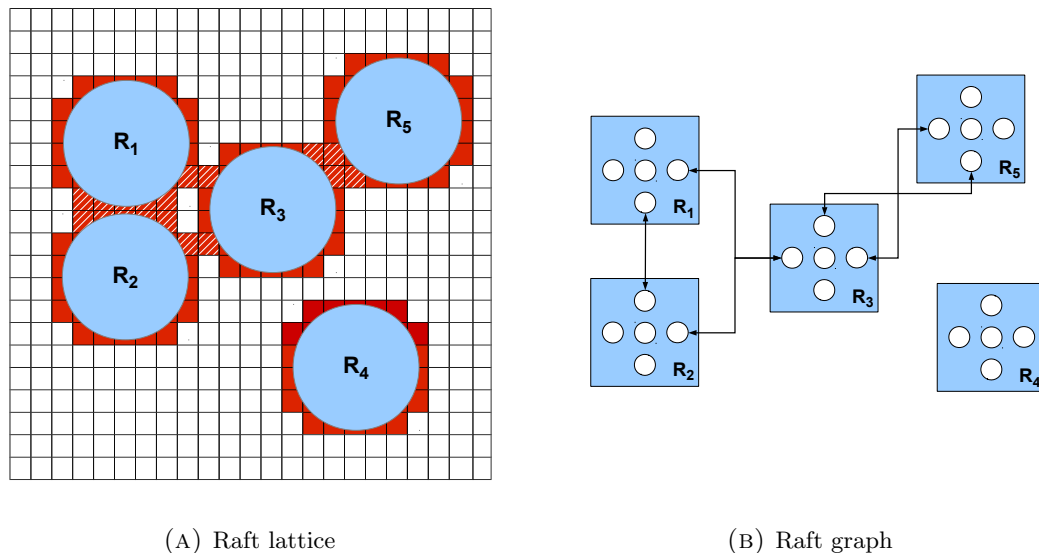


FIGURE 2.8: Neighborhood information in raft graph (C^{rg}) based on the positional information contained in the raft lattice (C^{rl}).

adjacent cells in the local raft lattice (see Fig. 2.8 for further clarification).

Accordingly the relative position results from the position of the adjacent lattice cells. The relative position of contiguous rafts plays a crucial role for the movement and collision handling.

Collision handling of Lipid Rafts

Basically, lipid rafts follow the same exclusion principle and thus perform the same random walk dynamics as described for particles. Accordingly, moving rafts are also subject to the two different types of collisions, i.e. direct and field collision, we previously defined in Section 2.2. However, the handling of raft collisions is far more complicated than for particles. Due to the spatial extension of rafts, any collision event has to be communicated through all lattice cells associated with the raft and multiple collision events might occur simultaneously/concurrently in a single raft.

In our model, we assume that any collision of rafts leads to a rejection of the scheduled move. This simplification is required to avoid a number of potential conflicts, in particular with regard to the interaction between rafts and particles. Due to the coupled motion of rafts and particles, a field collision of two individual rafts e.g. might result in an excessive accumulation of particles on a lattice cell, i.e. a situation when the number of particles approaching a cell exceeds the number of available velocity channels.

Field collisions of rafts are caused the same way as for particles, i.e. if two non-contiguous rafts approach the same lattice cell. In the example configuration, depicted in Figure 2.8,

a field collision would occur, if raft R_3 and raft R_4 were concurrently scheduled to move downwards and upwards, respectively. However, since field collisions occur between non-contiguous rafts, the neighborhood information required for collision detection is not available in the global raft model. This makes field collisions only detectable on the raft lattice.

Whereas, direct raft collisions may be detected on the global raft model solely. In our model a direct raft collision occurs as soon as a raft moves into the direction of a contiguous raft - except this particular raft moves into the same direction. Therefore we need the information about the local neighborhood and the scheduled directions of the involved rafts, which are stored in the global raft model. Consequently the collision detection for rafts has to be performed on both, the local (direct particle collisions and field collisions) and the global raft (raft collision) model and therefore demands an elaborate communication between both raft models during execution.

Transition operator of the coupled CxA model

Basically, the entire membrane model is composed of three coupled CA-based submodels in terms of CxA: the particle lattice, the raft lattice and the global raft model. Thereby the particle lattice defines the random movement of particles, while the remaining two models are required for the representation of the raft's random walk. However, the combined (individual-based) movement of rafts and particles cannot be incorporated in a single operator. This is due to the sweeping effect, according to which rafts impede the position of particles, i.e. particles are moved, independently of their own random movement. Since our individual based approach is restricted to $m = 1$ step length, raft and particle dynamics cannot be executed at the same time and have to be considered separately. Consequently, the entire membrane model evolves according to a consecutive execution of the raft (involving/including the particle drift due to sweeping effect) and particle movement. For each raft submodel C^{rl} and C^{rg} we thus apply similar variants of the shuffling, collision and propagation operators as for the individual-based particle model. Except that the individual operators now depend on the state of the related raft submodels. In the following the stepwise execution of the raft movement in terms of the transition operator Φ_r will be discussed in detail. Due to the close coupling between the local and global raft submodel, we will describe the execution of the update rule according to the shuffling, collision and propagation scheme, instead of describing each individual operator separately.

Initialization At first, however, both models have to be initialized accordingly. The basic goal of the initialization of the membrane model is to place the rafts (randomly)

on the grid without violating the exclusion principle. Accordingly we first initialize the local raft lattice by associating group of cells to a certain lipid raft entity and, based on that, subsequently build the raft graph of the global raft model:

$$\begin{aligned} \mathbf{s}^{rl}(0) &= \mathbf{s}_{\text{init}}^{rl} \\ \mathbf{s}^{rg}(0) &= \mathbf{s}_{\text{init}}^{rg}[\mathbf{s}^{rl}]. \end{aligned} \tag{2.21}$$

The initialization of the global raft model thus depends on the initial state of the raft lattice. Since rafts are assumed a circular shape, the group of cells we associate to an individual raft during initialization has the form of a discretized circle (c.f. Fig. 2.8).

Shuffling After the initialization or a completed update of the model, the connectivity of the global raft graph, i.e. the neighborhood information, is updated according to the configuration of the raft lattice. Following this, the succeeding update routine starts with the shuffling operator determining the direction of the next rafts movement. Thereby a new cell configuration is first calculated for each raft cell in the global model and subsequently transferred to all cells of the raft lattice that are associated with the respective raft entity:

$$\boldsymbol{\eta}^{\text{out}}(\mathbf{c}_{\nu}^{rl}, t) = \boldsymbol{\eta}^{\text{out}}(\mathbf{c}_{\nu}^{rg}, t) \tag{2.22}$$

where

$$\boldsymbol{\eta}^{\text{out}}(\mathbf{c}_{\nu}^{rg}, t) = \left(\Phi_{g(i)}^S(\boldsymbol{\eta}^{\text{in}}(\mathbf{c}_{\nu}^{rg}, t)) \right)_{i=1}^{\tilde{b}}, \text{ with } \mathbb{P}(\boldsymbol{\eta}^{\text{in}} \rightarrow \boldsymbol{\eta}^{\text{out}})(\mathbf{c}_{\nu}^{rg}, t) = 1/4$$

and ν specifying the global raft cell \mathbf{c}_{ν}^{rg} , to which the respective raft lattice cell \mathbf{c}^{rl} is associated. Note, that the shuffling step in the combined raft model is only responsible for scheduling the subsequent raft move and, in contrast to the particle model, does not contain any collision handling routine. This is because any movement resulting in a collision is rejected, which guarantees that any raft lattice cell is associated to at most one raft entity. However, the rejection of field collisions also requires an elaborate collision detection, before the actual raft move can be executed.

Collision Detection (local raft model) The first step of the collision detection routine is to check the system for field collisions. This is because any rejected movement due

to a field collision may lead to additional direct collisions. Moreover, field collisions cannot be detected in the global raft model, as they are caused by a pair of non-contiguous rafts, i.e. the corresponding global raft cells are not connected by an edge and thus do not possess any neighborhood information, which is required for collision detection in the global raft model, though. Consequently we have to use the raft lattice to detect and resolve potential field collisions. In case a field collision was detected, the information is propagated from the lattice to the global raft model, where the state of the involved raft entities is changed accordingly. The corresponding collision operator of the local raft model $\Phi_{rl(i)}^C$ is thus defined as:

$$\begin{aligned} \Phi_{rl(i)}^C(\mathbf{c}_\nu^{rg}, t) : \eta_i^{out}(\mathbf{c}_\nu^{rg}, t) \rightarrow \eta_i^{in}(\mathbf{c}_\nu^{rg}, t) \mid \\ \exists \mathbf{c}_\nu^{rl} \in \mathcal{L}^{rl} : \left(n_i(\mathbf{c}_\nu^{rl}, t) + n_k(\mathbf{c}_\nu^{rl} + 2\mathbf{v}_i, t) \right) > 1 \end{aligned} \quad (2.23)$$

$$k = i + 2 \cdot \sum_{l=0}^{d-2} \mathbf{v}_{i_l} ,$$

where ν again specifies the raft entity, to which the respective raft lattice cell \mathbf{c}^{rl} is associated.

Collision Detection (global raft model): As a result of the field collision detection routine, for all rafts that cause a field collision in the subsequent propagation step the scheduled movement has been rejected. However, we still have to detect and handle all direct collisions between rafts. For this we need the direct neighborhood information stored in the global raft model. As outlined before, any movement of a raft into the direction of a contiguous raft/direct neighbor is considered to cause a direct collision, despite the situation, when the contiguous rafts move in the same direction. Accordingly not only the directly adjacent raft, but all contiguous rafts in the direction of the scheduled movement have to be checked. We therefore apply the collision operator of the global raft model $\Phi_{rg(i)}^C$ as follows:

$$\begin{aligned} \Phi_{rg(i)}^C(\mathbf{c}_\nu^{rg}, t) : \eta_i^{out}(\mathbf{c}_\nu^{rg}, t) \rightarrow \eta_i^{in}(\mathbf{c}_\nu^{rg}, t) \mid \\ \exists \mathbf{c}^{rg} \in \mathcal{N}_i(\mathbf{c}_\nu^{rg}, t) : (n_i(\mathbf{c}_\nu^{rg}, t) + n_i(\mathbf{c}^{rg}, t)) \neq 2 \end{aligned} \quad (2.24)$$

where

$$\mathcal{N}_i(\mathbf{c}_\nu^{rg}) = \{ \mathbf{c}_\nu^{rg} + m\mathbf{v}_i \mid m \in \mathbb{N}, \\ \exists e \in E : e(\mathbf{v}_i(\mathbf{c}_\nu^{rg} + (m-1)\mathbf{v}_i), \mathbf{v}_k(\mathbf{c}_\nu^{rg} + m\mathbf{v}_i)) \}$$

The neighborhood thus contains all raft cells \mathbf{c}^{rg} that are contiguous to the movement direction of the raft under consideration (\mathbf{c}_ν^{rg}).

Raft Propagation After the successful collisions detection, the scheduled raft movement can be propagated to the raft and the particle lattice. However, before the actual propagation on the raft lattice is executed, the state of each raft-associated lattice cell is updated according to the result of the collision detection, i.e. $\boldsymbol{\eta}(\mathbf{c}_\nu^{rg}, t) \rightarrow \boldsymbol{\eta}(\mathbf{c}_\nu^{rl}, t)$. Based on the updated raft lattice, the configuration of each raft lattice cell is transferred to neighboring cell according to the movement of the associated raft.

$$\Phi_{rl}^P : \eta_i^{\text{out}}(\mathbf{c}^{rl}, t) \rightarrow \eta_i^{\text{in}}(\mathbf{c}^{rl} + \mathbf{v}_i, t + \tau) \quad (2.25)$$

Eventually the particle lattice is also updated according to the raft lattice.

$$\boldsymbol{\eta}(\mathbf{c}^p + \mathbf{v}_i, t + \tau) = \left\{ \boldsymbol{\eta}(\mathbf{c}^p, t) \mid n_i^{\text{out}}(\mathbf{c}^{rl}, t) = 1 \right\}_{i=1}^b \quad (2.26)$$

Thereby the raft movement is finalized and in the following the normal particle movement of the particle lattice, described in the previous section, is executed.

2.3 Concluding remarks

A CA-based membrane model has been implemented, that explicitly describes the combined diffusion dynamics of lipid rafts and membrane particles, i.e. receptors. Thereby local transition rules have been successfully designed and implemented to capture complex processes, like coordinated group movement and multi-level collision detection to represent lipid rafts diffusion. To achieve this, two concepts that extend the original CA formalism, i.e. Lattice Gas Cellular Automata (LGCA) and complex Cellular Automata (CxA) have been adopted. As a result, we demonstrated, that the CA formalism is capable of representing highly interdependent multilevel processes, such as the processes involved in the lipid rafts mediated receptor diffusion, as presented in this chapter.

Despite being a powerful modeling formalism with a resolution perfectly fitted for the dynamics addressed in this work, it has to be acknowledged that in terms of expressiveness, cellular automata are only partly suited for multilevel modeling. Especially the coordinated movement of lipid rafts implied rather complicated transition rules, which diminishes the reusability of the model and hampers potential extensions of the model.

Chapter 3

Studying raft-dependent receptor distribution and binding kinetics

In the previous section, a CA-based approach has been introduced, tailored to representing the dynamics of lipid rafts and their interaction with membrane-bound particles. Based on the presented approach we built a spatial membrane model, parametrized according to literature values, to perform various simulation studies exploring the impact of lipid rafts on membrane particle localization and signal transduction. Thereby the main emphasis is laid on receptor/raft interaction, as receptors and their spatial distribution within the membrane plays a crucial role in signal transduction (c.f. Section 1.2). Recent studies have already shown, that receptor clustering promotes protein receptor couplings [90, 202]. However, the influence of lipid rafts on the protein receptor binding rate has not been explored in detail yet. The aim of this study is to address this lack of knowledge and to explore the binding of cytosolic proteins to activated receptors with respect to varying binding conditions and lipid raft characteristics through modeling and simulation. Therefore we employ slow and fast dissociation/binding kinetics as well as considering raft properties such as size, fluidity and mobility. For simplicity, in the following we refer to membrane-bound particles as receptor, even though the insights gained by the simulation studies are not restricted to receptors, but may apply for any membrane-bound protein that can be associated with rafts.

3.1 Model and Parameters

In the following we give a short description of the lipid raft model applied to study the role of lipid rafts on the receptor aggregation (see Figure 3.1). The model setup with respect to the applied parameter is similar to the one proposed by Nicolau et. al. [150]. A

complete overview of the employed parameters can be found in table 3.1. All simulations were performed on a $\mathcal{L} = (500\text{nm} \times 700\text{nm})$ lattice, with step size $\delta = 2\text{nm}$ to approximate the average protein size and the volume exclusion effect. Periodic boundaries are applied. Receptors and Rafts are represented as described in previous section: Lipid rafts are represented as two-dimensional, discretized disks with diameter d_{lr} that occupy an approximate area of $A_{lr} = \frac{\pi d_{lr}^2}{4}$. Receptors are considered as membrane-bound particles. The model assumes only one type of receptor whose size and shape is solely represented by the dimension of a single grid cell ($2\text{nm} \times 2\text{nm}$). For simplicity further details, such as protein topology, structural properties or thermodynamic interactions are omitted. However, it should be noted, that these factors might have a strong impact on the partitioning of proteins into and out of rafts. Studying their influence on the model outcome, such as the binding kinetics would go beyond the scope of this work, but is of major interest for subsequent studies. In all simulation experiments performed, the standard diffusion speed of receptors is set to $D_r = 1$, i.e. one particle lattice cell per simulation time step ($\tau = 1$). This corresponds to a diffusion rate of $D = 0.5\delta^2/\tau$. Assuming a diffusion rate of $10^{-9} \text{ cm}^2/\text{s}$ ($0.1\mu\text{m}^2/\text{s}$) for a receptor performing undisturbed lateral movement, the unit time step τ is equivalent to $2\mu\text{s}$.

As illustrated before, diffusion in rafts is limited by the raft fluidity (ρ), i.e. a reduced diffusion coefficient of $D_r^* = \rho \cdot D_r$ applies within rafts. Further all raft associated receptors are subject to the raft's movement (D_{lr}) in addition to their own, reduced, mobility (D_r^*). Depending on the parametrization of the model, rafts may either be immobilized $mobile_{lr} = false$, or may perform lateral diffusion according to a size-dependent diffusion coefficient D_{lr} , that is determined according to the Saffman-Delbrück equation [170].

The fraction of the membrane that is covered by rafts is defined by the raft coverage ($cover_{lr}$). The same applies to the receptor coverage ($cover_r$). The initial distribution of receptors and lipid rafts is based on a normal distribution. Thus the grid is randomly seeded with receptors and lipid rafts, such that no receptor or raft occupies the same grid cell and according to the given coverage values ($cover_r$ and $cover_{lr}$ respectively). Values for raft properties, like size, mobility and fluidity are varied according to the ranges given in Table 3.1. However, during any simulation run, these parameters remain fixed. To analyse, how the system behaves under certain conditions, we applied parameter values within the ranges listed in Table 3.1. Simulations are run until either equilibrium or a maximum of 2000 time steps is reached. This corresponds to 4 seconds in real time, which is in agreement with the average life time of long-lived raft structures [16]. In fact, for some configurations equilibrium is not reached within 2000 time steps. However, in these cases the simulation run time to reach equilibrium would clearly exceed the average life time of long-lived raft structures. The number of replications for each simulation configuration has been chosen, such that the variance is below 0.1%.

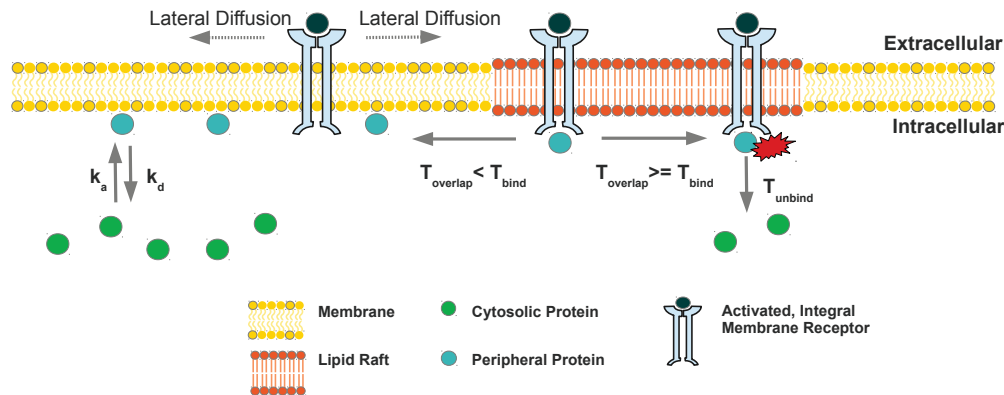


FIGURE 3.1: A schematic view of the plasma membrane illustrating the formation of a receptor-protein complex. Membrane-integral, activated receptors may overlap with cytosolic proteins that are localized at the membrane. When co-localized with an activated receptor, it depends on the time of overlap and the binding rate, whether the protein binds to the activated receptor or dissociates into the bulk solution.

Further simulation studies with varying grid sizes (doubled and quadrupled each side, particle lattice cell size constant 2nm x 2nm) showed no difference in the results (results not shown). Therefore the chosen grid size of 500x700 nm appears reasonable, as it obviously captures the essential membrane dynamics, while the computational effort is still manageable. The choice of a significantly smaller grid size would already be problematic, as not sufficiently many large lipid rafts of, for example, 25nm diameter can be mapped onto the grid.

3.2 Characterizing lipid rafts and receptor interaction

To explore the characteristics of the receptor/raft interaction under a wide range of different conditions we performed several simulation experiments with varying sets of parameter configurations. Therefore parameters referring to lipid rafts and receptor concentrations (in particular with regard to molecular crowding) as well as miscellaneous raft properties, like fluidity, mobility and diameter were varied within the ranges listed in table 3.1. The main focus of the first experiments was laid on studying the impact of lipid rafts on receptor localization. Accordingly the equilibrium mean receptor concentration within rafts $[R]^* = \frac{[R]}{[R]_{tr}}^1$ is defined as the main observable.

¹if the equilibrium is not reached within 2000 time steps, we consider the model configuration after 2000 ts as equilibrium state (c.f. Sec. 3.1)

3.2.1 Raft fluidity controls extend of receptor enrichment

Figure 3.4 shows the mean receptor concentration within rafts for decreasing values of ρ and different raft sizes reaching from 6 to 50 nm, based on a low (A & B) and a high receptor density (C & D). Obviously lower values of ρ lead to a higher concentration of receptors within lipid rafts. The high concentration is caused by the reduced fluidity inside the rafts. Thereby, the mobility of receptor is hampered, i.e. the probability of leaving the raft is reduced. Eventually this results in a localization, hence receptor enrichment inside the rafts.

However, we also observe that the receptor enrichment effect is slightly higher for mobile rafts compared to immobilized rafts. This difference is caused by the *sweeping effect* of mobile lipid rafts that has also been observed in earlier experiments [150]. This means receptors are picked up by diffusing rafts and subsequently dragged along with them.

TABLE 3.1: Parameters of Membrane Model

parameter	description	value range of model
$xdim_m, ydim_m$	dimension of the two dimensional membrane in nm	<i>fixed:</i> $xdim_m = 500$ $ydim_m = 700$
$xdim_v, ydim_v$	size of particle lattice cell inside the grid in nm	<i>fixed:</i> $xdim_v = ydim_v = 2$
$cover_{lr}$	degree by which the membrane is covered by lipid rafts	$cover_{lr} \in [0..0.5]$
$cover_r$	degree by which the membrane is covered by receptors	$cover_r \in [0.03..0.3]$
D_{lr}	diffusion coefficient of Lipid Rafts	$D_{lr} = 0$ or $D_{lr} = normal(x)$ with $x \in R^+$
D_r	diffusion of receptors	$D_r = 1$
d_{lr}	diameter of the lipid raft in nm	$d_{lr} \in [6..50]$
$mobile_{lr}$	mobility of lipid rafts	$mobile_{lr} \in \{true, false\}$
ρ	raft fluidity that reduces diffusion of receptors within the raft	$\rho \in [0.01..1]$
k_a	association rate of cytosolic proteins at a mesh-site	$k_a \in [0.01..0.0001]$
k_d	disassociation rates of cytosolic proteins	$k_d \in [0.01..1]$
t_{bind}	time that a cytosolic protein is required to stay at a receptor so that a binding can take place	$t_{bind} \in [1..2]$
t_{unbind}	time that a cytosolic protein is in complex with a receptor before dissociating into the cytosol	$t_{unbind} = 1$

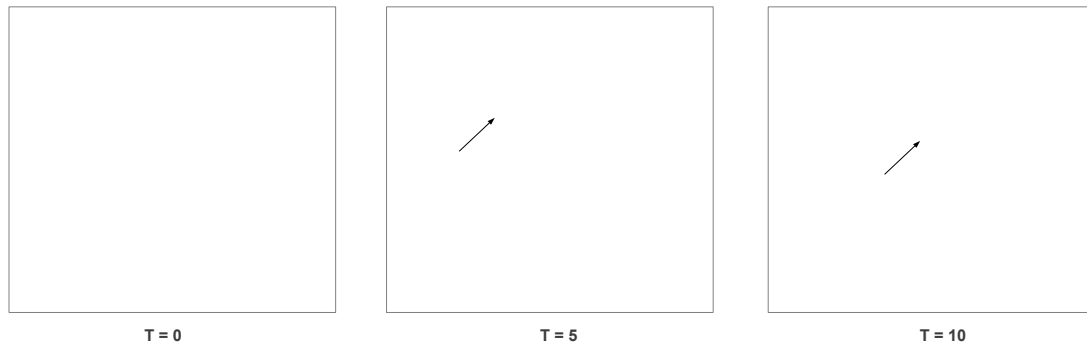


FIGURE 3.2: The figure depicts a small section of a larger grid, to illustrate the sweeping effect of moving rafts (14nm diameter and $\rho=1$, i.e. the diffusivity inside and outside rafts is the same for receptors). Lipid rafts are colored blue as well as their trails, which represent the previous 20 time steps. Whereas the trails of moving receptors are colored orange/red and represent the last 30 simulation time steps. The color is enhanced, if a cell is occupied multiple times by a receptor during these last 30 steps. The marked trail illustrates how the movement of a single receptor is influenced by both – the moving raft and the movement of the receptor itself.

The captured receptors are thus not only subject to their own movement but also to the lipid raft's movement (Figure 3.2). Consequently, the number of receptors entering rafts is slightly increased compared to immobile rafts, while the number of receptors leaving the raft remains unchanged. Likewise the concentration of receptors within mobile lipid rafts is slightly higher than in immobile rafts.

This accounts also for the case $\rho = 1$, where lipid rafts have no effect on the diffusion speed of receptors. Accordingly, the receptor concentration in rafts should approach a value of 25% that corresponds to the proportion of rafts on the membrane. Nevertheless, we still observe a minor aggregation of receptors in mobile rafts as shown in figure 3.4. This accounts in particular for larger raft sizes. What seems to be an apparent discrepancy in our results is due to the previously described *sweeping effect* of moving rafts which results in an increased uptake of receptors [128].

3.2.2 Under physiological conditions, receptor enrichment is raft size dependent

However, when seeding the membrane with a higher, more appropriate physiological concentration of receptors ($\sim 30\%$) [220] we observe a size-dependent receptor accumulation. As depicted in figure 3.4 the concentration of receptors in small rafts is significantly higher than in larger rafts and the difference observed increases as $\rho \rightarrow 0$. This applies to both immobile and mobile rafts, i.e. the effect on receptor accumulation that we observe referring to differently sized lipid rafts cannot be solely caused by the

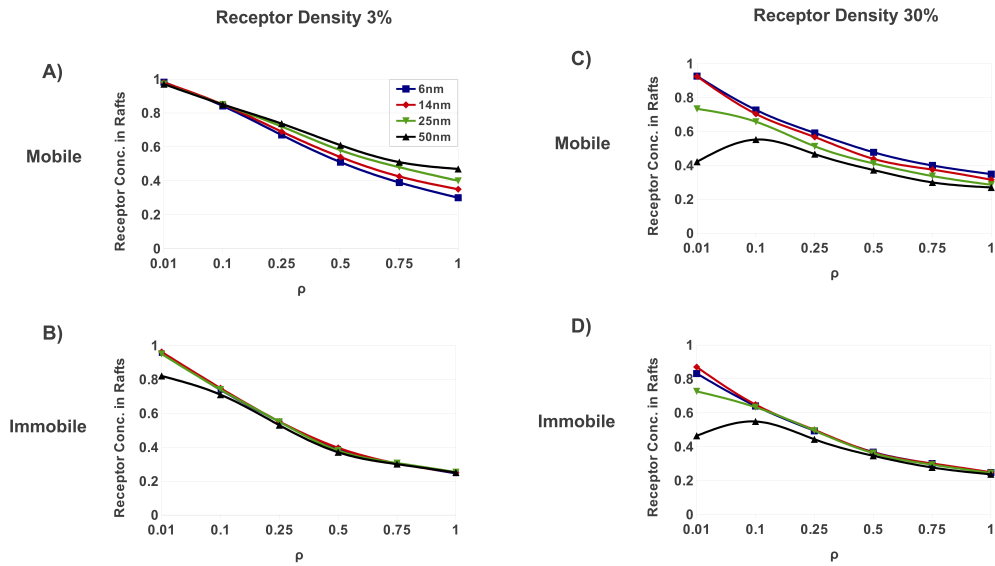


FIGURE 3.3: Equilibrium receptor concentrations inside lipid rafts with regard to raft fluidity (ρ) and lipid raft size. In the upper two figures (A & B) the results for a receptor density of 3% are depicted whereas the lower figures (C & D) show the results for a general receptor density of 30%.

sweeping effect. In fact, larger lipid rafts have a significantly smaller circumference-to-area ratio. As a result receptors have fewer raft boundaries to potentially collide with and so the rate of receptor uptake decreases with growing raft size. Additionally, as $\rho \rightarrow 0$ receptors become increasingly immobilized inside lipid rafts. As a consequence, receptors may also block the way for others as they become immobilized immediately after entering the raft. It is thus harder to obtain an even distribution of receptors inside larger lipid rafts, i.e. the area available to receptors is extremely reduced.

In summary the results of our study are in general agreement with the aforementioned publications [58, 150]. Further experiments in the physiological range of 20% - 35% receptor density [220] show only minor differences (results not shown). We therefore apply a fixed receptor concentration of 30% for the subsequent simulation studies.

3.3 The role of lipid rafts on Binding of peripheral proteins to membrane-bound receptors

The impact of lipid rafts on the diffusion and co-localization of membrane-bound receptors is meanwhile well accepted and has been underlined by several *in vivo* and *in silico* studies [58, 139, 150, 163]. Additionally rafts may also facilitate the interaction between membrane-bound receptors and membrane-anchored or peripheral proteins. [At first glance this seems not intuitive], since the movement of peripheral proteins is not

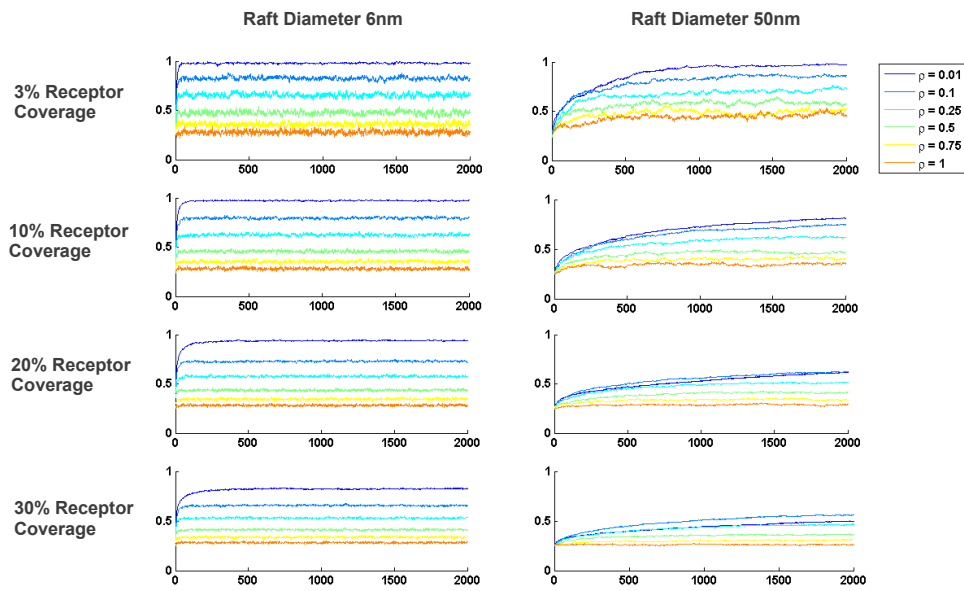


FIGURE 3.4: Equilibrium Plots showing the evolution of the receptor concentration inside rafts with simulation time and varying values of raft fluidity ρ , size and receptor coverage.

impeded by rafts. Though recent studies have already shown, that receptor clustering promotes protein receptor couplings [90, 202]. Accordingly, not only the interaction between membrane-bound molecules may be facilitated by lipid rafts, but also the binding of cytosolic molecules to transmembrane receptors under certain conditions. Protein receptor binding plays a pivotal role in this context, being the initial step in activating the intracellular signalling cascade [29, 181]. Once a receptor has been activated by extracellular signalling molecules (ligands), adaptor proteins, scaffolds and enzymes are immediately recruited and bound to the cytoplasmic side of the activated receptor. The time scale of the recruitment and binding process, however, strongly varies between different protein receptor couplings [90]. The recruitment of cytosolic proteins to the membrane, for instance, can be mediated by membrane-targeting domains and specific protein-lipid interactions [29, 67]. These interactions lead to a temporal localization of cytosolic proteins to the membrane (peripheral proteins)[67, 94, 192]. Thus, proteins recruited to the membrane exhibit slow or fast dissociation kinetics. The binding process, on the other hand, requires the correct mutual orientation of the involved molecules, such that potentially reactive groups are properly aligned [64, 134]. Depending on the electrostatic, steric or hydrophobic interactions between the binding partners, this process can be either accelerated or slowed down. Additionally, multiple state reactions may further slow down the formation of the protein receptor complex [147]. It should be noted that the lateral diffusion of membrane-bound receptors plays an increasing role

for the binding process the longer cytosolic proteins are localized to the membrane. Accordingly, for dissociation kinetics faster than lateral diffusion, the binding process solely depends on the local receptor density. But in the case of slow binding and dissociation kinetics of peripheral membrane proteins the protein receptor binding may indeed be influenced by the structural properties of the membrane and, in particular, by lipid raft dynamics.

Recent studies have already shown, that receptor clustering promotes protein receptor couplings [90, 202]. However, the influence of lipid rafts on the protein receptor binding rate has not been explored in detail yet. The aim of this study is to address this lack of knowledge and to explore the binding of cytosolic proteins to activated receptors with respect to varying binding conditions and lipid raft characteristics through modeling and simulation. Therefore we employ slow and fast dissociation/binding kinetics as well as considering raft properties such as size, fluidity and mobility.

3.3.1 Extending the model description

To represent the association of peripheral proteins to the membrane, the model was extended by incorporating cytosolic proteins and their respective association k_a and dissociation k_d rate constants. Accordingly, in the following any particle lattice cell of our CA-based model can be additionally associated with a cytosolic protein. Therefore we introduce three further parameters: the association rate constant k_a defining the probability that any particle lattice cell is marked as associated with a cytosolic protein; the dissociation rate constant k_d determining how long an associated protein stays at the respective particle lattice cell; and the binding rate constant t_{bind} , representing time needed to accomplish the binding complex. Further details can be found in the model description in the previous Section.

Cytosolic binding partners are considered as peripheral proteins being temporarily localized at the inner leaflet of the membrane (see Figure 3.1). The association rate constant k_a defines the probability of a cytosolic protein being recruited to the membrane. The time that the proteins reside at the membrane is determined by the dissociation rate k_d . Receptors may thus overlap with a cytosolic protein for a certain amount of time, i.e. occupy the same particle lattice cell, to which a protein is associated. Note that cytosolic proteins do not necessarily bind instantaneously upon contact with receptors, but after some time of being co-localized. In order to cover this fact a binding rate t_{bind} is introduced. A binding between protein and receptor is thus only accepted, if the time of overlap between receptor and protein is larger then the time needed to achieve the binding. We further assume a binding reaction rate of 1 ($t_{unbind} = 1$), i.e. cytosolic proteins dissociate into the bulk immediately after a successful binding event. Thus

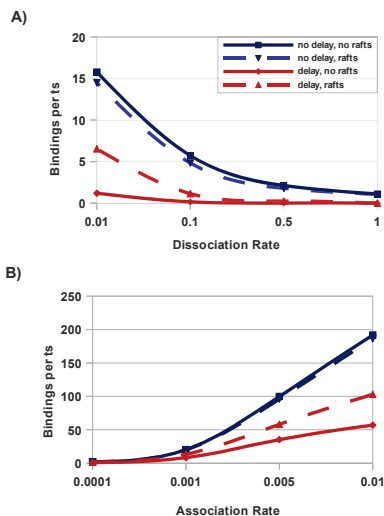


FIGURE 3.5: Plots showing the number of successful receptor-protein bindings per time step compared between a system with and without Lipid Rafts and in dependence of varying A) dissociation and B) association rate constants. Raft specific parameters are set to: Raft Size: 14 nm, $\rho = 0.25$. Lines marked with “no delay” and “delay” correspond to a binding time constant of 1 and 2, respectively.

receptors are not “bound” or occupied for certain amount of time.

Unfortunately, there is a lack of experimental data concerning dissociation and binding rate constants. Also these parameters will differ considerably between different biological systems. We therefore evaluate the impact of lipid rafts on the protein receptor binding, by applying various parameter values within the ranges given in Table 3.1. In the following the results of several simulation experiments studying the impact of lipid raft characteristics as well as raft and receptor densities on the receptor protein binding will be presented. Thereby different recruitment and binding kinetics are applied to study the general influence of lipid rafts on the binding process. Finally we present the influence of varying lipid raft characteristics on the binding process.

3.3.2 Lipid Rafts play ambivalent role in the protein-receptor binding

We now investigate the impact of global parameters, such as the association k_a , dissociation k_d and binding time constants t_{bind} on the formation of protein receptor complexes. Therefore we varied these parameters according to the ranges listed in table 3.1 and observed the number of successful binding events per time step. The experiments are executed on a system containing mobile lipid rafts of diameter 14 nm and medium fluidity of $\rho = 0.25$ and a system without lipid rafts.

3.3.3 Lipid rafts promote slow binding kinetics

The results of the study are depicted in figure 3.5. The average number of protein receptor bindings per time step is shown for different dissociation k_d and association k_a rate constants. The solid and dashed lines represent protein receptor bindings per time step for no rafts and rafts, respectively. Different values of the binding rate constants are indicated by the colour. In general, the protein receptor binding is greatly enhanced by a higher association rate and slightly promoted by smaller dissociation rate constants. Both parameters mainly control the number of cytosolic proteins localized at the membrane. However, the dissociation rate also controls the time, peripheral proteins reside in the proximity of the membrane, once associated. A longer residence time in turn increases the probability that diffusing receptors encounter associated proteins, and likewise increase the chance of a binding event.

In contrast, a binding rate larger than 1 significantly reduces the number of binding events. In this case protein and receptor must be co-localized for at least two time steps in order to accomplish a binding. However, since the step size of receptors equals 1 for freely diffusing receptors, this can only be achieved, if receptors are slowed down somehow. In raft-containing systems, receptors are slowed down when located inside raft regions. But in raft-free simulations, receptors can only stay at a certain particle lattice cell for more than one time step, if its movement is rejected due to a collision with neighbouring receptors. Therefore, a binding can be accomplished albeit by the unlikely event, when a receptor is overlapping with a peripheral protein and subject to a collision at the same time. Accordingly, in a system without lipid rafts and $t_{bind} = 2$, we observe very few but still some binding events for dissociation rates smaller than 0.1 (see fig. 3.5).

Interestingly, the impact of rafts on protein receptor binding is not consistent. While the impact of lipid rafts is slightly negative in the case of instantaneous bindings ($t_{bind} = 1$), we observe a significant promoting effect for $t_{bind} = 2$. This effect becomes more evident with increasing association and decreasing dissociation rate constants. Note that for a system with $\rho = 0.25$ the diffusion coefficient of receptors in raft regions is four times less compared to non-raft regions. Accordingly, receptors are significantly slowed down when located inside a raft. This is beneficial for the system with $t_{bind} = 2$, as it increases the chance that receptor and associated proteins overlap "long enough" to achieve an actual binding. This accounts especially for low dissociation rates.

3.3.4 Raft properties have significant impact on binding kinetics

The previously described experiments showed an ambivalent impact of lipid rafts on the receptor-protein binding. However, it remains unclear whether and how raft-specific parameters, such as fluidity, mobility or size affect the binding process. We therefore perform a sensitivity analysis to identify which of these parameters significantly influence the outcome of the model. As model outcome we define a ratio of mean binding events per time step for raft models to that of raft-free models (*binding ratio*). Values of global and raft-specific parameters are varied according to the ranges listed in table 3.1. For the sampling of parameter values, we apply the NOLH (nearly orthogonal Latin hypercube) approach, an extension of the Latin Hypercube sampling method, which provides a good space-filling experiment design already for low numbers of parameter combinations (design points) [32, 174]. Thereby a combination of 34 design points is sufficient to cover most relevant parts of the parameter space. To measure the correlation between parameter values and the model outcome (binding ratio) we compute partial ranked correlation coefficient (PRCC) values. The ranked correlation coefficient (like PRCC) is a robust sensitivity measure, particularly for non-linear, but monotonic relationships [135]. As for normal correlation coefficients, PRCC values vary between -1 and +1 indicating perfect negative and perfect positive correlation, respectively. To assess if a PRCC is significantly different from zero, p-values derived from Student's t test have to be calculated according to [4].

Table 3.2 lists all model parameters that yielded a significant PRCC value (p-value < 0.001) for models with undelayed/delayed binding -reactions and mobile/immobile rafts. Obviously the raft fluidity (ρ) has the most prominent influence on the receptor-protein binding. In all model configurations tested, ρ significantly correlates with the binding ratio, but depending on the binding delay the impact is either positive or negative. Note, that a positive correlation of ρ is not equivalent to a promoting effect of lipid rafts on the binding ratio. Considering the high equilibrium receptor concentration inside rafts for $\rho \rightarrow 0$ (see Fig. 3.4), a positive correlation of ρ rather indicates a disturbing effect of the presence of lipid rafts that diminishes with increasing raft fluidity. Whereas the opposite holds true for negative correlation of ρ , i.e. lower raft fluidity values strengthen the promoting effect of rafts on the binding process. This is supported by the fact that the correlation values for ρ and raft concentration ($cover_{lr}$) are of exactly opposite sign. Accordingly for delayed binding reactions we observe a beneficial effect for increasing raft concentrations (indicated by the positive correlation values), but negative correlation values for ρ and vice versa for undelayed bindings. This is in agreement with the ambivalent results described before (cf. Figure 3.5).

Besides the raft fluidity, several other parameters, such as dissociation rate and receptor

TABLE 3.2: PRCC values for input parameters significantly correlated with model outcome (binding ratio)

no binding delay		binding delay					
immobile	mobile	immobile	mobile	immobile	mobile		
ρ	0.840	ρ	0.507	ρ	-0.689	$cover_r$	-0.702
k_d	0.557			$cover_r$	-0.524	ρ	-0.535
$cover_{lr}$	-0.511			$cover_{lr}$	0.464	$cover_{lr}$	0.549

concentrations influence the binding ratio given different model configurations. Interestingly, the receptor concentration is significantly negatively correlated with the binding ratio, but solely for delayed binding reactions. This negative effect can be explained by the ratio of raft coverage to receptor coverage. As depicted in Figure 3.4, the equilibrium concentration of receptors within rafts decreases with receptor density, in particular for large lipid rafts. Consequently, the influence of rafts on the receptor-protein binding declines with an advanced receptor concentration.

3.3.5 Characterizing the ambiguous effects of raft properties on protein receptor bindings

The sensitivity analysis revealed a distinct, but ambiguous impact of raft-specific parameters on the binding of cytosolic proteins. However, the individual role of each raft parameter and its specific impact on the model outcome is still unclear. We therefore perform a full factorial experiment with all raft-specific parameters, i.e. raft coverage, size, mobility and fluidity. The values are chosen from the ranges defined in table 3.1, but aim to cover most of the realistic configurations with respect to lipid raft characteristics [163, 184] as well as dissociation and binding kinetics [90, 147].

In the previous simulation experiment the binding rate constants t_{bind} heavily influenced the results, in particular for the raft model. We therefore varied t_{bind} according to the previous experiment, i.e. $t_{bind} = 1$ and $t_{bind} = 2$ and kept the association as well as the dissociation rate constants fixed ($k_a = 0.001$, $k_d = 0.01$). Similar to the previous experiment we measured the binding ratio.

The results depicted in figure 3.6 suggest a complex and ambiguous interplay of different lipid rafts characteristics and their impact on the receptor protein binding process. Each graph in figure 3.6 illustrates how the binding kinetics evolve with decreasing raft fluidity ($\rho \rightarrow 0$), depending on varying raft diameter and raft coverage. In the case of moving lipid rafts (fig. 3.6 A-C), a change in the raft size directly implies a change in the diffusion speed of the rafts themselves. In contrast, for immobilized rafts (fig. 3.6

D-F) the diffusion coefficient is zero for all lipid rafts and thus not affected by the raft size.

The general impact of lipid rafts on the binding kinetics is limited by the raft coverage. In the case of low concentrated rafts (e.g. 5%), we observe only minor changes in the binding kinetics, regardless of any modification in the raft characteristics (see fig. 3.6 A & D). Whereas higher raft coverages, such as 25% or 50%, show a distinct, but similar pattern for the binding kinetics with respect to variations of raft parameters, although, the observed effects are more pronounced for 50% coverage, than for 25%. However, for subsequent discussion we will mainly consider the results for higher raft concentrations (25% - 50%).

As shown by the solid lines in figure 3.6, lower values of ρ hamper protein receptor bindings for $t_{bind} = 1$. The decline of binding events is directly related to the reduced mobility of receptors within lipid raft. Thereby the global lateral diffusion of receptors is considerably reduced [151]. As a result receptors cover a smaller area in a certain amount of time compared to freely diffusing receptors, which leads to less protein receptor interactions. Due to the “touch and bind” regime of undelayed bindings ($t_{bind} = 1$) any interaction automatically results in a binding event. Therefore a reduced amount of protein receptor interaction directly results in less binding events. This negative effect of lipid rafts (in the case of instantaneous binding) is even higher for immobilized rafts (3.6 E-F). While receptors located in a mobile raft are still subject to the lateral movement of the raft itself, they are almost completely immobilized in non-diffusing rafts, if $\rho \rightarrow 0$. On the other hand, in the case of $t_{bind} = 2$ (figure 3.6, dashed lines), lipid rafts clearly promote the protein receptor bindings. Again the impact of lipid rafts on the binding process mainly depends on the parameter ρ . As previously described, the reason can be found in the slow-down of receptors within rafts, which is now beneficial for the binding process. The reduced receptor mobility increases the chance of a successful binding, once receptors are in contact with membrane associated proteins. Surprisingly we also observe an enhanced binding rate for mobile lipid rafts with $\rho = 1$ (fig. 3.6 B-C). Again, this is due to the sweeping effect, that rafts exert on the receptors they contain. This may also cause opposite movement directions (of raft and receptor) forcing the respective receptor to stay at its position. The resulting delay facilitates the binding of associated proteins.

However, not only the lipid raft fluidity plays a major role, but also the mobility of rafts. As depicted in figure 3.6 (E & F), immobile rafts only promote the binding up to a value of $\rho = 0.25$. This is due to the diminishing number of protein receptor interactions with decreasing ρ . For $\rho \rightarrow 0$, the main fraction of receptors becomes completely immobilized inside non-diffusing rafts (see fig. 3.4). Due to their immobilization, receptors cannot co-localize with membrane associated proteins by lateral diffusion. Instead cytosolic proteins have to associate directly to a particle lattice cell, that is occupied by

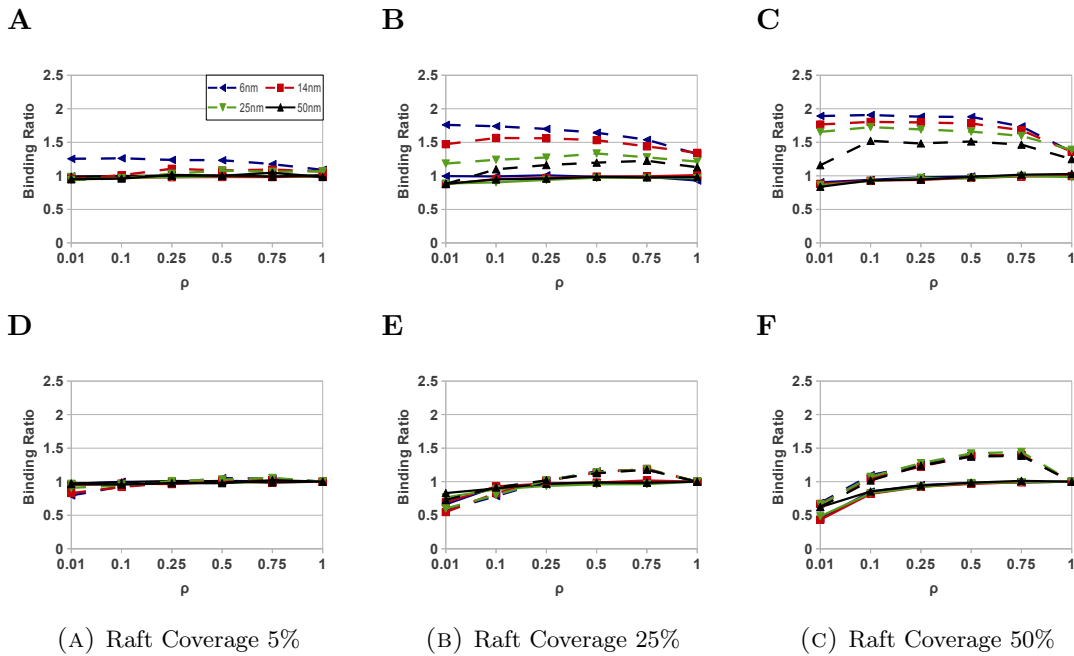


FIGURE 3.6: Binding Ratio with regard to lipid raft fluidity (ρ), size, mobility, coverage and binding delay. The upper and low rows (A-C & D-F) depict the results for mobile and immobile rafts, respectively. Whereas the three columns show the results for varying raft coverages. The dashed and solid lines correspond to delayed $t_{bind} = 2$ and undelayed $t_{bind} = 1$ binding reactions. The line colours indicate the size of the rafts. The simulations were performed with a dissociation rate constant of 0.01 and a fixed receptor concentration of 30% in all experiments.

a receptor. Thus, for immobile raft, lower values of ρ lead to a decline of binding events, even though the actual binding process is promoted.

To summarize, our results emphasize that the analysis of lipid rafts and their role on protein binding requires a differentiated approach. Specific lipid raft characteristics can either have beneficial or unfavourable effects depending on the chosen parameters. Especially, the parameter lipid raft fluidity (ρ) and the binding rate (t_{bind}) strongly influence the results.

3.4 Concluding remarks

In the former part of this work, the impact of lipid rafts on signal transduction has been studied on a high-detailed scale and valuable insights in particular regarding the formation of ternary signaling complexes under the influence of lipid rafts have been gained. Our simulation studies revealed, that lipid rafts have indeed a significant impact, not only on the accumulation of receptors, as shown in earlier studies, but also on the recruitment and binding of cytosolic proteins by the receptors. However, the impact depends on a variety of parameters, such as binding and dissociation kinetics as well as

lipid rafts characteristics.

Generally the impact of lipid rafts on the binding kinetics is limited by the raft concentration within the membrane. Thus a certain raft coverage is required to observe the raft related effects described in this study. In general fast binding reactions are slightly hampered by lipid rafts, while slow binding reactions are considerably enhanced. The extend to which lipid rafts influence protein receptor bindings becomes more prominent for proteins with slow dissociation kinetics.

With respect to raft characteristics, we observe the strongest impact when the fluidity of lipid rafts is low ($\rho \rightarrow 0$). Since the raft fluidity is mainly controlled by the cholesterol content of the membrane, our findings are consistent with recent studies showing that cholesterol depletion alters specific cellular responses in different cells (see [185] for review). In contrast to earlier studies we are able identify an impact of the raft size on receptor accumulation and consequently also on protein binding. Due to excluded volume effects at the border of lipid rafts, we observed a diminishing receptor accumulation with increasing raft sizes, e.g. 25nm or 50nm. Note, that the size-dependent effects can only be observed at physiological receptor density ($\sim 30\%$) and if rafts are rigid, that is if receptors are significantly slowed down inside rafts. Considering the crucial role of protein recruitment and binding for the assembly and activation of receptors, the results underline the diverse, but pivotal role of lipid rafts during signal transduction.

Chapter 4

Modeling raft-dependent WNT signaling

WNT signals are one of the five signal transduction pathways that shape virtually all cell fates and its malfunction is related to a wide range of pathologies, such as developmental disorder, degenerative or metabolic diseases and cancer. In the upcoming chapters we develop a model of raft-dependent WNT/ β -catenin signaling to analyze the role that lipid rafts play in canonical WNT signaling during early differentiation. Thereby we seize on a computational and numerous experimental studies previously done at the University of Rostock [119, 137, 138, 166]. These investigations demonstrated that WNT signaling is constantly active during the early cell fate commitment phase in human neural progenitor cells (hNPCs) (1-12h) [137] and provided strong evidence, that neuronal differentiation in hNPCs is regulated by WNT signaling [92]. In addition, simulation studies based on a computational model of the intracellular WNT/ β -catenin pathway, indicated that the WNT/ β -catenin pathway is activated in a auto-/paracrine manner [138]. The experimental results as well as the already existing WNT model provide a profound working basis to pursue our question of how lipid rafts influence WNT/ β -catenin signaling.

Several studies have confirmed a crucial involvement lipid rafts in canonical WNT signaling [155, 173, 183, 215]. However, the exact mechanism by which lipid rafts influence the signal transduction are still unclear. At the same time the lipid rafts have been completely disregarded in the existing WNT pathway models.

To tackle this deficiency we develop a detailed computational model of canonical WNT signaling that connects membrane-related and lipid rafts/receptor dynamics with the intracellular signal transduction chain. Notably, we first develop a purely qualitative model, that only describes the interaction and the corresponding kinetics, whereas the parametrization is done in the next chapter based on in vitro data derived from human

neural progenitor cells. With this approach we account for the dynamic nature of lipid rafts and their ambiguous effects on signaling. Depending on environmental factors, like the composition and the structural organization of the membrane, the actual impact of lipid rafts on signaling events may vary significantly between individual signaling pathways, as shown in the previous chapters and e.g. in [97]. Therefore, a general model of lipid rafts-dependent canonical WNT signaling will particularly contribute to the understanding of raft-dependent WNT signaling as it is independent of any cell-type specific dynamics and may be parametrized according to the cellular and environmental conditions that are used in the respective study. However, before actually developing the WNT/ β -catenin model, it is important to first assess the processes and dynamics that are of importance for our scientific question, i.e. raft-dependent WNT/ β -catenin signaling and to consider the already existing models. Based on this we evaluate conceivable modeling formalisms and select the modeling and simulation approach most suitable to capture the essential dynamics of the target system. After that the actual model is implemented.

4.1 Biological Background - Key regulatory aspects of WNT/ β -catenin pathway

Canonical WNT signaling is a central pathway in embryonic development and adult homeostasis, while its aberrant form is involved in a number of human cancers and developmental disorders [35, 126, 145]. The WNT/ β -catenin signal transduction is characterized by a reaction cascade, that is initiated by extracellular WNT molecules and eventually leads to an accumulation of cytosolic β -catenin and its subsequent shuttling into the nucleus. Beta-catenin is the key regulatory factor of WNT signaling. Once shuttled into the nucleus it associates with the Lef/Tcf transcription factors and triggers a pathway-specific gene response relevant for the regulation of various physiological and developmental processes [86, 126].

β -catenin levels - constant expression, dynamic degradation

Interestingly, β -catenin levels in canonical WNT signaling are regulated in a particular way. In most signaling pathways key regulatory proteins are kept at a certain concentration (stock level). Upon activation, the key regulatory protein is then activated, typically through phosphorylation, and the protein level rises due to an increased expression rate. In canonical WNT signaling however, the key regulatory or target protein

β -catenin is being constantly produced and, as long as there is no WNT stimulus, immediately phosphorylated and thereby targeted for degradation. Once canonical WNT signaling is activated the phosphorylation, hence degradation of β -catenin is disrupted, leading to an immediate increase of the intracellular β -catenin level while the expression rate remains unchanged. Accordingly, intracellular β -catenin levels in canonical WNT signaling are regulated by controlling its degradation instead of its targeted expression. However, this raises the question, why the cell expends such an astonishing effort in keeping a constant, but transient pool of its key regulatory key protein β -catenin? In fact, the described mechanism has one major advantage over the typical expression-based regulation of protein levels: it permits a much more rapid and versatile regulation of β -catenin levels in response to WNT signals. Due to the high expression rate of β -catenin already in the inactive state, the increase of β -catenin levels in response to WNT stimulation is almost instantaneous. The same applies to the negative regulation - as soon as the WNT stimulation diminishes the destruction complex is reactivated and β -catenin is immediately degraded, decreasing its protein level. In contrast to that, expression-based regulation of protein levels is rather ponderous. This is due to the number of time consuming and elaborately regulated processes involved in the regulation of gene expression, translation, protein folding and post-transcriptional modifications. Indeed the degradation-based regulation of β -catenin facilitates a precise temporal activation or inhibition of WNT target genes that is necessary during development [193].

Structure and regulation of the destruction complex

The proteasomal degradation of β -catenin is mainly controlled by a large, dynamic multi-protein assembly, termed *destruction complex*. Apart from β -catenin itself, the destruction complex comprises the tumor suppressors AXIN and adenomatosis polyposis coli (APC), the kinases glycogen synthase kinase 3 (GSK3) and casein kinase 1 α (CK1 α) as well as the E3-ubiquitin ligase β -TrCP [193], as depicted in Fig. 4.1.

The key components of the destruction complex and their binding interactions are well understood, yet several molecular mechanisms underlying β -catenin degradation remain unclear. In particular the relationship between the destruction complex and the ubiquitination machinery as well as the crucial role of APC (APC mutations occur in >80% of all colon cancers) in the destruction complex are largely unknown [167, 193].

The mechanism best understood is the phosphorylation of β -catenin, which marks β -catenin molecules for ubiquitination, hence degradation. The β -catenin phosphorylation crucially depends on the scaffold protein AXIN [41, 72, 95], even though AXIN has no apparent effect on the catalytic capabilities of the involved kinases [190, 193]. In fact,

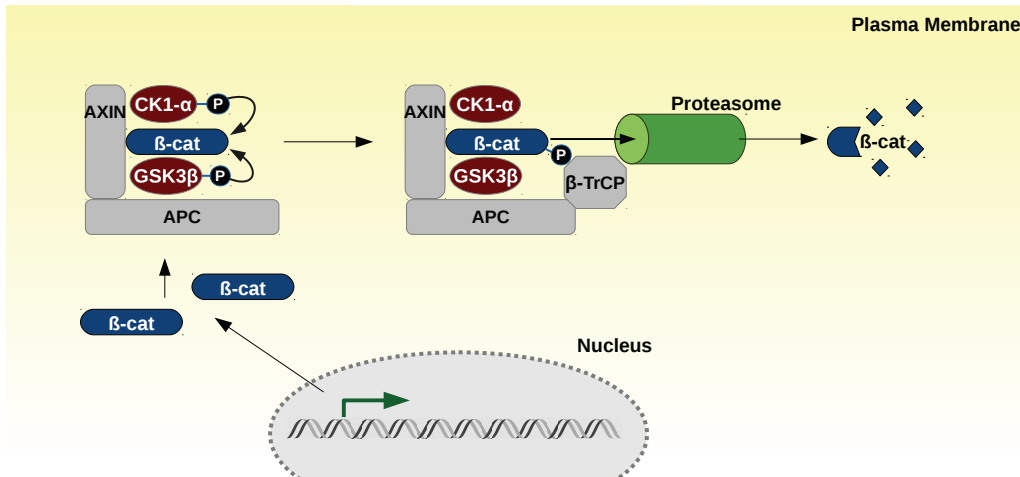


FIGURE 4.1: Schematic representation of the structure and function of the *Destruction Complex*.

the function of AXIN is purely based on the scaffolding effect, i.e. the correct assembly of the destruction complex. AXIN provides several binding sites for CK1 α , GSK3 and β -catenin, allowing a simultaneous binding of these components [95, 123, 169, 214]. Thereby kinases and substrate are brought in close proximity, such that CK1 α and GSK3 may sequentially phosphorylate β -catenin at several phosphorylation sites at the carboxy terminus [3, 123]. Note, that GSK3 and CK1 α are also involved in various other signal pathways. Thus, the binding to AXIN does not only promote phosphorylation of β -catenin, but also prevents the interaction of GSK and CK1 α with other regulatory proteins not involved in canonical WNT signaling. Thereby GSK3 and CK1 α are uncoupled and shielded from interacting with other signal pathways. [50].

Dvl and LRP6 as main transducer of canonical WNT signals

In addition AXIN comprises binding sites for DVL and LRP6, which are of particular relevance for the inhibition of the β -catenin degradation machinery, hence activation of WNT/ β -catenin signalling. LRP6 is a cell surface receptor that initiates the signal cascade upon an extracellular WNT stimulus whereas cytosolic DVL functions as a relay between receptor and downstream signaling effectors. Even though LRP6 and DVL do not *directly* interact with each other (see Table 1 [65]), both proteins are the main transducer of canonical WNT signaling. Note that Dvl is also involved in a number of different WNT pathways, whereas LRP5/6 induces no other WNT signal pathway than the canonical. The crucial role of Dvl and LRP6 for the activation of canonical

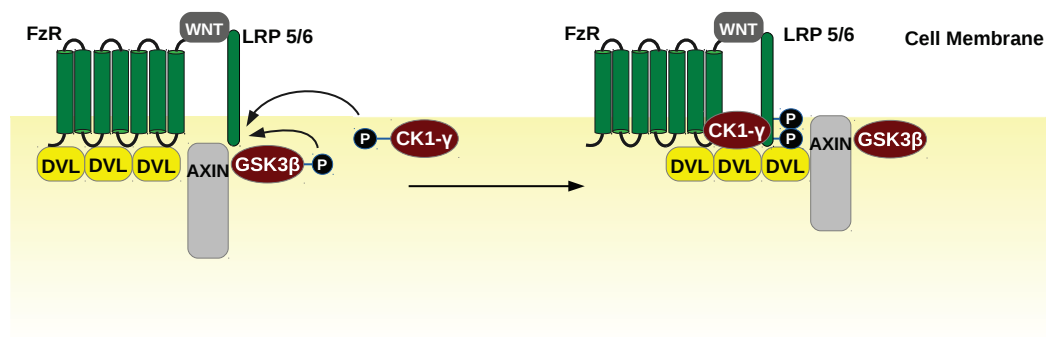


FIGURE 4.2: Schematic representation of the structure and function of the formation of the protein-receptor complex, that forms the *signalosome*. Note, that the clustering of several protein-receptor complexes into the actual macroscopic signalosome is omitted in the figure

WNT/ β -catenin signaling is explained in the following.

LRP6 Signalosome formation upon WNT binding

Secreted WNT proteins initiate canonical WNT signaling by interacting with LRP6 and its co-receptor Frizzled (Fz). In response to the extracellular WNT stimulus, LRP6 co-localizes with its co-receptor Frizzled (Fz). In the following Dvl is recruited by Fz and oligomerizes at the cell membrane (c.f. Fig. 4.2). The oligomerization of Dvl leads to a clustering of LRP6 and Fz receptors and further promotes the recruitment of AXIN as well as other cytosolic proteins, like CK1 γ and GSK-3 β [11, 36]. The resulting receptor-protein complex is termed signalosome. The stable aggregation of the signalosome triggers the phosphorylation of several intracellular phosphorylation sites (mainly PPSPXS motifs) in the cytosolic tail of LRP6, primarily through CK1 γ and GSK-3 β (c.f. Fig. 4.2). The phosphorylation of the cytosolic tail of LRP6 generates high-density platforms for the recruitment of AXIN [142, 152, 218]. Due to the binding of AXIN (and GSK-3 β) to LRP6, key components of the destruction complex are inhibited, which in turn leads to an accumulation and translocation of β -catenin into the nucleus and eventually to the well known gene transcription signal (see right hand side of Fig. 4.3).

Dvl polymers act as binding platform

However, Dvl does not only promote the clustering of LRP5/6 and Fz to form signalosomes. It is also crucially involved in the phosphorylation of LRP6 and the subsequent binding of AXIN [11]. Active Dvl molecules form dynamic protein assemblies that interact with WNT pathway components, like GSK3 β , CK1 α and AXIN. Accordingly,

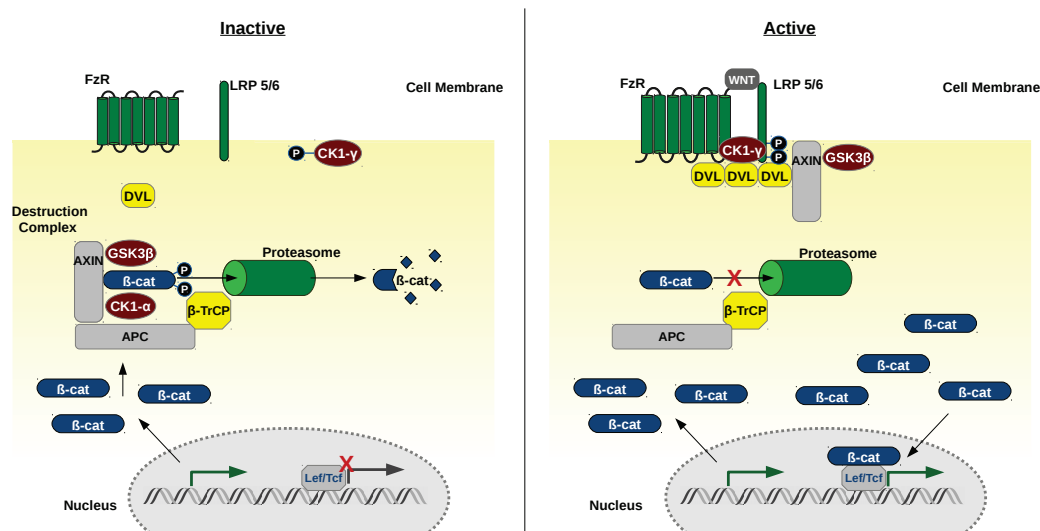


FIGURE 4.3: Schematic representation of the inactive and active state of canonical WNT signaling.

in response to a WNT stimulus dynamic Dvl polymers are recruited to the membrane where they bind to FZ. However, Fz-bound DVL polymers also interact with LRP6, which is bridged to FZ by WNT molecules. Thereby Dvl-bound GSK3 β , CK1 α and AXIN get in close proximity to LRP6, which promotes their interaction. After its binding to FZ, Dvl thus acts as a binding platform providing a major part of the kinases required for LRP6 phosphorylation. Thus, the stable accumulation of the signalosome driven by LRP6 and Dvl is vital for the activation of canonical WNT signaling [11].

The decisive role of Dvl and LRP6 for the activation of the pathway is underlined by a number of studies demonstrating that for both proteins the presence of extracellular WNT molecules is not necessarily required to induce β -catenin accumulation [10, 11, 36, 101, 124, 188]. Even though they bypass the need for WNT stimulation, these artificially induced signaling events give valuable indication of the intricate regulation of canonical WNT signaling.

Dishevelled competes with AXIN polymerization, thereby interfering with its regulatory function.

As previously described, DVL has the ability to self-associate via its DIX domain, forming elongated head-to-tail polymers, observable as regularly shaped cytoplasmic puncta [60, 180, 216, 217]. Intriguingly AXIN has an almost identical domain (DAX), which is also known to mediate self-association in vitro as well as in vivo [91, 104, 130, 168, 172]. DIX/DAX domains is highly conserved and essential for the effector function of both Dvl and AXIN. NMR spectroscopy demonstrated, that the purified DIX/DAX domains

of the two proteins interact with each other directly through their polymerization interfaces [60]. Thereby the same residues mediate homo- as well as heterotypic interactions. This means, Dvl may potentially compete for the polymerization interface of AXIN. Accordingly AXIN monomers copolymerize with Dvl into more dynamic Dvl-AXIN signalosomes instead of AXIN polymers [60, 180], which in turn disrupts the self-assembly and thereby the effector function of AXIN. This process, however, is highly concentration dependent. AXIN polymers are relatively stable and Dvl-AXIN affinity is rather low. Therefore only high-grade DVL polymers, that form upon WNT binding to its Fz receptor and LRP6 coreceptor as described in the previous paragraph, generate a binding avidity high enough to break up AXIN polymers in the cytosol [60]. This process is further amplified by the binding sites presented by phosphorylated LRP6, after DVL/AXIN polymers have been recruited to the membrane. Nevertheless it has to be acknowledged that Dvl has the potential of inhibiting AXIN directly, given its local concentration exceeds a certain threshold.

LRP6 self-accumulation and phosphorylation

LRP6 possesses a similar concentration-dependent self-activation mechanism as Dvl. As soon as the local receptor density of LRP5/6 crosses a certain threshold, it starts to self-aggregate into signalosomes. The oligomerization of LRP5/6 in turn promotes the phosphorylation of the cytoplasmic tail of LRP5/6 by CK1 γ and GSK3 β . When accumulated, phosphorylated LRP6 is capable of recruiting and binding AXIN, thereby inhibiting the destruction complex. Intriguingly, the previously described artificial oligomerization and subsequent phosphorylation of LRP6 is also completely independent of Dvl [11]. The phosphorylation sites of LRP6 signalosomes apparently provide a local concentration of binding sites high enough for AXIN recruitment and binding. Thus, a forced oligomerization by mutation or simply a significant overexpression of LRP6 is sufficient to induce canonical WNT signaling hence bypassing the need for Dvl polymers, Fz or even WNT molecules [11, 18].

Given the central role of the WNT signaling, the local concentration levels of LRP6 and Dvl have to be elaborately regulated. Experimental studies demonstrate that WNT-induced phosphorylation of Dvl differentially regulates canonical and noncanonical WNT signaling [9]. For instance, phosphorylation of WIP sites reduces the formation of DVL polymers and attenuates β -catenin signaling [68]. Thereby DVL activity is shifted from canonical to non-canonical WNT signaling. It should also be noted, that the general availability of free Dvl is rather restricted due to its involvement in various other WNT pathways and the high number of interaction partners [65].

In contrast to that, LRP6 is exclusively involved in canonical WNT signaling. Accordingly LRP6 concentration and activation is tightly regulated through recycling, inhibitors (DKK) and most importantly an intricate regulation mechanism that is based on lipid rafts [155, 173, 183, 215].

LRP6 phosphorylation is restricted to Lipid Rafts

In fact, the localization of LRP6 in lipid rafts is crucial for its successful phosphorylation, implying a major impact of lipid rafts on the activation of the signalosome, hence WNT/ β -catenin signaling [155, 173]. Interestingly, LRP6 is not raft-associated, but evenly distributed throughout the membrane independent of the presence of WNT ligands, whereas its main kinases, membrane-bound CK1 γ , is primarily located in lipid rafts. This means receptor and kinase are separated to a large extent, which effectively reduces the interaction between LRP6 and CK1 γ attenuating the phosphorylation of LRP6 and signalosome formation. However, additional mechanisms are required to [completely] restrict the phosphorylation of LRP6 to lipid rafts as observed in the experiments. Recent experimental results have identified *LY6/PLAUR domain-containing 6* (Lybd6) as additional interaction partner of LRP6. Lybd6 is GPI-anchored to the membrane and therefore partitions into lipid rafts, where it interacts with FZ and LRP6 and promotes LRP6 phosphorylation upon WNT stimulation. However, the exact mechanism of raft-specific phosphorylation and the role of CK1 γ and Lybd6 still remains elusive.

Endocytotic regulation of WNT/ β -catenin pathway

An ever growing number of studies underline the various role of endocytosis for the regulation of WNT/ β -catenin pathway. Thereby endocytosis has been shown to have inhibiting as well as promoting effects, depending on the endocytotic pathway, that is activated [15]. Endocytosis induced by the inhibitor Dkk, e.g. is mediated by clatherin and specifically depletes LRP6 from the lipid raft, hence attenuates the receptor and signal activation. Whereas WNT induced endocytosis is controlled by caveolin and leads to the inhibition of the destruction complex by transferring GSK3 β to multivesicular bodies, where it is separated from the cytosol and eventually targeted for lysosomal degradation [173, 196].

4.2 Existing WNT/ β -catenin models

There exists a huge number of WNT models and each considers a specific aspect of WNT/ β -catenin signaling hence employs a different level of detail. Here we want to focus on the models describing the detailed intracellular processes of canonical WNT signaling. Therefore we particularly emphasize the Lee model and its extensions. For a thorough survey of the existing WNT models, the interested reader is referred to one of the excellent reviews of *Kofahl and Wolf* as well as *Lloyd-Lewis et. al.* [107, 125].

Lee et. al. (2003) The first mathematical model of canonical WNT signaling was proposed in 2003 by Lee and Heinrich [116]. The model is deterministic and captures the essential dynamics of β -catenin in the cytosol. It is considered as reference model for the canonical WNT signal pathway, for the majority of the kinetic parameters and protein concentrations are based on experimental measurements [125]. Lee et al used *Xenopus* oocyte as experimental system, which is a decent choice, because in contrast to e.g. cell populations, it provides a well-stirred cytosolic environment of a single cell without compartmentalization. Thus *Xenopus* oocytes fulfill most of the assumptions for deterministic models and therefore serve as a perfect reference system for the model. The original model is composed of 15 ODEs, which describe the regulation of the transcriptional activity of WNT target genes by β -catenin. Accordingly the model comprises β -catenin, its target transcription factor TCF and the main species involved in the regulation of β -catenin levels, i.e. WNT, Dishevelled (Dsh in *Xenopus*) as positive regulators and the main components of the β -catenin destruction complex: GSK3 β , APC and AXIN. The reactions between the species describe the following processes: protein synthesis and degradation, de-/phosphorylation, and protein complex dis-/assembly. Note, that in the model only AXIN and β -catenin are subject to production and turnover processes, whereas the concentrations of Dsh, GSK3 β , APC and TCF are considered as constant over time. WNT on the other hand is not represented as a species, but by a rather abstract signal, which has a value between 0 and 1 and its decay is described by an arbitrary exponential function.

Apart from the model, one of the main insights of the study by Lee et. al. is the crucial role of AXIN for the assembly and function of the degradation complex. Indeed, quantitative determination of all species concentrations revealed a significantly lower concentration of AXIN compared to the other species of the degradation complex, i.e. 0.02 nM versus 50 nM for GSK3 β and 100 nM for APC. Further *in silico* experiments showed that the increase and duration of β -catenin accumulation in response to WNT stimulation is directly affected by the turnover rate of AXIN. Thus, according to the

Lee model AXIN is the limiting factor in β -catenin degradation process, hence canonical WNT signaling.

Model analysis and simplifications The Lee model has been thoroughly analysed in a number of studies and several simplifications have been proposed.

Kruger et. al.

Kruger and Heinrich were one of the first to perform a thorough analysis of the Lee model. They identified varying time scales involved in the WNT pathway and the existence of conservation laws, which allowed them to reduce the model to 7 ODEs and 8 algebraic equations [111]. Further Kruger and Heinrich performed a sensitivity analysis to analyse the robustness of the WNT model to variation of parameter values. Remarkably, the robustness of the model differs between active and inactive state. In the inactive state, i.e. without WNT stimulation, parameter variations resulted in inappropriate pathway activations, whereas in the active state, i.e. during WNT stimulation, the model appeared rather robust against perturbations.

Mirams et. al.

In an attempt to reduce the amount of parameters used in the Lee model Mirams et al performed a detailed asymptotic analysis of the Lee model to identify the dominant component involved in WNT signaling. Based on their analysis they suggest to simplify the Lee model to one single ODE describing the dynamics of active β -catenin under the dependence of WNT signals. In this simplified model only three reactions are considered: the basal production and decay reactions of β -catenin, which are preserved from the Lee model, and the AXIN-dependent degradation of β -catenin. Finally the inclusion of an additional equation for the formation of the β -catenin/TCF complex is suggested. Remarkably the simplified model, consisting of the four reaction previously described reactions, is capable of reproducing the essential dynamics of WNT/ β -catenin signaling [143].

Geontoro et al

Extended analysis of the Lee model revealed, that WNT-induced β -catenin fold changes, i.e. the ratio of β -catenin concentration before and after WNT stimulation, are insensitive to certain perturbations of pathway parameters (in a certain range). This means, perturbations that affect the concentration values of certain key components of the WNT/ β -catenin pathway, affect the total β -catenin level, but not the WNT-induced fold change of β -catenin. However, data from *Xenopus* and mammalian cells show that

the robustness of the β -catenin fold change strongly varies between individual parameters. While WNT-induced β -catenin fold changes are sensitive to β -catenin overexpression, the perturbations of the degradation of β -catenin has hardly any effect on the fold change in β -catenin. Further in vivo and in vitro experiments in *Xenopus* and ROK cells demonstrated, that cellular responses are coupled to WNT-induced fold changes, instead of absolute β -catenin levels, i.e. not the absolute concentration of β -catenin/TCF, but the fold change controls transcriptional outcome of WNT signaling. As a consequence transcriptional and phenotypic responses to WNT signaling are robust to natural variations in proteins levels, either of genetic, environmental or stochastic nature.

Model extensions Apart from model simplifications, a number of studies have build upon the Lee model and introduced additional components, such as feedback mechanisms or compartments and the diffusion between them.

Feedback Mechanisms - (Cho 2006, Wawra 2008)

A key aspect for several WNT regulators is that they are positive or negative transcriptional targets of the canonical WNT pathway, hence modulate WNT pathway activity in terms of a feedback mechanisms [125]. Several extensions of the Lee model exist, that include negative feedback loops by coupling the expression and production of pathway inhibitors, like AXIN or Dkk with the WNT-induced β -catenin accumulation [28, 211]. The inclusion of feedback mechanisms can result in a robust oscillation of β -catenin and its inhibitor [103]. Though, analyses of the extended models demonstrate, that oscillation of the WNT/ β -catenin pathway occurs only under certain conditions, i.e. parameterizations of the model [28, 211]. For instance, the original configuration of the Lee model cannot establish a stable oscillation under permanent WNT signal, despite the inclusion of negative feedback [211]. Instead an increase between 2 and 20 fold of the original parameter configuration is required to reach stable oscillation of β -catenin/TCF and AXIN2.

Compartments / Subcellular models

A major limitation of the previous models is the assumption of homogeneity, i.e. the models consider the cell as a homogeneous, well-mixed solution. This simplification

neglects the facts, that cells comprise distinct compartments, like the nucleus or endosomes, that proteins migrate between these compartments through active or passive transport and that specific reactions can be localized to a particular compartment or region. This also accounts for the canonical WNT pathway, where crucial processes are spatially restricted to certain compartments, like the complexation of β -catenin and TCF in the nucleus after the nucleo-cytoplasmic shuttling of β -catenin or the formation of the ligand activated receptor complex (signalosome) in the membrane. Recent extensions of the Lee model address this issue in a compartmental approach. Van Leeuwen et al's model was one of the first to consider different pools of β -catenin and their distribution between the three compartments membrane, nucleus and cytosol. This work was followed by several models that explicitly include the nucleo-cytoplasmic shuttling of WNT pathway components, as done by *Mazemondet et al* for β -catenin [138] or *Schmitz et al* for β -catenin and its regulator APC [176, 177]. Indeed *Tan et al* recently demonstrated that compartmental models provide more realistic results than purely cytosolic models [200].

However, to our knowledge only the model of *Kogan et al* includes receptor-ligand interaction and receptor complex formation at the membrane [108]. The model is capable of not only describing the coordinated activation and formation of the WNT/Frizzled/LRP6 complex, but also the synergistic effect of common WNT inhibitors, like secreted Frizzled-related protein (sFRP) and Dickkopf (Dkk) [108]. In view of these results and the fact, that the WNT-induced formation of the receptor complex is a key step in canonical WNT signaling, it remains illusive, why there exists only one model that considers signaling at the receptor level.

4.3 Modeling membrane-related processes in signal transduction

While in the two previous chapters of this thesis, the impact of lipid rafts on signal transduction has been studied on the microscopic temporal and spatial scale, i.e. microseconds and micrometers, a much higher temporal and spatial scale is required to explore the impact of lipid rafts on an entire signal transduction chain, like canonical WNT signaling. Indeed, the time that generally passes between the initial ligand-receptor binding and the cellular response, e.g. in terms of gene expression or target protein activation, lies in the range of seconds to minutes rather than microseconds. The same applies to the spatial scale - typically a single or a colony of cells has to be considered when studying signal transduction and cell communication, with an average cell volume of $V \approx 2.25 \cdot 10^3 \mu\text{m}^3$, not to mention the enormous amount of proteins involved. Therefore we need computational modeling approaches that have a much lower

level of detail in terms of spatial and temporal scales. This section is focused on how to construct a hierarchically structured model of WNT/ β -catenin signaling that features both the membrane-related and intracellular dynamics described in section 4.1. At the same time, we address the problems and challenges that arise when developing models of signaling pathways in general and in particular with regard to spatial aspects, such as lipid rafts dependent signal transduction dynamics.

4.3.1 Modeling features required to capture membrane-related processes in signal transduction

Cell biological models usually require different modeling features depending on the interactions within the model network and the individual properties of the model components [131]. In signal transduction, for instance, a low number of extracellular signaling molecules is often sufficient to activate membrane-bound receptors, which in turn induce an intracellular signaling cascade. Therefore features such as stochasticity, multi-state components and compartments are important for signal transduction models. In the following major modeling features are summarized, that are specifically required to capture membrane-related processes in signal transduction and in particular in canonical WNT signaling, as described in Sec. 4.1. These modeling features help to derive the requirements in search for the proper modeling formalism that is later used for the actual model implementation. The set of model requirements is based on the review of *Machado et. al.* [131].

Multi-state components

Proteins are typically subject to several modifications, such as phosphorylation, ubiquitination or glycosylation. This also applies for the proteins involved in canonical WNT signaling. WNT-bound LRP6, for instance, has to be phosphorylated at several phosphorylation sites, before it can bind and inhibit AXIN [11, 142, 152, 218]. CK1 γ is palmitoylated, which anchors the protein at the membrane, where it preferably partitions into lipid rafts [173]. Also WNT proteins are glycosylated, which is essentially required for membrane localization and ligand receptor interaction [7]. These examples already illustrate the major impact that protein modifications have on the protein's localization, its functionality and the reactions it participates in. Therefore different modification states of proteins ought to be included in model descriptions. The easiest approach for this, and most commonly used for mathematical modeling (in terms of ODEs), is to represent each modification state by an individual entity. However, such a

straight-forward approach results in a combinatorial explosion of entities and reactions (a protein like LRP6 with n phosphorylation sites will have 2^n possible states, hence entities), and therefore becomes rapidly infeasible, in particular for models that contain several multi-state components [56, 87]. The problem of combinatorial complexity can be avoided by formalisms that allow the specification of attributed entities and state-dependent reactions [131]. Since the majority of proteins involved in the regulation of canonical WNT signaling possess multiple modification states, a modeling formalism supporting multi-state components is apparently more suited for a combined membrane- and intracellular model of canonical WNT signaling than a pure mathematical approach.

Spatial structure and compartmentalization

The cell is well structured in terms of static and dynamics compartments, such as organelles (e.g. nucleus, mitochondrion or endoplasmatic reticulum) and cytoplasmic vesicles (e.g. endo -or lisosomes). Compartments are enclosed by a semi-permeable membrane, which separates the compartments contents from the surrounding environment. Molecules, like proteins, nucleotides (RNA) or ions, migrate between these compartments in terms of active or passive transport, depending on the molecule's size and the porosity of the compartment. As a result, molecule concentrations, hence diffusion and reaction kinetics may strongly vary between individual compartments. Note, that the membrane itself is also considered as separate functional unit, because membrane-bound proteins are restricted to lateral diffusion and therefore only interact with other membrane-bound and peripheral proteins or ligands.

Compartments play a major role in canonical WNT signaling. β -catenin can only function as transcription factor, when present in the nucleus. Whereas the destruction complex can degrade only cytoplasmic β -catenin. An even greater role plays the compartmentalization of the membrane in terms of lipids rafts. Thereby membrane-bound proteins like, LRP6 and CK1y are not only heterogeneously distributed throughout the membrane, but their interaction is completely restricted to lipid rafts. A model combining membrane-related and intracellular WNT/ β -catenin models thus has to be realized in a compartmental approach.

Modularity and hierarchy

As described in the previous paragraph, the cell is organized into a set of separate compartments, each with its own specific functionality [79, 165]. Shuttling molecules, driven

by active or passive diffusion, interconnect the individual compartments. This modularity provides the basis for composition-based approaches, meaning that a model can be composed into separate submodels, which may be eventually aggregated into one model without changes to any of the submodels. Taking advantage of the modular organization of the cell in terms of model composition can help to reduce their complexity facilitating the development, extension and analysis of models in general [160].

While modularity and compartmentalization represents the horizontal organization of the cell, living systems also comprise a vertical, i.e. hierarchical organization [27, 131]. The most prominent example is the organization of any vertebrate organism into organs, tissue, cells and molecules. However, already a single cell has multiple hierarchical layers, reaching from the extracellular space, over the plasma membrane to intracellular compartments, like the nucleus of mitochondria, each of which may be further hierarchically structured (e.g. lipid rafts domains within the membrane). Capturing the described complex, hierarchical organization of the cell poses a great challenge for the modeling formalism. It has to support hierarchical, and [bestenfalls], dynamic nesting of compartments and cope with the interaction across compartment boundaries. Let's consider the formation of the WNT/LRP6 receptor complex in canonical WNT signaling as an illustrative example. In this reaction extracellular WNT molecules directly interact with membrane-bound LRP6 receptors, which can further be located within lipid rafts. The complex hierarchical nesting of the LRP6 receptor, being located in within three compartments (Cell, Membrane, Lipid Rafts), is necessary due to the specific restriction of LRP6 phosphorylation to Lipid Rafts (c.f. Sec. 4.1). At the same time WNT directly interacts with LRP6, crossing several compartment boundaries. Therefore, the formation of the WNT/LRP6 complex can best be represented by a model formalism that supports hierarchical nesting of proteins and that connects the hierarchical layers with a bottom up approach to allow direct ligand receptor interaction.

Dynamic Model Structures

Cells are dynamic systems, where not only molecules are being produced and degraded, but also larger structures, i.e. compartments. Typical examples for dynamic structures, that continuously emerge and disappear are endocytotic vesicles and endosomes. Endocytotic vesicles emerge from or merge with the Golgi apparatus and the plasma membrane and they are mainly responsible for trafficking, sorting and recycling processes in cells. Another dynamics structure is the cell itself, as it is subject to growth, division and also cell death/apoptosis. The modeling of dynamic model structures like endosomes or cell division provides one of the greatest challenge for modeling formalisms, for a number of reasons. First, endosomes and in particular cells, are compartments, that contain

an arbitrary number of molecules. If modeling approaches support compartments at all, the compartmental structure of the model is typically fixed and a dynamic handling of compartments, like the emergence of new compartments, is not explicitly designated in most of the formalisms. Also the dissection of model structures, for instance in cell division, requires a procedure for the distribution of the containing molecules to the resulting structures/compartments. Lastly it would be desirable, if dynamic structures could also be associated with individual properties, i.e. attributes. For instance, the function of endosome changes with its characteristics, in particular with its pH value. This means for normal (neutral) pH values, endosomes serve as trafficking vesicles, while acidic endosomes transfer to the lysosomal pathway, which is responsible for the degradation of proteins and the break down of cellular waste products. Since endocytosis also plays a crucial role in canonical WNT signaling (cf. Section 4.1), a proper modeling formalism should provide means for the representation of dynamic and preferably attributed structures.

Stochasticity

Stochasticity becomes crucial, when very low molecule numbers are involved in the reaction network of a model. The most prominent example is gene regulatory networks, but this also applies for signal transduction, as signaling cascades are often triggered by a low number of signaling molecules and then further amplified. In canonical WNT signaling, a small concentration of WNT molecules are sufficient to induce a transient, but robust activation of the WNT/ β -catenin pathway [76, 116]. Further, AXIN and thereby another key player in canonical WNT signaling is present in a comparably low concentration [116, 138, 152, 203]. Accordingly, for the simulation of signaling networks in general and in particular of the WNT/ β catenin signaling network, a stochastic approach should be preferred over a deterministic approach.

4.3.2 Rule-based modeling approaches

There exists numerous modeling formalisms, a lot of which provide an ever increasing amount of extensions, each specifically addressing different aspects of the previously elucidated challenges in modeling of canonical WNT signaling and complex signal transduction pathways in general. According to the previously described model features that are required to effectively capture the dynamics of canonical WNT signaling, rule-based approaches appear to be the method of choice for a number of reasons. Rule-based formalisms are a specific class of modeling languages that employ sets of rules to describe

state changes in the model. Thereby each rule comprises a precise formal statement about the conditions that have to be fulfilled for the rule to be executed (or fired) and the consequences of its execution. There exists numerous rule-based approaches that are tailored to quantitative systems biology, such as BioNetGen Language (BNGL), κ , which are probably the most prominent and commonly used approaches, and the recently developed ML-Rules. In these approaches the model is typically described in terms of chemical solutions, i.e. mappings from molecules to discrete numbers, while the rule specification follows the notation of (bio)chemical reactions. Thereby the left-hand site of each rule describes what condition have to apply for the rule to be executed/fired; whereas the right hand site describes what happens, when the rule is executed/fired.

Due to the similarity of rule-based languages to chemical reaction systems, the description of transduction pathways in rule-based formalisms is rather intuitive. The main advantage of rule based approaches, however, is that it can avoid the combinatorial explosion problem in the development and simulation of complex models. This is because most rule-based formalisms provide means for a structured definition of model components (or species) with multiple, arbitrary states (attributes). This allows to define rules with reaction patterns, where a single rule represents a set of multiple reactions, depending on the attribute values of the species [57, 99, 136]. On the one hand, this significantly reduces the model complexity, because the interactions of an attributed species can be defined by schematic rules instead of specifying reactions per each possible state of the species. On the other hand, the computational complexity is also decreased, since species and reactions only need to be instantiated as they become available. In the following BNGL, κ and ML-Rules will be shortly introduced and discussed whether they are suited to implement the processes involved in canonical WNT signaling (cf. Section 4.1).

BioNetGen Language

BioNetGen is a framework and language for modeling and simulation of rule-based models. It is primarily dedicated to model biochemical systems, and has been particularly applied in the modeling of different signaling pathways [8, 14, 201]. The basic building blocks of BNGL models are molecules. Molecules are structured objects that are organized in terms of components. Components allow to specify molecule specific properties (i.e. attributes), like phosphorylation or binding sites and may be associated with a predefined list of possible/arbitrary state values. Components of different molecules can be linked through bonds in order to describe the binding of molecules. This means, the association of molecules is explicitly described in a binding-site specific way (example WNT-LRP6).

With respect to canonical WNT signaling, the attribution of molecules in terms of components provides mean to describe the various phosphorylation states of e.g. LRP6 and in particular its interactions with its numerous binding partners, like WNT, CK1 and AXIN. Rules specify the formation and degradation of molecules as well as their biochemical transformations, i.e. state changes of the molecule's components. Like in most common rule-based language, BNGL employs reaction patterns, i.e. a single rule represents a set of multiple reactions. Thereby BNGL follows the premise "don't care, don't write", which means, that if component/attribute values of a molecule/species are not explicitly specified in the rule, it applies to all entities of the molecule/species, independently of their attribute values. However, as soon as concrete component/attribute values are specified, the rule is restricted to the set of molecules that matches the given attribution/component values. This way the phosphorylation of LRP6 can be restricted to LRP6 molecules that are bound to WNT or the AXIN-dependent degradation of β -catenin is restricted to free, unbound AXIN molecules. BNGL further supports conditional expressions as well as arbitrary rate kinetics. Arbitrary kinetics can be specified by user-defined functions, which may further depend on global observables [189]. Observables relate to quantities of a set of chemical species that match a search pattern or set of search patterns.

However, due to the need for global observables to access the total amounts of certain molecular species, rule schemata can only be applied in a limited way. For instance, a model with numerous compartments, e.g. several cells, or endocytotic compartments, would require the definition of an own global observable as well as the respective reaction rules for each of the modeled compartments, and therefore would soon become very complex and cumbersome.

To encounter the apparent need to explicitly describe the hierarchical topology of the cell, the BGNL formalism has been extended [78]. The compartmental BNGL (cBNGL) explicitly distinguishes between three-dimensional (compartment volume) and two-dimensional (surface, i.e. membrane) compartments, taking into account their effects on reaction rates. This means in cBNGL the localization of molecules restricts the scope of rule application, and the reaction rate is inherently scaled to the predefined volume of the compartment. By explicitly specifying the compartment name, transport rules may change the location of individual molecules and entire molecular complexes respectively.

In summary BNGL and its extension compartmental extension cBNGL provide a powerful modeling formalism that serves most of the modeling features, we identified earlier as being crucial for the development of a canonical WNT signaling model. Namely, BNGL allows the definition of multi-state model components, it supports an explicit

notion for molecule binding and protein assemblies and with its extension cBNGL provides a mean to describe the hierarchical topology of cells in terms of compartments. However, the major drawback of the BioNetGen formalism is its lacking support for dynamic structures. The restriction to a finite, predefined list of attribute values for each component, hampers the description of dynamic entities. As a consequence e.g. growth processes are difficult to capture, which might be important for modeling raft and cell growth in the context of canonical WNT signaling. A way to circumvent this problem is the specification of an observable, which can then be used for volume dependent rate calculations. However, observables only capture species numbers, thus cannot replace dynamic attributes.

The compartment topology of a model is fixed too, i.e., cBNGL does not provide means for dynamic structures, and, apart from the volume, it is not possible to equip compartments with an own state. Moreover, the volume of a compartment denotes merely a constant model parameter rather than a state variable that may change over time. This for instance hampers the description of newly emerging structures and abrupt volume changes, e.g., due endocytosis/recycling or lipid rafts dynamics, such as growth, merge and fission of rafts. Moreover, downward causation and certain high-level aspects of the WNT signaling, such as varying diffusion regimes, for instance caused by molecular crowding or increased viscosity in lipid rafts cannot be captured in the current BNGL notation.

κ -calculus

A similar rule-based formalism as the previously described BNGL is the κ language [42, 43, 59]. While BNGL was originally conceived as a language for describing ODEs in a higher level fashion, the κ -calculus was early on intended as modeling language providing a direct and transparent formalization of molecular agents in signaling networks [42]. Hence, κ follows an agent-based approach where species are defined by agents that have a structured interface for the interaction with other agents. However, even though their original motivation is completely different, κ and BNGL are astonishingly similar regarding synthax and semantics. In the following we shortly describe the elemental building blocks of the κ -calculus and evaluate, why this formalism is generally more limited than BNGL, particularly regarding its expressiveness, except for certain, tailored modeling approaches.

κ description consists of a collection of agents and rules. Similar to the components of molecules in BNGL, agents can be arbitrarily attributed in terms of labeled sites. Sites describe the internal state of the agent and typically refer either to protein modifications, like phosphorylation, ubiquitination or binding sites. Thereby domain-level

modifications and bindings can be presented in a similar way as in BNGL.

At the same time, rules provide concise descriptions of the interaction, i.e. under which conditions agents may interact and what the result of this interaction is. Elemental interactions refer to binding and unbinding of two agents or changes in the modification state of a site of an agent, but also the creation and deletion of an agent. Similar to BNGL κ also follows the "don't care don't write" convention, i.e. if sites are omitted in the rule description, the rule applies for all agents, regardless of the current state of the omitted site. Thereby rule schemata can be specified, representing a set of different rule instances, that are generated when there exist agents that fulfill the conditions on the left-hand side of the reaction. Rules are associated with reaction rate constants and the set of reactions contained in a model is typically executed in terms of the Gillespie algorithm. To this point the κ language provides a similar functionality as the native BGN language (not cBNGL), hence covers a substantive body of events sufficient to describe a majority of mechanistic interactions in cellular signaling. Though more sophisticated aspects of signaling, such as compartmentalization, space in general and dynamic structures are not yet addressed. Another major drawback is the restriction to mass action kinetics. In contrast to BNGL, no arbitrary rate calculations can be defined in κ . Also explicit description for compartmentalization, like in the extended version cBNGL, is not available.

However, also for κ a number of extensions have been developed to represent agents in a hierarchical way or to provide a spatial representation of compartments. [43, 191]

The hierarchical extension of κ allows the definition of generic species and rules. Thereby agents can be derived from already specified agents in a similar way as in object-oriented programming. This means newly defined agents may specifically modify, add or remove individual sites of the agent from which it is derived from, while the remaining sites, inherited from its ancestor agent remain unchanged. This implies an hierarchical organization of agent entities and allows the definition of generic rules that mention agents that have many descendants in the hierarchy. [43] This allows a convenient exploration of arbitrary model perturbations, as for instance ligands, mutations or drugs [43]. Also, spatial aspects in terms of neighborhood can be easily expressed in a condensed and concise manner. Thereby cell-to-cell communication in a cell colony can be represented without suffering from combinatorial explosion as in BNGL. For these specific modeling purposes κ provides crucial advances in comparison to BNGL. However, for the implementation of the canonical WNT signal pathway, these aspects only play a minor part. Spatial Kappa is an extension of κ to embed Kappa-based models in space, i.e. that captures the location and the movement of species [191]. For this, the formalism has been extended in terms of voxel-based compartments, connections between them (known as channels) and respective translocation rules for species. Spatial Kappa thus supports the definition of purely compartment-based models, similar to cBNGL, as well as more

spatially resolved models, where compartments are additionally discretized in terms of a regular lattice, i.e. voxels. Agents can move along channels, that connect voxels within or across compartments. The diffusion and transport dynamics of species shuttling between voxels is based on the next-subvolume approach [53]. Spatial Kappa thus provides means to describe heterogeneous protein distributions within single compartments, given the discretization of the compartment is sufficiently small. In addition, the reaction rate of a rule may now contain agent descriptions, i.e. the rate of a diffusion rule may be defined as a function of the size of the species being diffused. This is a major advance compared to basic Kappa and BNGL. However, also in Spatial Kappa reactions rates are still restricted to mass action kinetics, which limits its applicability severely. Moreover, Spatial Kappa suffers from the lack of dynamic structures, which, similar to BNGL, hampers the description of cellular processes like endocytosis, cytokinesis or the merging and fission of lipid rafts.

ML-Rules

ML-Rules is the newest development in the line of rule-based model languages that are tailored to bio-chemical systems. ML-Rules puts a special emphasis on representing dynamics at different levels of a nested hierarchy [136, 210]. The basic model entities in ML-Rules are called *species*, which may represent any object of interest, e.g. a cell or a protein. Each species consists of a name and a fixed tuple of attributes, i.e. in the basic language concept attributes do not have names and are identified by their position only. In addition, ML-Rules supports the concept of *nested species* to build hierarchical model structures, i.e. species can be enclosed by other species and can enclose other species themselves. That means, species are not only characterized by their names and attributes, but also by their context (the species they are enclosed by) and content (the set of species they contain, called *solution*). Note that species at any level within such a hierarchy may still have assigned attributes. Since ML-Rules belongs to the reaction-centric family of rule-based formalisms, the dynamics of a model are described by *rule schemata*, each of which may encode for possibly infinitely many concrete rule instantiations, helping to effectively reduce redundancy and thereby facilitating compact model descriptions [43]. A rule schema can be instantiated at any (sub-)solution of the current model state to which the set of reactants would match. The firing rate of a rule determines the frequency with which a rule is being executed. To let the rate depend on the amount of matched reactants, so called *species identifiers* can be defined through which the according species population size can be dynamically accessed. In contrast to many other formalisms, e.g. the κ -calculus, rate kinetics in ML-Rules are not restricted to the law of mass-action, which is an important feature for multi-level modeling in

general [136, 137]. Complex mathematical expressions and conditional constraints are allowed to manipulate the reaction rate of a rule schema, e.g. to specify thresholds that control a rule to only fire if a certain amount of reactants is available. To model upward and downward causation between different hierarchical levels, ML-Rules supports the specification of rule schemata that involve nested reactant and product species. Most importantly, in ML-Rules it is possible to change the model structure dynamically, which is another important feature for specifying biological multi-level models, since many biological processes, e.g. endocytosis, cell division, and death, change the hierarchical composition of the system. The support for variable model structures during runtime and the fact that species are allowed to have attributes (states) at any organizational level, distinguishes ML-Rules clearly from cBNGL and κ .

4.3.3 Multi-level, rule-based modeling in ML-Rules

For the following model implementations we apply ML-Rules, a multi-level, rule-based modeling language [136]. The semantics of ML-Rules is based on continuous time Markov chains (CTMC). ML-Rules models are executed by stochastic, discrete event execution algorithms [66]. All entities are expressed in terms of concrete numbers, like molecules, compartments or cells, instead of concentrations. In our model stochastic events play a crucial role due to the comparatively low molecule number of the key player AXIN. In this setting, a deterministic ODE based execution might miss important dynamics as has been shown in [138]: in comparison to the ODE based execution, the stochastic execution revealed artifacts in simulating β -catenin signaling within hNPCs-cells if adopting the very low AXIN concentration as given by [116]. Therefore in [138], a still comparatively low but ~ 10 times higher number of AXIN molecules was determined as more realistic, a result that was later confirmed for various mammalian cells by wet-lab studies [199]. The implemented WNT/ β -catenin signaling model makes extensive use of rule-schemata provided by the ML-Rules syntax. This is necessary, since the model contains several hierarchical levels as well as protein specific binding and phosphorylation states, that are in particular necessary for the representation of the signalosome.

Model description in ML-Rules

Next we shortly introduce the rule-schemata provided by the ML-Rules syntax. For more details the interested reader is referred to Maus et. al. [136]. A model description in ML-Rules typically consists of four different elements that are specified in a certain order. We will introduce each of these elements with the help of exemplary ML-Rules

model specifications, that represent a simple ligand-receptor interaction, i.e. extracellular ligands bind to membrane-bound receptors and the degradation of the receptor, independent of its binding state.

Parameter specification

At first a list of optional constant model parameters is defined, like initial molecule number or reaction rate constants. The parameter definition consists of the parameter name, a colon and its value. The values assigned to parameters can be a numerical value, a string or even an expression, as shown in the example below. In this example, the number of ligands is calculated based on the number of receptors and corresponds to 250:

```
k1: 2.3e-02;  
k2: 1.0  
nReceptor: 1e03;  
nLigand: nReceptor / 4;  
nCell : 1;  
stateB: 'b';
```

Species definition

Any entity in the model is defined as species type with a unique name and its number of attributes. For example the rule specification below states, that the species `receptor` is attributed with one attribute, whereas the species `ligand` does not contain any attributes:

```
Receptor(1);  
Ligand(0);
```

However, note that the species type definition does not contain any information about the type or the value of the attributes. Attributes are explicitly specified when defining the initial solution or the rule schemata. As seen in the next paragraph, the attribute of `receptor` correspond to its binding state.

Initial solution

The initial model state is defined by the initial solution `>>INIT[...]`. Here, the species that are initially present, their species count and attributes are (explicitly) specified.

Distinct species are separated by a + symbol. Note that the same species type may occur several times in the initial solution, if differently attributed. For example, in our example the `receptor` may initially be present in the unbound and bound state. Accordingly the initial solution contains two species of type `receptor` - one with attribute `'ub'` (unbound) and one with `stateB`, i.e. `'b'` (bound) with the corresponding molecule counts:

```
>>INIT[
  nReceptor Receptor('ub') +
  25 Receptor(stateB) +
  nLigand Ligand
];
```

Note, that attributes are now explicitly specified. These values are changed during the simulation according to the rules defined later on.

Since ML-Rules supports hierarchical nesting, the initial solution may also comprise sub-solutions contained by certain species. The hierarchical structure is indicated by square brackets, i.e. a nested species `Cell` that encloses a `Nucleus` and a `Membrane` is, in the simplest case (without further attributes or nested structures), defined as follows:

```
Cell [Nucleus+Membrane]
```

Assume in our exemplary model the initial solution comprises extracellular ligand molecules and a single `Cell` holding the nested species `membrane`, which in turn contains the two differently attributed receptor species. The corresponding definition of the (extended) initial solution is shown below:

```
>>INIT[
  nLigand Ligand +
  nCell Cell[
    1 Membrane[
      nReceptor Receptor('ub') +
      25 Receptor(stateB)
    ]
  ]
];
```

Rule schemata

Eventually the dynamics of the model are defined in terms of rules or rule schemata. A rule (schemata) consists of an arbitrary number of reactants, products and a stochastic

rate, that defines the reaction kinetics. Reactants and products are separated by an arrow \rightarrow followed by the rate definition after the @ symbol:

```
reactants -> products    @ rate;
```

In our model we only consider biochemical reactions following mass action kinetics. The stochastic rate of the reaction is thus determined by the amount of reactant species and the speed of the reaction, i.e. the reaction rate constant. To access the amount of a certain reactant, it can be assigned to an identifier x . The corresponding variable $\#x$ then holds the current number of the assigned species, as depicted in the rule for the ligand-receptor binding:

```
Ligand:l + Receptor('ub'):r -> Receptor('b') @ k1*#l*#r;
```

As indicated in the rule specification above, attribute values can easily be changed as a result of a reaction. Accordingly, the binding of the ligand to the receptor is reflected by the change in the receptor's binding attribute ('ub' \rightarrow 'b') and the consumption of the ligand.

However, the given specification disregards the hierarchical nesting of the species and is therefore incomplete yet. In its current form the rule would not be executed, since ligand and receptor are not at the same hierarchical level. Instead, the nesting of the species has to be specified explicitly:

```
Ligand:l + Cell[Membrane[Receptor('ub'):r + s_m?] + s_c?] ->
Cell[Membrane[Receptor('b') + s_m?] + s_c?] @ k1*#l*#r;
```

Please note, that when applying rules to nested species, one typically wants to preserve the remaining molecules (sub-solution) within the nested species (e.g. cell, nucleus or membrane) without specifying them explicitly. Therefore an additional, arbitrary variable with the suffix ? occurs on the reactant and product site. In the example above, $s_m?$ and $s_c?$ thus refer to the -unknown- sub-solution of the membrane and the cell respectively, which remain unchanged, except for the change in the receptor's attribute. The next example illustrates the use of schematic rules. Instead of specifying each potential (binding) state of the receptor ('ub' and 'b') explicitly for its degradation, one can specify a schematic rule with a variable (bind) rather than a defined attribute value. For example, the first order decay reaction with reaction rate constant k_2 is described by the following rule:

```
Receptor(bind):r ->    @ k2*#r;
```

where $\#r$ relates to the current amount of ligand molecules. This however also implies, that the degradation rate constant is the same for unbound and bound receptors.

4.4 A rule-based model of raft-dependent WNT/ β -catenin signaling

In this section a detailed description is given how membrane-related and intracellular processes are combined in a comprehensive WNT/ β -catenin model and specified in terms of the ML-Rules formalism. To evaluate what model could potentially be used in our model, the existing WNT/ β -catenin models are first described, before the model is described that has been developed.

4.4.1 Membrane WNT Model in ML-Rules

This component represents lipid rafts-dependent receptor dynamics, receptor-ligand interaction and receptor activation through kinase-dependent phosphorylation. Unfortunately, there exists hardly any model that describes these processes for the canonical WNT pathway. To our knowledge only the model of *Kogan et. al.* includes receptor-ligand interaction [108]. However, the model neglects the impact of lipid rafts, membrane-bound kinases which are apparently essential mechanism for canonical WNT signaling. Therefore we have to develop the membrane WNT model basically from scratch.

Model assumptions The model is compartment-based, but for rate calculation we consider the membrane as a two-dimensional layer with lipid rafts being (immobile) circular-shaped entities within the membrane, whose radius and coverage control the rate of receptor-raft collision. Lipid rafts are included as individual compartments within the membrane, similar to the nucleus being a single compartment within the cell. Membrane bound proteins and receptors may enter and leave individual lipid rafts by diffusion. Note that the mobility inside lipid rafts is reduced. Accordingly the diffusion coefficient of raft-associated receptors is reduced by a constant factor R_ρ . The value of R_ρ controls the extend of receptor aggregation inside lipid rafts [58, 73, 150]. In addition to R_ρ , the aggregation also depends on the protein's specific raft affinity R_φ . The value of R_φ is mainly determined by the structure and the hydrophobic character of the membrane-bound protein, in particular of its membrane integral domain. This corresponds to the observation, that only a specific set of proteins are accumulated by lipid rafts [61, 207].

With regard to the membrane compartment, we reduce the representation of the receptor-complex and the signalosome. Accordingly, the FZ-LRP6 receptor complex is only represented by LRP6, such that in our model WNT directly binds to the LRP6 receptor. This simplification is reasonable for canonical WNT signaling, because crucial events, like AXIN binding, mainly depend on LRP6 and its activation through phosphorylation. We further employ a simplified representation of LRP6 phosphorylation. LRP6 has to be phosphorylated at several phosphorylation sites to recruit and bind AXIN. Thereby the dual phosphorylation of the phosphorylation sites T1479 and S1490 by CK1 γ and DVL/GSK3 β is crucial [152, 173, 219]. In our model, we consider solely the interaction between CK1 γ and LRP6, whereas a detailed representation of DVL mediated unspecific phosphorylation of LRP6 by GSK3 β is omitted. This assumption is justified by several studies indicating that the LRP6 phosphorylation site targeted by GSK3 β , S1490, is constitutively phosphorylated and not or only weakly responsive to WNT stimulation, while the phosphorylation of the CK1 γ specific phosphorylation site, T1479, is clearly induced by WNT stimulation [46, 152]. In addition several studies revealed accordantly that CK1 γ -mediated phosphorylation of LRP6 is confined to lipid rafts [155, 173]. We include this finding in our model by restricting the phosphorylation to rafts-associated proteins, i.e. only LRP6 that are located within a lipid raft may be phosphorylated by CK1 γ .

Eventually we allow two types of WNT stimulation. WNT molecules can either be initially provided (transient stimulation) or continuously synthesized and secreted by the cell. Since WNT is a highly lipophilic protein that is localized at the membrane after its secretion [39, 213], we assume, that released WNT molecules can directly induce the WNT/ β -catenin signaling at the cell surface in an autocrine manner. Note that in our model we consider only one cell, instead of a heterogeneous cell population. As shown in our aforementioned study, the impact of the cell cycle asynchrony on the average β -catenin dynamics in cell populations is negligible [138]. Naturally, in a cell population, the released WNT molecules will most likely induce WNT/ β -catenin signaling in the neighboring cells as well (paracrine activation).

Molecules and Interactions The membrane model of WNT signaling comprises two subcomponents. The first model subcomponent represents the diffusion-driven receptor shuttling between raft and non-raft membrane regions, while the second model subcomponent includes the receptor interactions with extracellular ligands (WNT) and membrane-bound kinases (CK1 γ). Both subcomponents are depicted in Fig. 4.4. Each labeled arrow in the figure refers to a specific rule in the model code 4.6. Note that, if not stated otherwise, all reactions are reversible, e.g. the rules for WNT binding to LRP6 (R7–8) relate to the respective binding and dissociation reaction. To illustrate

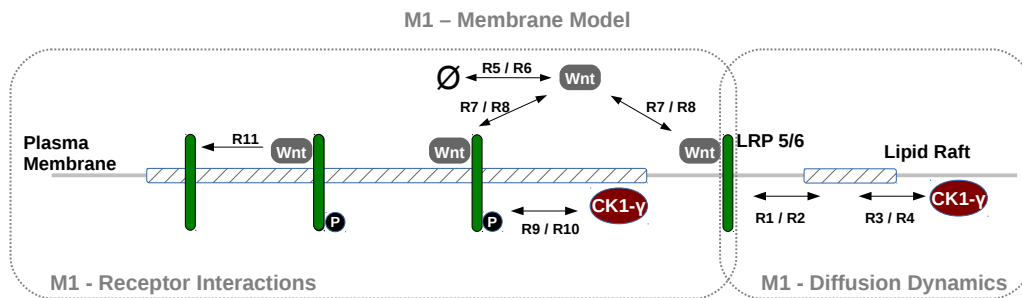


FIGURE 4.4: Schematic representation of the *membrane WNT model*. The left-hand site depicts the modeled receptor interactions with WNT ligands and membrane-bound CK1 γ kinases. On the right-hand site the diffusion-driven receptor shuttling between raft and non-raft regions is illustrated. Two-sided arrows indicate reversible reactions.

Arrow labels correspond to rule numbers

the implementation of the membrane model components using ML-Rules, each individual process, such as receptor-raft shuttling or ligand-receptor binding, will be shortly described with the aid of exemplary rule definitions.

Receptor-raft shuttling

To start with, we consider the raft-dependent diffusion dynamics of LRP6 and CK1 γ . LRP6 and CK1 γ are located in the membrane, both diffusing into and out of Lipid Rafts. This means LRP6 and CK1 γ are either nested within the membrane or within lipid rafts. At the same time, lipid rafts are a nested species of the membrane, which itself is a nested species of the cell. The actual transition of LRP6 (or CK1 γ) between the nested compartments *Membrane* and *LR* is best illustrated in a reduced, exemplary rule specification, that solely considers the nesting of LRP6 and disregards any other attributes and additional nested structures:

```
// LRP6 diffusion into Lipid Rafts
Cell[Membrane[LR[] + LRP6]] -> Cell[Membrane[LR[LRP6]]]

// LRP6 diffusion out of lipid rafts
Cell[Membrane[LR[LRP6]]] -> Cell[Membrane[LR[] + LRP6]]
```

LISTING 4.1: Simplified ML-Rules specification for LRP6-Raft shuttling

However, the specification of the shuttling process in ML-Rules requires not only hierarchical nesting but also attributed species. Let's consider the exact specification of LRP6 shuttling into and out of lipid rafts, as shown below:


```

// (R1) LRP6 diffusion into Lipid Rafts
Membrane(A)[LR(radius, p)[s?]:l + LRP6(d, ra, phos, bind):r ] ->
Membrane(A)[LR(radius, p)[LRP6(d*p, ra, phos, bind) ]] @ k_1*#l*#r*ra

// (R2) LRP6 diffusion out of lipid rafts
Membrane(A)[LR(radius, p)[LRP6(d, ra, phos, bind) + s?]:r ] ->
Membrane(A)[LR(radius, p)[s?] + LRP6(d/p, ra, phos, bindW) ] @ k_2*#l*#r

```

LISTING 4.2: ML-Rules specification for LRP6 lipid raft shuttling. Please note, in this and any of the following rule specifications the rest solutions of the nested species, i.e. Cell, Membrane and LR have been omitted for simplicity. The exact ML-Rules implementation can be found in the model code at the end of the subsection

As depicted in rule 4.2 LRP6 is attributed with four different attributes:

1. *d* - diffusion rate
2. *ra* - raft affinity (corresponding to $R_\varphi(LRP6)$)
3. *phos*- phosphorylation state
4. *bindW*- WNT binding state

For the raft shuttling, the diffusion rate and the raft affinity are of major relevance, because they are required for the calculation of the kinetic rates k_1 and k_2 . Further, note that in rule 4.2 the diffusion rate *d* of LRP6 is modified during the transition by a raft-specific factor *p*. *p* refers to the raft fluidity R_ρ and determines how strong receptors are slowed down within lipid rafts (c.f. model assumptions & Section 1.2). Therefore, any receptor in the model is attributed with parameters for the diffusion rate *d* and the raft affinity *ra*. Also the value of the diffusion rate is adapted whenever receptors enter or leave lipid rafts.

The kinetic rates k_1 and k_2 correspond to the stochastic diffusion constant, that describes the discrete event-based diffusion of a particle between separate compartments [53]. In our case, however, we do not consider cubic sub-volumes, but concentric spheres, where one sphere (the lipid rafts) is contained in the other (membrane). Accordingly the kinetic rate corresponds to the analytical solution of the Smoluchowski rate equation [208], which determines the rate at which a particle collides with the reaction surface of another stationary particle:

$$k_a = 4\pi D \cdot a \quad (4.1)$$

where D is the diffusion constant of the particle, and a is the reaction criterion, i.e. the minimum separation required for the particles to interact.

We thus consider the receptors as moving particles that interact with stationary lipid rafts of circular shape and the lipid raft's radius serves as reaction criterion. Under consideration of the surface of the compartment, where the particle/receptor starts (i.e.

either raft or non-raft regions), the kinetic rates k_1 and k_2 are obtained:

$$k_1 = \frac{4\pi D \cdot r_{raft}}{V_m} \quad (4.2)$$

$$k_2 = \frac{4\pi D \cdot r_{raft}}{V_{raft}} \quad (4.3)$$

where r_{raft} , A_m and A_{raft} correspond to the raft radius and the available surface of the membrane and lipid rafts, respectively. Note that k_1 and k_2 only refer to the stochastic diffusion constant of one receptor and one lipid rafts and that k_1 further depends on the receptor specific raft affinity. Therefore these values are included in the calculation of the kinetic rates, as depicted in rule 4.2.

Receptor Interactions

Next, we consider the receptor-protein interactions. As previously described (c.f. paragraph assumptions), we employ a reduced model of the signalosome and solely consider the dynamics of its key component LRP6. Accordingly extracellular WNT proteins bind to LRP6 (R7–8) and subsequently LRP6 in complex with WNT gets phosphorylated by CK1 γ (R9–10). Importantly, we assume that CK1 γ -mediated phosphorylation of LRP6 is restricted to lipid rafts, as indicated by experimental studies [155, 173]. In fact, this restriction will be further confirmed by our simulation experiments as described in the paragraph "parameter adjustment" 5.3.1.

For the specification of the LRP6 interaction, both hierarchical nesting and species attributes are required once again. The specification for the binding and dissociation reaction of WNT and LRP6 in ML-Rules is shown below.

```
// (R7a) Binding of WNT to LRP6 (representing Fz,LRP6 receptor complex)
Wnt:w + Cell[Membrane(A)[LRP6(diff, ra, 'uP', 'uB'):1]] ->
Cell[Membrane(A)[LRP6(diff, ra, 'uP', 'B')] ] @ k_7a**w**1;

// (R7b) Binding of WNT to raft-associated LRP6
Wnt:w + Cell[Membrane(A)[LR(radius, p)[LRP6(diff, ra, 'uP', 'uB'):1]]] ->
Cell[Membrane(A)[LR(radius, p)[LRP6(diff, ra, 'uP', 'B')] ] ] @ k_7b**w**1;
```

LISTING 4.3: ML-Rules specification for WNT-LRP6 binding.

Notably the binding reaction, as implemented in rule 4.3 stretches over several compartment/species boundaries, i.e. extracellular WNT interacts with LRP6, which is nested within three or two species depending on whether LRP6 is raft-associated or not. Also the latter two attributes of LRP6, that represent phosphorylation and binding states,

come into play. Note, that these attribute are LRP6 specific now. Consider the change of the binding attribute of LRP6 ('uB' \rightarrow 'B') in rule 4.3 indicating the binding of WNT, which is thereby consumed in the reaction. However, the bound WNT protein is not ultimately lost. The dissociation reaction is just vice versa, i.e. one WNT protein is released (produced) in the extracellular space and the binding attribute of LRP6 is reverted to 'uB' (c.f. 4.6). Note, that the dissociation reaction occurs only for unphosphorylated LRP6, i.e. once LRP6 is phosphorylated, the receptor is committed to signaling and WNT will eventually be consumed and degraded when the signalosome is recycled.

```
// (R11) Recycling of Wnt/LRP6 complex (representing signalosome)
LRP6(diff, ra, 'P', 'B'):1 ->
LRP6(diff, ra, 'uP', 'uB') @ k_11*#w*#l;
```

LISTING 4.4: ML-Rules specification for dissociation/recycling of the activated WNT/LRP6 complex under the consumption of WNT.

The first order reaction depicted in rule 4.4 occurs independently of the localization of LRP6. Therefore, the specification of the exact nesting of LRP6 can be omitted in this rule. Next we consider the CK1 γ mediated phosphorylation of the WNT/LRP6 complex:

```
// (R9) Phosphorylation of WNT/LRP6 complex in Lipid Rafts
LR(radius,p)[CK1y(diff_ck,ra_ck):ck + LRP6(diff_l,ra_l,'uP','B'):1 ]:r ->
LR(radius,p)[LRP6(diff_l,ra_l,'P','B') + CK1y(diff_ck,r_ck,ra_ck) ]
@ k_9*#l*#ck / (3.14*radius*radius*#r/vol) * p;
```

LISTING 4.5: ML-Rules specification for CK1 γ mediated phosphorylation of LRP6.

As mentioned before, the phosphorylation of LRP6 solely occurs in lipid rafts. In ML-Rules this is reflected by explicitly restricting the reaction to LR contained species, as done in 4.5. Also this reaction applies only for “bound” LRP6 molecules, i.e. LRP6 receptors that are in complex with WNT proteins. As a result of the reaction the second LRP6-specific attribute is changed ('uP' \rightarrow 'P'), indicating the phosphorylation of the phosphorylation site in LRP6. Note that in contrast to WNT CK1 γ is not consumed in this reaction. Since this reaction is restricted to lipid rafts, the reduced diffusion in lipid rafts and their reduced volume/surface have to be regarded when calculating the kinetic rate. Since reaction rate constants are already scaled according to the cell specific membrane volume/surface, the reaction rate constant has to be divided/scaled by the relative raft surface, i.e. the raft coverage.

```

// ++++++
// +++++ species definitions (number of attributes) +++++
// ++++++

Cell();
Membrane(1);
LR(2);
Wnt(0);
LRP6(4);
CK1y(2);

// ++++++
// +++++ initial solution +++++
// ++++++

>>INIT[
  nWnt Wnt +
  nCells Cell[
    (1) Membrane(A)[
      nLR LR(radius, rho) +
      nLRP6 LRP6(1, ra_lrp, 'uP', 'uB') +
      nCK1y CK1y(1, ra_ck)
    ]
  ]
];

// ++++++
// +++++ reaction rules ++++++
// ++++++

// **** Lipid Raft Dynamics ****

// (R1) LRP6 diffusion into lipid rafts
Membrane(A)[LR(radius,p)[s?]:1 +LRP6(d,ra,phos,bindW):r +s_m?] ->
Membrane(A)[LR(radius,p)[LRP6(d*p,ra,phos,bindW) +s?] +s_m?] @ k_1*#1*#r*ra;

// (R2) LRP6 diffusion out of lipid rafts
Membrane(A)[LR(radius,p)[LRP6(d,ra,phos,bindW):r +s?]:1 +s_m?] ->
Membrane(A)[LR(radius,p)[s?] +LRP6(d/p,ra,phos,bindW) +s_m?] @ k_2*#1*#r;

// (R3) CK1y diffusion into lipid rafts
Membrane(A)[LR(radius,p)[s_lr?]:1 +CK1y(d,ra):r +s_m?] ->
Membrane(A)[LR(radius,p)[CK1y(d*p,ra) +s_lr?] +s_m?] @ k_3*#1*#r*ra;

// (R4) CK1y diffusion out of lipid rafts
Membrane(A)[LR(radius,p)[CK1y(d,ra):r +s_lr?]:1 +s_m?] ->
Membrane(A)[LR(radius,p)[s_lr?] + CK1y(d/p,ra) +s_m?] @ k_4*#1*#r;

// **** Membrane Signalling ****

// (R5) Wnt production
Cell[s?] -> Wnt + Cell[s?] @ k_5;

```

```

// (R6) Wnt degradation
Wnt:w -> @ k_6*#w;

// (R7a) Binding of Wnt to LRP6 (representing Fz,LRP6 receptor complex)
Wnt:w+Cell[Membrane(A)[LRP6(diff,ra,'uP','uB'):1 +s_m?] +s_c?] ->
Cell[Membrane(A)[LRP6(diff,ra,'uP','B') +s_m?] +s_c?] @ k_7a*#w*#1;

// (R7b) Binding of Wnt to raft-associated LRP6
Wnt:w+Cell[Membrane(A)[LR(radius,p)[LRP6(diff,ra,'uP','uB'):1 +s_lr?]
+s_m?] +s_c?] -> Cell[Membrane(A)[LR(radius,p)[LRP6(diff,ra,'uP','B')
+s_lr?] +s_m?] +s_c?] @ k_7b*#w*#1;

// (R8) Dissociation of Wnt from LRP6 (representing Fz, LRP6 receptor complex)
Cell[Membrane(A)[LRP6(diff,ra,'uP','B'):1 +sm?] +s_c?] ->
Cell[Membrane(A)[LRP6(diff,ra,'uP','uB') +sm?] +s_c?]+Wnt @ k_8*#1;

// (R9) Phosphorylation of activated LRP6 in LR
Membrane(A)[LR(radius,p)[CK1y(diff_ck,ra_ck):ck +
LRP6(diff_l,ra_l,'uP','B'):1 +s_lr?] +s_m?] -> Membrane(A)[LR(radius,p)[
LRP6(diff_l,ra_l,'P','B') + CK1y(diff_ck,ra_ck) +s_lr?] +s_m?] @
k_9*#1*#ck / (3.14*radius*radius/A) * p;

// (R10) Dephosphorylation of LRP6
LRP6(diff,ra,'P','B'):1 -> LRP6(diff,ra,'uP','B') @ k_10*#1;

// (R11) Recycling of Wnt/LRP6 complex (representing signalosome)
LRP6(diff,ra,'P','B'):1 -> LRP6(diff,ra,'uP','uB') @ k_11*#w*#1;

```

LISTING 4.6: ML-Rules implementation of the membrane WNT model as depicted in Figure 4.4.

4.4.2 AXIN/ β -catenin model

In the following the intracellular WNT model component is described. This model component primarily describes the dynamics of β -catenin, i.e. its synthesis, its interaction with the destruction complex and the resulting degradation process as well as its shuttling between nucleus and cytosol.

In contrast to the membrane WNT model, there already exist several experimentally validated models capturing these dynamics (cf. Section 4.2). Most of the models addressing the WNT-dependent regulation of intracellular β -catenin levels are based on the Lee model [116]. Interestingly, mathematical analyses have shown, that a reduced version of the Lee model containing only three proteins (β -catenin, AXIN and WNT) is capable of reproducing the essential dynamics of WNT-induced β -catenin signaling. Accordingly [we will] employ a stochastic ML-Rules implementation of the reduced Lee model, which will be subsequently discussed.

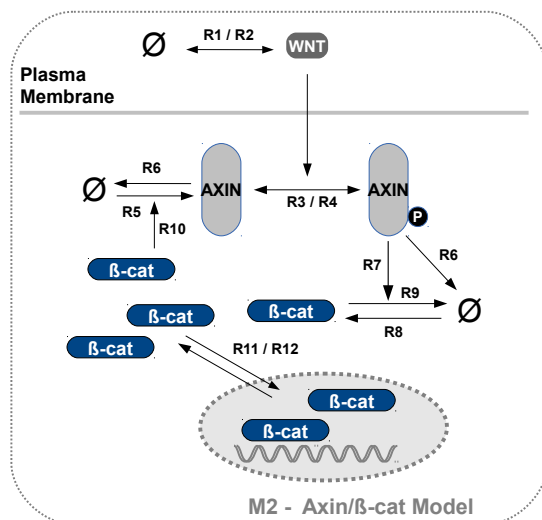


FIGURE 4.5: Schematic representation of the *intracellular WNT model*. Two-sided arrows indicate reversible reactions. Arrow labels correspond to rule numbers

Model assumptions As depicted in Fig. 4.5, the intracellular model provides three different proteins, Beta-catenin, AXIN and WNT as well as two compartments, cytosol and nucleus, with the nucleus being nested within the cytosolic compartment. AXIN is considered as a condensed representation of the destruction complex, i.e. its remaining components, like GSK3 β , APC and CK1 α are disregarded. This simplification is based on the fact, that AXIN is the main component of the destruction complex and is present in a very low concentration [116]. Although AXIN has been found to be less rare in mammalian cells than e.g. in *Xenopus* egg extracts, AXIN is still the rate-limiting component in WNT/ β -catenin signaling and its inhibition is one of the crucial events for pathway activation [138, 152, 203].

To differentiate between single AXIN molecules and the fully assembled, functional destruction complex (including the kinases required for β -catenin phosphorylation), a phosphorylation site has been added to AXIN. This means the phosphorylation state of cytosolic AXIN determines the activation state of the destruction complex, i.e. unphosphorylated AXIN is inactive, whereas its phosphorylated form is active and promotes the degradation of β -catenin.

In accordance with the reduced Lee model, WNT proteins directly trigger the dephosphorylation of AXIN. Thereby AXIN is attenuated in its regulatory function in degrading cytosolic β -catenin, which in turn leads to an immediate increase of the β -catenin levels. Thus, WNT directly interacts with AXIN, neglecting any membrane-related processes, like receptor ligand interaction or activation.

Note, that β -catenin is subject to nucleo-cytoplasmic shuttling and therefore located in the cytosol as well as within the nucleus. The nucleo-cytoplasmic shuttling is regarded as a simple diffusion process with rate constants based on experimental data (cf. [138]).

When located in the nucleus, β -catenin promotes AXIN expression, i.e. the WNT-induced accumulation of nuclear β -catenin promotes the synthesis of AXIN, resulting in a negative feedback loop upon WNT stimulation.

Molecules and interactions Without WNT stimulation AXIN is subject to frequent autophosphorylation and dephosphorylation (R3–4). In these first order reactions, the attribute that represents the phosphorylation state of AXIN is simply changed, similar to the phosphorylation of LRP6:

```
// (R3) Basal AXIN autophosphorylation
AXIN('p', 'f'):a -> AXIN('p', 'f') @ k_3**a;

// (R4) Basal AXIN dephosphorylation
AXIN('p', 'f'):a -> AXIN('u', 'f') @ k_4**a;
```

LISTING 4.7: ML-Rules specification of autophosphorylation of AXIN.

Similar to the basal dephosphorylation, AXIN is also subject to WNT-induced dephosphorylation (R13). Thereby extracellular WNT crosses the cell boundary and interacts with phosphorylated AXIN, inducing its dephosphorylation. Note, that in this reaction WNT molecules are consumed:

```
// (R13) Wnt-induced AXIN dephosphorylation
Wnt:w + Cell[AXIN('p', 'f'):a] -> Cell[AXIN('u', 'f')] @ k_13**a**w;
```

LISTING 4.8: ML-Rules specification of WNT-induced dephosphorylation of AXIN.

AXIN and β -catenin are subject to production and degradation processes (R5 & R6, R8 & R9). In addition to its basal degradation, β -catenin is subject to an AXIN mediated enhanced degradation (R7). While the degradation of β -catenin and AXIN is unspecific regarding their attribution, the AXIN mediated degradation of β -catenin is constrained to phosphorylated AXIN and further restricted to the cytosol. This is also reflected in the rule specifications:

```
// (R6) AXIN degradation
AXIN(phos, 'f'):a -> @ k_6**a;

// (R7) Activated $\beta$-catenin degradation
Cell[AXIN('p', 'f'):a + Bcat:b + s?]:c ->
Cell[AXIN('p', 'free) + s?] @ #c*((k_7**a**b));
```

LISTING 4.9: ML-Rules specification of degradation of AXIN and p-AXIN-mediated degradation of β -catenin.

The nucleo-cytoplasmic shuttling of β -catenin (R11–12) is included in the model and, apart from the kinetic rate, its specification resembles the raft-shuttling of CK1 γ and LRP6. To obtain the kinetic rate of nucleo-cytoplasmic shuttling, equation 4.3 has to be transformed from 2D (membrane layer) to 3D (cytosole):

$$k_{.11} = \frac{4\pi D \cdot r_{nuc}^2}{V_{cyt}} \quad (4.4)$$

$$k_{.12} = \frac{4\pi D \cdot r_{nuc}^2}{V_{nuc}} \quad (4.5)$$

where r_{nuc} is the radius of the nucleus and V_{cyt} and V_{nuc} are the volumes of cytosole and nucleus.

```
// ++++++
// +++++ species definitions (number of attributes) +++++
// ++++++

Cell();
Wnt();
AXIN(1);
bCat();
Nuc();

// ++++++
// +++++ initial solution +++++
// ++++++

>>INIT[
  nWnt Wnt +
  nCells Cell[
    nAXINU AXIN('u') +
    nAXINP AXIN('p') +
    nbCat bCat +
    1 Nuc[nbCatNuc bCat]
  ]
];

// ++++++
// +++++ reaction rules ++++++
// ++++++

// **** Membrane Signalling ****

// (R1) Wnt production
Cell[s?] -> Wnt + Cell[s?] @ k_1;
```



```

// (R2) Wnt degradation
Wnt:w -> @ k_2*#w;

// **** Beta-catenin signalling ****

// (R3) Basal AXIN autophosphorylation
AXIN('u'):a -> AXIN('p') @ k_3*#a;

// (R4) Basal AXIN dephosphorylation
AXIN('p'):a -> AXIN('u') @ k_4*#a;

// (R5) Basal AXIN synthesis
Cell[s?]-> Cell[AXIN('u') + s?] @ k_5*#b;

// (R6) AXIN degradation
AXIN(phos):a -> @ k_6*#a;

// (R7) Activated  $\beta$ -catenin degradation
Cell[AXIN('p'):a + Bcat:b + s?]:c ->
Cell[AXIN('p') + s?] @ #c*((k_7*#a*#b));

// (R8) Beta-catenin synthesis
Cell[s?] -> Cell[Bcat + s?] @ #c*k_8;

// (R9) Basal  $\beta$ -catenin degradation
Bcat:b -> @ k_9*#b;

// (R10) Beta-catenin driven AXIN synthesis
Nuc[Bcat:b + s?] -> Nuc[Bcat + s?] + AXIN('u') @ k_10*#b;

// (R11) Beta-catenin shuttling into the nucleus
Bcat:b + Nuc[s?] -> Nuc[Bcat + s?] @ k_11*#b;

// (R12) Beta-catenin shuttling out of the nucleus
Nuc[Bcat:b + s?] -> Bcat + Nuc[s?] @ k_12*#b;

// (R13) Wnt-induced AXIN dephosphorylation
Wnt:w + Cell[AXIN('p'):a] -> Cell[AXIN('u')] @ k_13*#a*#w;

```

LISTING 4.10: ML-Rules implementation of the intracellular AXIN/ β -catenin model as depicted in Figure 4.5.

4.4.3 Putting it together - a combined lipid raft and β -catenin WNT model

In the previous sections, the membrane and intracellular model components have been discussed in detail. Now it is the question, how these separate components are best to be composed into a single comprehensive model. Let's consider the unrealistic assumption, that WNT directly interacts with AXIN, as modeled in the intracellular model component. Apparently, this assumption neglects any membrane-related processes and also

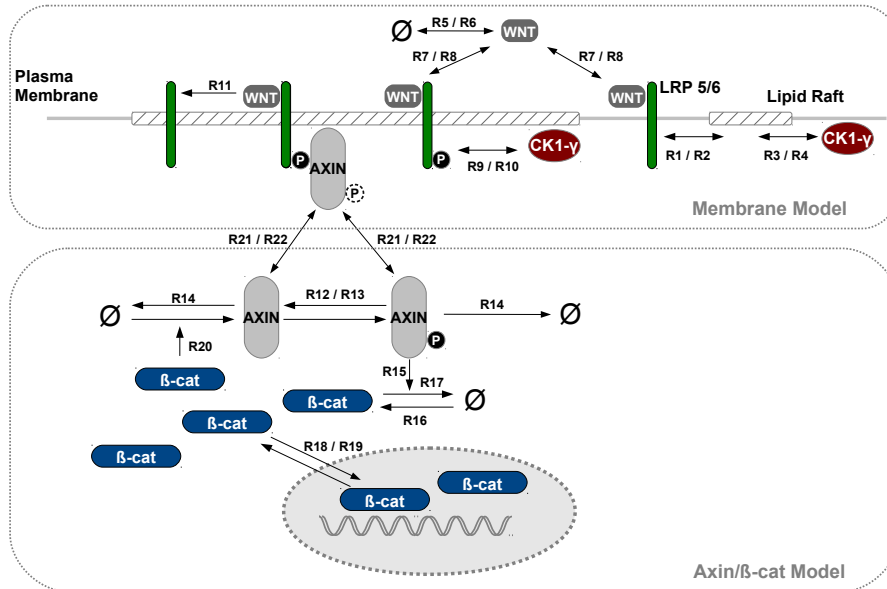


FIGURE 4.6: Schematic representation of the *combined intracellular and membrane WNT model*. Two-sided arrows indicate reversible reactions. Arrow labels correspond to rule numbers

the membrane's function as semi-permeable barrier which extracellular proteins can only overcome in terms of active transport. These important aspects however, are addressed in detail by the membrane model component. Thus, the membrane model component provides a more detailed view on the processes occurring between WNT stimulation and AXIN inhibition.

As described in 4.1, upon extracellular WNT stimulation, the destruction complex, can be inhibited by the direct binding of AXIN to membrane-bound phosphorylated LRP6 (p-LRP6), which renders AXIN unavailable for other reactions. This particular reaction, i.e. the interaction between AXIN and phosphorylated LRP6 connects the intracellular AXIN/ β -catenin dynamics with the membrane-related dynamics. Fig. ?? shows a schematic representation of the combined model, i.e. the two main model components of membrane-related LRP6/CK1 γ and axin/ β -catenin signaling and their interaction.

Model assumptions Importantly, almost all assumptions made for the separate model components also apply for the composed model. The only exception is the direct interaction of WNT and AXIN, which is not part of the composed model anymore. Instead AXIN reversibly binds to p-LRP6, which attenuates the AXIN-dependent degradation of β -catenin. Note, that the AXIN/p-LRP6 binding is independent of the phosphorylation state of AXIN. The impact of Dvl, which is supposed to be involved in this process, is neglected.

In addition the recycling of the receptor complex is altered in the combined model. In

contrast to the membrane model, not the phosphorylation of WNT-bound LRP6, but the binding of AXIN leads to signal commitment, hence recycling and WNT consumption (c.f. rule 4.4).

Molecules and interactions As depicted in Fig. 4.6, the rule numbering, particularly for the intracellular model components changed. The specification of the rules, as explained in Section ??, however, remains unchanged. Though, rule 4.8 specifying the WNT-induced dephosphorylation of AXIN is obsolete and replaced by a rule specifying the reversible binding of p-LRP6 and AXIN:

```
// (R21a) AXIN binding by LRP6 in membrane
AXIN(phos,'f'):a + Membrane(A)[LRP6(diff,ra,'P','B','f'):1] ->
Membrane(A)[AXIN(phos,$link) +LRP6(diff,ra,'P','B',$link)] @ ((k_21a*#1*#a));

// (R21b) AXIN binding by LRP6 in lipid rafts
AXIN(phos,'f'):a + Membrane(A)[LR(radius,p)[LRP6(diff,ra,'P','B','f'):1]] ->
Membrane(A)[LR(radius,p)[AXIN(phos,$link) + LRP6(diff,ra,'P','B',$link)]] @
((k_21b*#1*#a));

// (R22a) Dissociation of receptor/AXIN complex (signalosome) in membrane
Cell[Membrane(A)[LRP6(diff,ra,'P','B',bind):1a +AXIN(phos,bind)]] ->
Cell[Membrane(A)[LRP6(diff,ra,'uP','uB','f')] +AXIN(phos,'f')] @
if (bind=='f') then 0 else (k_22a)*#1a;

// (R22b) Dissociation of receptor/AXIN complex (signalosome) in LR
Cell[Membrane(A)[LR(radius,p)[LRP6(diff,ra,'P','B',bind):1a +AXIN(phos,bind)]]] ->
Cell[Membrane(A)[LR(radius,p)[LRP6(diff,ra,'uP','uB','f')]]] +
AXIN(phos,'f')] @ if (bind=='f') then 0 else (k_22b)*#1a;
```

LISTING 4.11: ML-Rules specification of p-LRP6 and AXIN binding.

According to the rule specification 4.11 p-LRP6 recruits and binds AXIN (R21a/b) which is subsequently unavailable for the destruction complex, i.e. inhibiting the enhanced degradation of β -catenin (R15). Thus β -catenin accumulates and is transported into the nucleus (R18–19).

Similar to the binding and dissociation reaction of WNT and LRP6 (c.f. rule 4.3), the binding and dissociation reactions between AXIN and pLRP6 have to be defined for raft-associated and non raft-associated p-LRP6 species separately. Also, please note that in contrast to all previous binding complexes, the binding between LRP6 and AXIN is represented by the binding operator \$ (4.11). This means, instead of changing LRP6-specific attributes, e.g. 'uB' \rightarrow 'B' for LRP6/WNT binding (c.f. 4.3) as done in the previous binding complexes, LRP6 and AXIN are both attributed with a unique identifier, which explicitly connects both individual species. This specification of a bimolecular binding is strongly related to the binding concept of BNGL. The reason

for this is, that this time, the binding reaction involves species that are both attributed. Therefore the binding operator is used here to capture all attributes, whose values are not unique in rule R21a/b. In rule (4.11) the phosphorylation and binding state of LRP6 are unique, because their values are a requirement for the reaction, i.e. LRP6 has to be in complex with WNT ('B') and phosphorylated ('P'). In contrast, the phosphorylation state of AXIN or the diffusion rate of LRP6 (depending on the location of LRP6) are not relevant for the reaction and may thus have arbitrary values. Accordingly these values have to be stored after the binding, so that these values are available for the dissociation reaction (R22a/b).

Further, note that the dissociation of the LRP6/AXIN complex (R22a/b) is supposed to mimic the recycling of the receptor/protein complex. Consequently in contrast to LRP6 and AXIN, WNT is not released, but consumed in this reaction.

```

// ++++++
// +++++ species definitions (number of attributes) +++++
// ++++++

Cell();
Membrane(1);
LR(2);
Wnt(0);
LRP6(5);
CK1y(2);
AXIN(2);
bCat();
Nuc();

// ++++++
// +++++ initial solution +++++
// ++++++

>>INIT[
  nWnt Wnt +
  nCells Cell[
    (1) Membrane(A)[
      nLR LR(radius,rho) +
      nLRP6 LRP6(1,ra_lrp,'uP','uB','f') +
      nCK1y CK1y(1,ra_ck)
    ]
    nAXINU AXIN('u','f') +
    nAXINP AXIN('p','f') +
    nbCat bCat +
    1 Nuc[nbCatNuc bCat]
  ]
];

// ++++++
// +++++ reaction rules ++++++
// ++++++

// **** Lipid Raft Dynamics ****

// (R1) LRP6 diffusion into lipid rafts
Membrane(A)[LR(radius,p)[s?]:l +LRP6(d,ra,phos,bindW,'f'):r +s_m?] ->
Membrane(A)[LR(radius,p)[LRP6(d*p,ra,phos,bindW,'f') +s?] +s_m?] @ k_1*#l*#r*ra;

// (R2) LRP6 diffusion out of lipid rafts
Membrane(A)[LR(radius,p)[LRP6(d,ra,phos,bindW,'f'):r +s?]:l +s_m?] ->
Membrane(A)[LR(radius,p)[s?] +LRP6(d/p,ra,phos,bindW,'f') +s_m?] @ k_2*#l*#r;

// (R3) CK1y diffusion into lipid rafts
Membrane(A)[LR(radius,p)[s_lr?]:l +CK1y(d,ra):r +s_m?] ->
Membrane(A)[LR(radius,p)[CK1y(d*p,ra) +s_lr?] +s_m?] @ k_3*#l*#r*ra;

// (R4) CK1y diffusion out of lipid rafts
Membrane(A)[LR(radius,p)[CK1y(d,ra):r +s_lr?]:l +s_m?] ->
Membrane(A)[LR(radius,p)[s_lr?] + CK1y(d/p,ra) +s_m?] @ k_4*#l*#r;

```

```

// **** Membrane Signalling ****

// (R5) Wnt production
Cell[s?] -> Wnt + Cell[s?] @ k_5;

// (R6) Wnt degradation
Wnt:w -> @ k_6*#w;

// (R7a) Binding of Wnt to LRP6 (representing Fz,LRP6 receptor complex)
Wnt:w+Cell[Membrane(A)[LRP6(diff,ra,'uP','uB','f'):l +s_m?] +s_c?] ->
Cell[Membrane(A)[LRP6(diff,ra,'uP','B','f') +s_m?] +s_c?] @ k_7a*#w*#l;

// (R7b) Binding of Wnt to raft-associated LRP6
Wnt:w+Cell[Membrane(A)[LR(radius,p)[LRP6(diff,ra,'uP','uB','f'):l +s_lr?]
+s_m?] +s_c?] -> Cell[Membrane(A)[LR(radius,p)[LRP6(diff,ra,'uP','B','f')
+s_lr?] +s_m?] +s_c?] @ k_7b*#w*#l;

// (R8) Dissociation of Wnt from LRP6 (representing Fz, LRP6 receptor complex)
Cell[Membrane(A)[LRP6(diff,ra,'uP','B','f'):l +sm?] +s_c?] ->
Cell[Membrane(A)[LRP6(diff,ra,'uP','uB','f') +sm?] +s_c?]+Wnt @ k_8*#l;

// (R9) Phosphorylation of activated LRP6 in LR
Membrane(A)[LR(radius,p)[CK1y(diff_ck,ra_ck):ck +
LRP6(diff_l,ra_l,'uP','B','f'):l +s_lr?] +s_m?] -> Membrane(A)[LR(radius,p)[
LRP6(diff_l,ra_l,'P','B','f') + CK1y(diff_ck,ra_ck) +s_lr?] +s_m?] @
k_9*#l*#ck / (3.14*radius*radius/A) * p;

// (R10) Dephosphorylation of LRP6
LRP6(diff,ra,'P','B','f'):l -> LRP6(diff,ra,'uP','B','f') @ k_10*#l;

// (R11) Recycling of Wnt/LRP6 complex (representing signalosome)
LRP6(diff,ra,'P','B',bind):l -> LRP6(diff,ra,'uP','uB',bind) @
if (bind=='f') then 0 else k_11*#w*#l;

// **** Beta-catenin signalling ****

// (R12) Basal AXIN autophosphorylation
AXIN('u','f'):a -> AXIN('p','f') @ k_12*#a;

// (R13) Basal AXIN dephosphorylation
AXIN('p','f'):a -> AXIN('u','f') @ k_13*#a;

// (R14) AXIN degradation
AXIN(phos,'f'):a -> @ k_14*#a;

// (R15) Activated  $\beta$ -catenin degradation
Cell[AXIN('p','f'):a + Bcat:b + s?]:c ->
Cell[AXIN('p','f') + s?] @ #c*((k_15*#a*#b));

// (R16) Beta-catenin synthesis
Cell[s?] -> Cell[Bcat + s?] @ #c*k_16;

// (R17) Basal  $\beta$ -catenin degradation
Bcat:b -> @ k_17*#b;

```

```

// (R18) Beta-catenin shuttling into the nucleus
Bcat:b + Nuc[s?] -> Nuc[Bcat + s?] @ k_19*#b;

// (R19) Beta-catenin shuttling out of the nucleus
Nuc[Bcat:b + s?] -> Bcat + Nuc[s?] @ k_12*#b;

// (R20) Beta-catenin driven AXIN synthesis
Nuc[Bcat:b + s?] -> Nuc[Bcat + s?] + AXIN('u', 'f') @ k_20*#b;

// **** AXIN LRP6 signalling ****

// (R21a) AXIN binding by LRP6 in membrane
AXIN(phos,'f'):a + Membrane(A)[LRP6(diff,ra,'P','B','f'):1] ->
Membrane(A)[AXIN(phos,$link) +LRP6(diff,ra,'P','B',$link)] @ ((k_21a*#l*#a));

// (R21b) AXIN binding by LRP6 in lipid rafts
AXIN(phos,'f'):a + Membrane(A)[LR(radius,p)[LRP6(diff,ra,'P','B','f'):1]]->
Membrane(A)[LR(radius,p)[AXIN(phos,$link) + LRP6(diff,ra,'P','B',$link)]] @
((k_21b*#l*#a));

// (R22a) Dissociation of receptor/AXIN complex (signalosome) in membrane
Cell[Membrane(A)[LRP6(diff,ra,'P','B',bind):1a +AXIN(phos,bind)]] ->
Cell[Membrane(A)[LRP6(diff,ra,'uP','uB','f')] +AXIN(phos,'f')] @
if (bind=='f') then 0 else (k_22a)*#1a;

// (R22b) Dissociation of receptor/AXIN complex (signalosome) in LR
Cell[Membrane(A)[LR(radius,p)[LRP6(diff,ra,'P','B',bind):1a +AXIN(phos,bind)]]]->
Cell[Membrane(A)[LR(radius,p)[LRP6(diff,ra,'uP','uB','f')]] +
AXIN(phos, 'f')] @ if (bind=='f') then 0 else (k_22b)*#1a;

```

LISTING 4.12: ML-Rules implementation of the combined WNT/ β -catenin model as depicted in Figure 4.6.

4.5 Concluding remarks

Here, we provide a rule-based model of WNT/ β -catenin signaling that, for the first time, combines intracellular and membrane-related processes including lipid rafts dynamics. However, we are well aware, that our model is a simplified representation of WNT/ β -catenin signaling. As for instance, it does not include any endocytotic processes, like recycling or the sequestration of the destruction complex inside multivesicular endosomes as currently discussed [141, 196]. Though our model does neither contradict nor exclude these hypotheses. Instead we concentrate on the fact, that phosphorylation of LRP6 is a raft-dependent process being crucial for canonical WNT/ β -catenin signaling as demonstrated by [173] and our investigations. LRP6 phosphorylation is a prerequisite for WNT-mediated endocytosis [196, 215].

Moreover, this model provides an ideal use-case to analyze how well model formalisms cope with the challenges imposed by a complex, but typical signal transduction pathway. This is because the WNT/ β -catenin model comprises most of the motifs (or modeling features), that occur in common signal pathways and that have been thoroughly discussed in Sec. 4.3.1. Notably, ML-Rules, the model formalism that has eventually been chosen to implement model, provides all the modeling features that were required to implement a hierarchical compartment-based model of raft-dependent WNT signaling. However, it should be emphasized that the model in its current form could have also been implemented in other rule-based formalisms as well. In particular BNGL provides solutions for nearly all modeling features present in the WNT/ β -catenin model. Though, in contrast to ML-Rules, the expressivity of BNGL is already stretched to its limits when it comes to the arbitrary rate kinetics that additionally depend on compartmental properties or dynamic structures.

In the presented WNT model arbitrary rate kinetics are in particular required to depict the change of the diffusion and reaction kinetics into and out of lipid rafts. This means reaction kinetics within the membrane do not only depend on the localization of the proteins, but in case of raft-associated proteins also on the lipid rafts characteristics, such as fluidity and size. As discussed in Sec. 4.3.2, the compartmental extension of BNGL, cBNGL, provides means for describing two dimensional compartments of arbitrary size and the respective changes in the reaction kinetics. Therefore different reaction kinetics between raft and non-raft regions can well be incorporated in cBNGL. However, since it is not possible to equip compartments with an own state, representing the kinetic changes due to the reduced mobility inside rafts appears already problematic and reasonable extension, like dynamic lipid rafts characteristics in terms of growth, fusion and fission give a cutting edge to this problem.

The same applies to dynamic compartments, which are e.g. required to represent processes like endocytosis and recycling. The current WNT model does not contain the endocytotic cycle - for reasons that will be explained in the following chapter. Its implementation in ML-Rules is straight forward though:

```
Cell[Membrane[LR[LRP6(diff, ra, 'P', 'B', bind):rec + AXIN(phos, bind)]]] ->
Cell[Membrane[LR[s_l?] + s_m?] + Endosome[LRP6(diff, ra, 'P', 'B', bind) +
AXIN(phos, bind)] + s_c?] @ if bind == 'free' then 0 else kEndo*#rec;

Cell[Endosome[LRP6(diff, ra, 'P', 'B', bind):e + AXIN(phos, bind)] + Membrane]->
Cell[Membrane[LRP6(1, 0.15, 'uP', 'uB') + s_m?] + s_c?]
@ if bind == 'free' then 0 else kRecycling*#e;
```

LISTING 4.13: ML-Rules specification for a simplistic endocytotic cycle that controls the recycling of the signalosome.

Whereas in (c)BNGL, due to the missing support of dynamics structures, complicated workarounds might be found that provide the desired functionality, but only at the great cost of model complexity, readability and eventually usability.

In summary, the model of lipid raft-dependent WNT signaling developed here greatly demonstrates two important aspects - 1. that considering spatial aspects and dynamic structures in signal transduction is of prime importance, and 2. that sophisticated modeling approaches are required to describe such complex model features in terms of assessable and (re-)usable models.

Chapter 5

Studying Raft-dependent WNT signaling in Neural Differentiation using an integrative in-vitro and in-silico approach

5.1 Background (Early differentiation in human neural progenitor cells)

WNT/ β -catenin signaling has been reported to be involved in the neuronal differentiation process of human neural progenitor cells (hNPCs) [92]. NPCs provide a new, promising basis for the in-vitro growth of neuron populations that can be used in replacement therapies for neurodegenerative diseases, such as Parkinson's or Huntington's diseases [34, 121]. However, controlling NPC differentiation in stem cell engineering demands a thorough understanding of neuronal and glial cell fate determination and its endogenous regulation.

To investigate WNT-signaling during the in-vitro differentiation a new cell line of immortalized human neural progenitor cells (ReNcell VM197) has been established [51, 89]. The ReNcell VM197 cell line was derived from the ventral mesencephalon region of a human fetal brain tissue and is characterized by a rapid differentiation. Upon growth factor removal ReNcell VM197 cells differentiate into neurons and glial cells within a few days and without any additional external stimulation. This allows to study WNT signaling in the context of cell fate commitment in a time dependent manner. A first characterization of ReNcell VM197 hNPC cell fate commitment uncovered a spatio-temporal regulation of WNT/ β -catenin key proteins, like LRP6, Dvl, Axin and β -catenin throughout the

entire phase of early differentiation [137]. However, the exact mechanisms that drive the WNT/ β -catenin signaling and therewith control the cell fate commitment in hNPC remain unclear.

To explore the potential mechanisms that drive the spatio-temporal regulation of β -catenin signaling during cell fate commitment we analyze the impact of lipid rafts disruption on WNT/ β -catenin signaling in untreated as well as raft-deficient human progenitor cells during early differentiation using a combined in-vitro and in-silico approach.

5.2 In vitro Exploration

In the following we describe experimental data, retrieved from ReNcell VM197 human progenitor cells. The ReNcell VM197 is a well-characterized cell line, that has been successfully applied in several studies and proven to be a simple and accepted model to investigate different aspects of neural differentiation [92, 113, 118, 119, 137]. The major advantage of this cell line is its rapid differentiation. Within three days after growth factor removal, ReNcell VM197 cells differentiate into neurons, astrocytes, and oligodendrocytes without any additional exogenous stimulation. We evaluate the impact of lipid raft disruption on WNT/ β -catenin signaling during differentiation by measuring the temporal progress of WNT signaling in terms of nuclear β -catenin concentrations in methyl- β -cyclodextrin-treated and untreated cells in the process of cell fate commitment. Accordingly proliferating ReNcell VM197 cells were used as reference (0h), whereas all following time points were measured after initiating the differentiation by growth factor removal. Note, that we only consider the first 12 hours after induction of differentiation. Typically most of the cells commit themselves for differentiation within the first 12 hours. Also, at later time points the cell population of ReNcell VM197 is already so heterogeneous due to differentiation, that potential signal activities may originate from multiple sources.

5.2.1 Materials and methods

Culture of neural progenitor cells and lipid rafts Disruption Our experimental results are retrieved from ReNcell VM 197 cells - a cell line, that is derived from the ventral midbrain of a 10-week-old human fetus and immortalized by retroviral transduction with v-Myc oncogene (ReNeuron Ltd, Guildford, UK). VM cells were cultivated according to the protocol described previously [89]. Briefly, cells were cultured in laminin coated cell culture flasks and maintained at 37°C with 5% in media containing DMEM/F12 supplemented with B27 media supplement, glutamine, heparin sodium salt and gentamycin (Invitrogen, Karlsruhe, Germany). Cells were kept in proliferative state

by applying 10 ng/mL basic fibroblast growth factor (bFGF, Invitrogen) and 20 ng/mL epidermal growth factor (EGF, Sigma-Aldrich, Steinheim, Germany). Every three to four days the cells were passaged, i.e. when a confluency reached $\sim 80\%$. Differentiation was initiated at a confluence of $\sim 70\%$ according to a standard differentiation protocol, i.e. cells were washed with HBSS, and new medium without growth factors EGF and bFGF was added [51]. For the continuous lipid rafts disruption throughout differentiation 2mM M- β -cyclodextrin (MbCD) was added to the differentiation medium. To exclude potential side effects caused by the MbCD treatment, proliferating cells were also treated 30 minutes in advance of fixation (Immunocytochemistry) or lysis (Western Blot).

Fixation and immunostaining for fluorescence microscopy Before fixation, lipid rafts were labeled with Vybrant lipid rafts labeling kit (Invitrogen). Cells cultured on coverslips were incubated with 0.5mM fluorescent Cholera Toxin B-Subunit (CT-B, Alexa 594) for 10 minutes at 4°C. After washing with PBS, cells were treated with anti-CT-B antibody (dilution 1:200) for another 10 minutes at 4°C. In the following fixation and immunofluorescence staining was performed as described previously [1]. Accordingly, cells were washed with PBS and fixed with 4% paraformaldehyde for 20 min (Sigma-Aldrich). To reduce non-specific binding, cells were treated with 1% gelatin. First, cells were labeled with rabbit anti-LRP6 (Santa Cruz, dilution 1:150) and subsequently incubated with Alexa Fluor 488 (Invitrogen, dilution 1:300). Afterwards, cell membranes were permeabilised with 0.2% Triton X-100 (Sigma-Aldrich) followed by labelling with mouse anti-active- β -catenin (Millipore, dilution 1:250) and subsequent incubation with Alexa Fluor647-conjugated anti-mouse secondary antibody (Invitrogen, dilution 1:300) and Hoechst for nuclei staining (Sigma-Aldrich, dilution 1:1000). Finally, cells were mounted on microscope slides using ProLong Gold antifade reagent (Invitrogen).

Western blotting Protein concentration was determined by Western blotting. Briefly cells cultured were washed twice with phosphate-buffered saline (PBS) and lysed in 29 sodium dodecyl sulfate (SDS) sample buffer followed by sub-cellular fractionation. Cell fraction lysates were separated by SDS-polyacrylamide gel electrophoresis (PAGE) using a 10% SDS polyacrylamide gel and proteins were transferred onto nitrocellulose membrane by electro blotting. For time-dependent β -catenin expression, the following anti-bodies were used: Anti-rabbit IgG (Cat. A9169; Sigma-Aldrich, dilution 1 : 80 000) and anti-mouse IgG (Cat. NA931V; GE Healthcare, Freiburg, Germany, dilution 1 : 10 000) antibodies conjugated with horseradish peroxidase were used and bound antibodies were detected with ECL Western blot detection reagent (GE Healthcare). Membranes were exposed to light-sensitive film and quantified by IMAGEJ software.

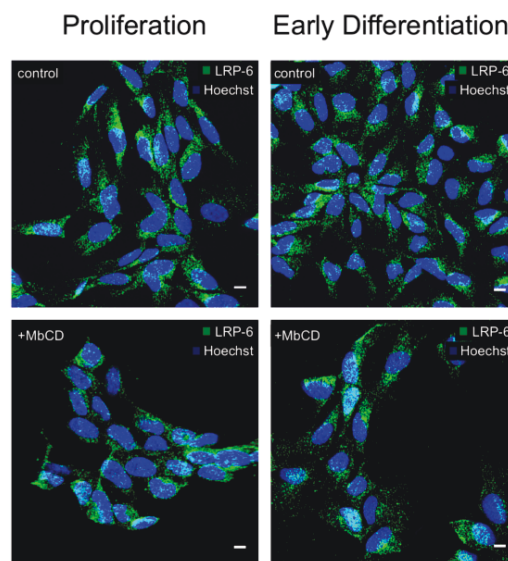


FIGURE 5.1: Confocal microscopy images of LRP6 staining (no Lipid Rafts staining) in proliferating and early differentiating cells. The first row shows untreated (control) cells, while cells depicted in the lower row are treated with 2mM MbCD. Scale bar $10\mu\text{m}$

5.2.2 Experimental Results

Lipid Rafts Disruption Before evaluating the potential impact of Lipid Rafts on WNT/ β -catenin signaling, we first show their existence in ReNcell VM197 cells and whether they can be disrupted by methyl- β cyclodextrin (MbCD) treatment. MbCD is commonly applied to disrupt the formation of lipid rafts by withdrawing cholesterol from the membrane. Previous studies reported an involvement of lipid rafts in the canonical WNT signaling pathway, but these studies were mainly based on detergent resistant membranes (DRM) and applied to proliferating cells, like HEK293 [155, 173, 183, 215]. For differentiating cells, however, lipid rafts and their impact on WNT/ β -catenin signaling have not been documented so far.

Indeed, fluorescence microscopy images of ReNcell VM197 cells stained with Vybrant lipid rafts labelling kit confirm the existence of lipid rafts also in human neural progenitor cells (see Fig. 1A). Further, signal intensity of lipid rafts staining is clearly reduced for cells treated with 2mM MbCD in comparison to untreated control cells. Treatment with 2mM MbCD thus successfully disrupts lipid rafts in ReNcell VM197 cells. Also MbCD has little to no effect on the lateral distribution of LRP6 in the membrane. LRP6 staining without application of Lipid Rafts staining shows a homogeneous distribution of LRP6 throughout the entire membrane for both control and MbCD-treated cells 5.1 This is in line with previous studies, that reported no specific partition of LRP6 into Lipid Rafts, but rather a homogeneous distribution among all membrane compartments [173, 215].

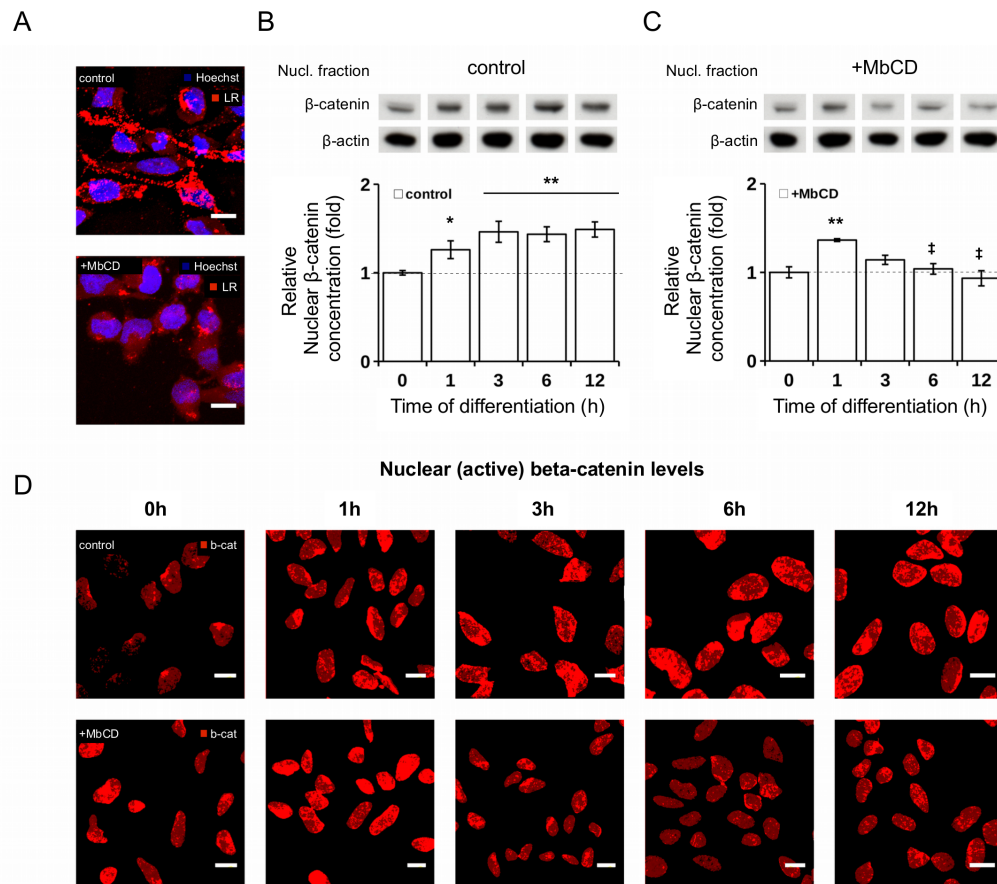


FIGURE 5.2: Impact of raft disruption on temporal regulation of nuclear β -catenin concentration after induction of differentiation in ReNCell VM197. (A) Confocal microscopy images of Lipid Rafts staining (red) in control (upper row) and raft-deficient, MbCD treated cells (lower row). Cell surface was stained with Vybrant Lipid Raft Labelling kit and nuclei were stained with Hoechst staining. Scale bar $10\mu\text{m}$. (B-C) Time-dependent relative concentration levels of nuclear β -catenin during differentiation with (C) and without (B) MbCD treatment. Graphs show data of four and three independent experiments for control and MbCD-treated cells, respectively, as mean \pm SEM, Student's t-test (* $p < 0.05$; ** $p < 0.01$; significant difference from 0h (proliferation); [‡] $p < 0.05$; significant difference between control and MbCD treated cells at specific time point), β -Actin was used a loading control. (D) Confocal microscopy images of nuclear β -catenin signal intensity in control and MbCD treated cells during differentiation confirm western blot data. Cells were labeled with anti- β -catenin antibody (red) and Hoechst Nuclei staining. Scale bar = $10\mu\text{m}$. For illustration purpose, only the β -catenin concentration within the nuclei are shown and other cell compartments, like cytoplasm and membrane are excluded from the view.

The impact of lipid raft disruption on β -catenin signaling in human neural progenitor cells

To determine the actual impact of lipid rafts on WNT signaling, we treated ReNcell VM197 cells with 2mM methyl- β cyclodextrin and measured the nuclear β -catenin concentration during early differentiation. Note that cholesterol depletion by MbCD is a concentration dependent and reversible process [161]. To assure a stable and continuous raft inhibition, we thus continuously exposed ReNcell VM197 cells to 2mM MbCD throughout the differentiation. The resulting effects in terms of the nuclear β -catenin concentration have been studied qualitatively by fluorescence microscopy and

quantitatively by Western Blot.

As a result we register a continuous β -catenin signal during differentiation for untreated cells, i.e. for all time points from 1h to 12h the measured nuclear β -catenin concentration is significantly higher as compared to proliferating cells (0h) (see Fig. 5.2 B, D). For the MbCD treated cells, however, we observe a significant increase of nuclear β -catenin at 1h, but no signal activity after that, i.e. the nuclear β -catenin concentration returns to its base line for the remaining time points (3 - 12 hours) (see Fig. 5.2 C, D). Apparently WNT/ β -catenin signaling is inhibited by raft disruption after 3 hours of differentiation, but not during the early immediate cell response at 1h. As demonstrated by earlier and recent studies, the deployment of lipid rafts from the plasma membrane prevents the raft dependent LRP6 phosphorylation and thereby inhibits the WNT induced receptor activation and subsequent signal transduction [155, 173]. This could explain the inhibition of WNT/ β -catenin signaling by MbCD treatment after 3 hours of differentiation. However, the early immediate activation at 1h in raft deficient cells remains puzzling. A delayed raft inhibition cannot be held responsible because MbCD treatment has an immediate effect on the deployment of lipid rafts from the plasma membrane [161]. From this we deduce that lipid rafts are successfully disrupted by MbCD treatment throughout the entire differentiation process and further conclude that, in accordance with previous studies, WNT/ β -catenin signaling is inhibited by lipid rafts disruption [155, 173], whereas the early immediate β -catenin activation at 1 hour was not affected by MbCD treatment for unknown reasons.

5.2.3 Discussion

The aim of the formerly described experiments was to confirm the existence and regulatory impact of lipid rafts on WNT/ β -catenin signaling in hNPCs as well as to obtain experimental data required to parametrize the raft-dependent WNT/ β -catenin model. Indeed, our experimental results confirmed both - lipid rafts are expressed in human neural progenitor cells and WNT/ β -catenin crucially depends on functioning lipid rafts. At the same time, however, our experimental results showed an early immediate β -catenin activation in raft-deficient cell, which is contradictory to the statements above.

What was thought as a control experiment now revealed further questions of what the mechanisms are involved in the spatio-temporal regulation of β -catenin signaling. In fact, chances are, that nuclear β -catenin levels are not exclusively regulated by canonical WN signaling during the early phase of differentiation. Instead a second signaling mechanism might be involved, that is independent of the raft-dependent WNT/ β -catenin pathway. To explore the signaling mechanisms of both, the continuous activation pattern in untreated and in particular the inexplicable early immediate response in raft-deficient

cells, we perform a number of simulation studies based on the formerly presented computational model of WNT signaling.

5.3 In silico Exploration

To explore the signaling mechanisms of both, the continuous activation pattern in untreated and in particular the early immediate response in raft-deficient cells, we perform a number of simulation studies. The simulation studies are based on a computational model of WNT signaling that has been derived in the previous chapter. The model will now be parametrized by using literature values and fitting routines, such that the model parameterization yields simulation trajectories that fit the experimental data, i.e. the measured nuclear β -catenin concentrations during the early phase of differentiation.

5.3.1 Experiment specification and execution

As indicated in the previous chapter, the WNT/ β -catenin model is based on the multi-level, rule-based modeling language ML-Rules. ML-Rules is implemented on top of the modeling and simulation framework JAMES II [85]. JAMES II is implemented in Java and provides various plug-ins to realize complex simulation experiments, e.g., for parameter optimization, sensitivity analysis, and output data storage [54]. In our experiments, we used the approximative τ -leaping simulator for ML-Rules [83] to speed up the simulation. We set up most experiments with the domain-specific language SESSL [55]. SESSL is based on the Scala programming language [154] and allows to concisely specify JAMES II experiments. In the following two typical experiment setups (a parameter scan and an optimization experiment) are described that illustrate the specification of simulation experiments in SESSL.

Parameter Scan

A typical SESSL experiment specifying a parameter scan is shown in SESSL Code 1. After importing basic language constructs (line 1) and the support for JAMES II (l. 2), we define a file to store the results (l. 4) and execute the simulation experiment (l. 6–30). The experiment supports the observation of model variables and a parallel execution, as declared in line 7. After specifying the model file to be used (l. 8), a full factorial parameter scan is set up in lines 11–17. For each parameter either a list of values is given (e.g. `kLWNTBind`), or an (inclusive) range of values is defined (e.g.

```

execute {
  new Experiment with Observation with ParallelExecution {
    model = "file-mlrj:/" + dir + "/Wnt_apCrine.mlrj"

    // Set model parameters for parameter scan:
    scan("kLWNTBind" < $\sim$ (0.01, 10, 1000))
    scan("kLWNTUnbind" < $\sim$ (0.05, 0.5, 5))
    scan("kApA_act" < $\sim$ (0.1, 0.5, 1, 5, 10))
    scan("kLA_diss" < $\sim$ (0.001, 0.01, 0.1, 1))
    scan("kLWNTBind" < $\sim$ (0.1, 10, 50, 100))
    scan("kLphos" < $\sim$ range(0.1, 0.1, 1))
    scan("kLdephos" < $\sim$ range(0.01, 0.01, 0.1))

    simulator = MLRulesReference()
    stopTime = 720
    replications = 15
    parallelThreads = 3
    observe("Cell/Nuc/Bcat()") // Observe species Bcat
    observeAt(range(1, 10, 720))
    withRunResult { results =>
      // Store results to file:
      modelOutput << results.trajectory("Cell/Nuc/Bcat()")
    }
  }
}

```

FIGURE 5.3

`kLphos`. In line 19, JAMES II is configured to simulate the model with the ML-Rules reference implementation (see [136]). Alternatively the faster τ -leaping variant from [83] could be used as well. Then, the simulation time at which each run shall stop (l. 20), the number of replications per parameter combination (l. 21), and the number of parallel threads (l. 22) is specified. Lines 23–24 state that model variable `Cell/Nuc/Bcat()`, i.e., the number of β -catenin molecules in the nucleus, shall be observed at fixed time points, again given as a `range` of values. The last lines of the experiment specification (l. 25–28) write, for each run, the observations for `Cell/Nuc/Bcat()` into the file specified in line 4.

Optimization

We use the Opt4J framework [129] to optimize the parameter values of our WNT model. An exemplary optimization experiment specification is shown in SESSL Code 2. All SESSL constructs shown in SESSL Code 1. have the same meaning as explained above. The execution of the actual simulation experiment is defined in lines 11–40. It is now embedded in the call to the optimization interface of SESSL, which allows to set up a minimization experiment by defining an anonymous function that takes two arguments, `params` and `objectives` (l. 10). The `params` object (l. 10) contains the current parameters of the objective function, retrievable via `params("name")` (l. 16), and can be used to set parameters of the simulation model. The argument `objectives` represents a container to store the values of the (potentially multivariate) objective function (l. 35).

Here, the objective to be minimized is the mean squared error between the simulated amount of β -catenin in the nucleus and the reference data from the wet lab (l. 8, 28–29), averaged over all replications (l. 20, 35). Note that the anonymous function to handle the results of all replications (l. 33–38) is called only once, after the last simulation replication is complete.

The second part (l. 41–53) of the optimization experiment specification determines which optimization software to use (l. 41), which parameters to optimize within which bounds (l. 42–43), and which optimization algorithm to rely on (l. 45). Optionally, Opt4J's graphical user interface allows to display intermediate results (l. 46). Again, event handlers are used to store the results of each optimization iteration (l. 47–49) and to print the overall results to standard output (l. 50–52).

```

val ref = Set(0, 7561, 8247, 7772, 7918, 7814, 7702)

minimize { (params, objective) => // Minimize the following function
  execute {
    new Experiment with Observation with ParallelExecution {
      model = "file-mlrj:/" + dir + "/WNT_apCrine.mlrj"

      // Set model parameters as defined by optimizer:
      set("kLphos" < $\sim$ params("p"))
      set("kLdephos" < $\sim$ params("d"))

      stopTime = 721
      replications = 10
      observe("Cell/Nuc/Bcat()")
      observeAt(range(0, 120, 720))

      var runResults = 0.0 // Variables for result aggregation
      var count = 0

      withRunResult(results => {
        val numbers = results.values("Cell/Nuc/Bcat()").asInstanceOf[Iterable[Long]]
        runResults += scala.math.sqrt(mse(numbers, ref))
        count += 1
      })

      withReplicationsResult(results => {
        // Store value of objective function:
        objective < $\sim$ runResults / count
        runResults = 0.0
        count = 0
      })
    }
  }
} using (new Opt4JSetup {
  param("p", 0.1, 0.1, 10) // Optimization parameter bounds
  param("d", 0.01, 0.001, 0.1)
  // Configure optimization algorithm:
  optimizer = sessl.opt4j.SimulatedAnnealing(iterations = 15)
  // showViewer = true //Switches on Opt4J GUI
  withIterationResults { results =>
    optOutput << results
  }
  withOptimizationResults { results =>
    println("Overall results: " + results(0)) // print results to stdout
  }
})

```

FIGURE 5.4

5.3.2 Model Parametrization

We use literature values as often as possible and fit the remaining parameters to experimental measurements of nuclear β -catenin dynamics during in-vitro differentiation of ReNcell VM 197 cells. To further test the calibrated/fitted model we apply cross-validation by reproducing existing in-silico and in-vitro data (measurements of β -catenin concentration under different WNT stimuli). However, we also have to verify whether the model predictions are still in accordance with experimental data when it comes to perturbations, like raft disruption.

Due to the lack of literature values, some parameter values, especially regarding the membrane model, had to be fitted by simulation experiments. The values of the fitted parameters are listed in *italics* in Table 5.1. The model itself is compartment-based, but for rate calculation we consider the membrane as a two-dimensional layer with lipid rafts being (immobile) circular-shaped entities within the membrane, whose radius and coverage control the rate of receptor-raft collision. In our model we set the radius and number of rafts such that $R_A = 25\%$ of the membrane surface is covered by lipid rafts [162]. First, we adjust the parameters related to the lipid raft/protein interaction, i.e. determine the fraction of LRP6 and CK1 γ that are associated to lipid rafts. Fortunately, the concentrations for raft associated LRP6 and CK1 γ have been determined in a previous study [173]. About 30% of LRP6 and 80-85 % of CK1 γ have been found in detergent resistant membranes (DRM). To match these experimentally measured values, we apply different raft affinity values for LRP6 and CK1 γ . Based on the values in 5.1, the system almost immediately reaches a stable equilibrium with the desired concentration of raft-associated proteins, as depicted in Fig. 5.5.

In addition several recent studies also revealed that CK1 γ dependent phosphorylation of LRP6 is confined to lipid rafts [155, 173]. We include this finding in our model by restricting the phosphorylation to rafts-associated proteins, i.e. only LRP6 that are located within a lipid raft may be phosphorylated by CK1 γ . Interestingly, without this constraint we were not able to determine a parameter configuration matching the simulation results to in vitro measurements. This means, the restriction of LRP6 phosphorylation to lipid rafts in the model is not only motivated by the aforementioned studies, but necessary to yield the dynamics observed in vitro.

In the following we fitted the remaining parameter values of the combined intracellular and membrane model against in vitro measurements we derived from human neuronal progenitor cells (ReNcell VM197). More details about the experimental data and in vitro experimentation are described in the previous Section and in the Material and Methods Section respectively. Briefly, we measured the temporal progress of endogenous WNT

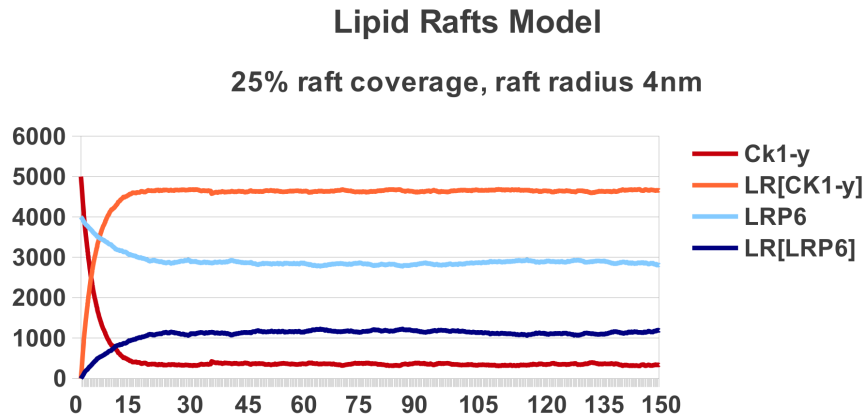


FIGURE 5.5: Simulation result for Raft/Receptor dynamics. Representative simulation trajectory demonstrating the separation of membrane bound Ck1 γ and LRP6 molecules into lipid rafts and non-raft regions depending on their individual raft affinity. In equilibrium $\sim 85\%$ of Ck1 γ molecules are located within rafts (LR[Ck1 γ]), whereas only $\sim 25\%$ LRP6 molecules are raft-associated (LR[LRP6]), which corresponds to experimentally derived values in [173].

signaling in terms of nuclear β -catenin concentration fold changes during early differentiation in ReNcell VM197 cells. Differentiation of ReNcell VM197 cells is induced solely by growth factor removal and proceeds without any additional external stimulation. The established parameter values of the fitting routine are listed in Table 5.1. As a result of the parameter adjustment, we were able to reproduce the temporal dynamics of nuclear β -catenin measured in ReNcell VM197 cells. Before we extensively discuss the simulation results, we first thoroughly validate the model and its current parametrization.

TABLE 5.1: **Parameter Table of the WNT/ β -catenin model.**

<i>Molecule Numbers</i>			
Species	Description	Value	Reference
WNT	WNT	220	
LRP6 (mem)	membrane-bound LRP6	4000	[6]
CK1y (mem)	membrane-bound CK1y	<i>5000</i>	
Beta-cat (cyt)	cytosolic β -catenin	12989	[116, 138]
Beta-cat (nuc)	nuclear β -catenin	5282	[116, 138]
Axin (cyt)	cytosolic AXIN	252	[138]
Axin-P (cyt)	cytosolic phosphorylated AXIN	219	[138]

<i>Raft Parameters</i>			
Raft Parameter	Description	Value	Reference
R in %	Raft coverage	25	[162]
R_r (a.u.)	Raft radius	4	[162]
R_ρ	Raft fluidity	<i>0.1</i>	
$R_\varphi(LRP6)$	Raft affinity LRP6	<i>0.15</i>	
$R_\varphi(CK1y)$	Raft affinity CK1y	<i>1</i>	
k_1	Raft entry of LRP6	<i>25.12</i>	
k_3	Raft entry of CK1y	<i>250.12</i>	
k_2/4	Raft exit	<i>25,12</i>	

<i>Reaction Rate Constants</i>			
Rule/Parameter	Description	Value	Reference
R5 / k_5	WNT production	<i>1.9</i>	
R5 /kW_delay	Delay for WNT production	<i>90</i>	
R6 /k_6	WNT degradation	<i>0.27</i>	
R7 /k_7	LRP6-WNT binding	<i>100</i>	
R8 /k_8	LRP6-WNT dissociation	<i>0.1</i>	
R9 /k_9	Phosphorylation of LRP6 by CK1y	<i>6.73E1</i>	
R10 /k_10	Dephosphorylation of LRP6	<i>4.7E-2</i>	
R11 /k_11	Dissociation of signalosome	<i>3E-4</i>	
R12 /k_12	Basal dephosphorylation of AXIN-P	0.03	[138]
R13 /k_13	Basal phosphorylation of AXIN	0.03	[138]
R14 /k_14	AXIN degradation	4.48E-3	[138]
R15 /k_15	AXIN-driven degradation of β -catenin	2.1E-4	[138]
R16 /k_16	β -catenin synthesis	600	[138]
R17 / k_17	basal degradation of β -catenin	1.13E-4	[116, 138]
R18 /k_18	β -catenin shuttling into nucleus	0.0549	[110, 138]
R19 /k_19	β -catenin shuttling out of nucleus	0.135	[110, 138]
R20 / k_20	AXIN synthesis	4E-4	[138]
R21 / k_21	LRP6-AXIN association	<i>5</i>	
R22 / k_22	LRP6-AXIN dissociation	<i>6.5E-4</i>	

Parameter and reference values of the WNT/ β -catenin model as depicted in Fig. 2.

Bold: literature values, *Italics:* fitted values.

5.3.3 Validation of the model

We validated the presented model of WNT/ β -catenin signaling against independent in-silico and in-vitro data [76, 116]. Thereby, we evaluated how the model reacts on transient and continuous WNT stimulation in comparison to already published data. For the transient stimulation we assume an initial amount of 250 WNT molecules that is degraded over time (see k.6 in Table 5.1). This resembles the simulation experiment performed by *Lee et. al.* based on their mathematical model of WNT/ β -catenin signaling. When comparing the simulation outcome of *Lee et. al.* and our model, it appears that the amplitude or excitation level of the transient signal activity, is similar in both models, but the corresponding temporal resolution differs significantly: In our model the peak of the activation curve (which translates to maximum β -catenin concentration) is reached at about 90 minutes and the base line is reached within five hours, while in the Lee model it takes about 5 hours to reach the peak and 16 hours to return to the base line, respectively (cf. Fig. 5.6). Apparently, the two models relate to a different temporal scale. However, we can adapt the temporal scale of our model by reducing *all* parameter values by a constant factor. Thereby the system's kinetics are slowed down, but the inherent system dynamics remain unchanged. To match the temporal level of the Lee model, we apply a constant factor of 2/7. The simulation results with the adapted model are depicted in Fig. 5.6 B and show a good fit between β -catenin concentration in our and in the Lee model over the course of time (Fig. 5.6 B). Thus our core model yields the same increase of β -catenin concentration in response to a transient WNT stimulus, as predicted by the Lee model when adapting the temporal scale. In this context, we would like to emphasize the rapid differentiation process of ReNcell VM197 cells. This cell line differentiates into neurons and glial cells within 72 hours after growth factor removal, which might explain the faster time scale of our model compared to the Lee model. To model the continuous WNT stimulation, however, we have to compensate the fact, that *in vitro* a single cell is faced with a constant concentration of WNT molecules. This means ligands consumed by the cell (e.g. by receptor binding, endocytosis or unspecific decay) can be immediately replaced by new ones from the bulk solution. This is not the case in our stochastic, single cell model, where we have molecule numbers instead of concentrations. Therefore we apply a production rule for extracellular WNT molecules (modeled as constant flux, R6) with varying rate values according to [76]. To avoid an over saturation of the system, i.e. the number of produced molecules is greater than its consumption, the execution of this *production rule* is restricted to WNT molecule numbers less than a given threshold. This restriction is reversible. Hence, the production of WNT is suspended once the number of WNT molecules exceeds a previously defined value (threshold ϵ), but resumed as soon as the molecule concentration falls below this threshold. For the given validation experiment, the threshold always corresponds to the

TABLE 5.2: **Table of varying WNT stimuli.**

[WNT] ng/ml	k ₁
1.56	0.3225
6.25	1.29
12.5	2.58
25	5.15
50	10.31
100	20.62
200	41.25
400	82.5

Varying WNT stimuli applied *in vitro* by *Hannoush* and corresponding input parameter (k₁) for model simulations. Concentration values have been recalculated to molecule numbers per available volume (membrane) (details see Text).

concentration of WNT molecules tested in the respective simulation run.

Given this slight modification of our model, we run several simulation experiments with the WNT concentrations listed in Tab. 5.2 and measured the rate of β -catenin accumulation after 2 hours of WNT stimulation [76].

Note, that *Hannoush* measured the accumulation in terms of fluorescence intensities instead of concentration or fold changes. We thus scaled the simulated β -catenin concentration values by a linear scaling factor to compare our simulation results with the experimentally derived values. Intriguingly our results (red line) almost perfectly match the experimental data obtained by *Hannoush* (blue line). Regardless of the applied WNT3a concentration, our model always predicts an equivalent β -catenin accumulation as obtained *in vitro* (see Fig. 5.6C). This is underpinned by the fact, that both unscaled data sets - *in silico* and *in vitro* - are significantly correlated ($P = 0.9963$, with p-value < 0.001). To summarize, our WNT/ β -catenin model, which has been fitted against experimental data retrieved from ReNcell VM197 cells solely, is capable of exactly reproducing β -catenin kinetics reported for different cell types and stimuli (transient and continuous WNT3a stimulation) [76, 116]. Consequently our WNT/ β -catenin model is not only in agreement with data published earlier, but conclusions about WNT/ β -catenin signaling drawn from ReNcell VM197 cells do not appear to be cell line specific and, hence, seem generally applicable.

5.3.4 Simulation results

Hidden biphasic activation pattern Before we analyze the effect of lipid rafts disruption on canonical WNT signaling and execute the corresponding simulations, let us take a closer look at the simulation results achieved so far. As previously mentioned, all

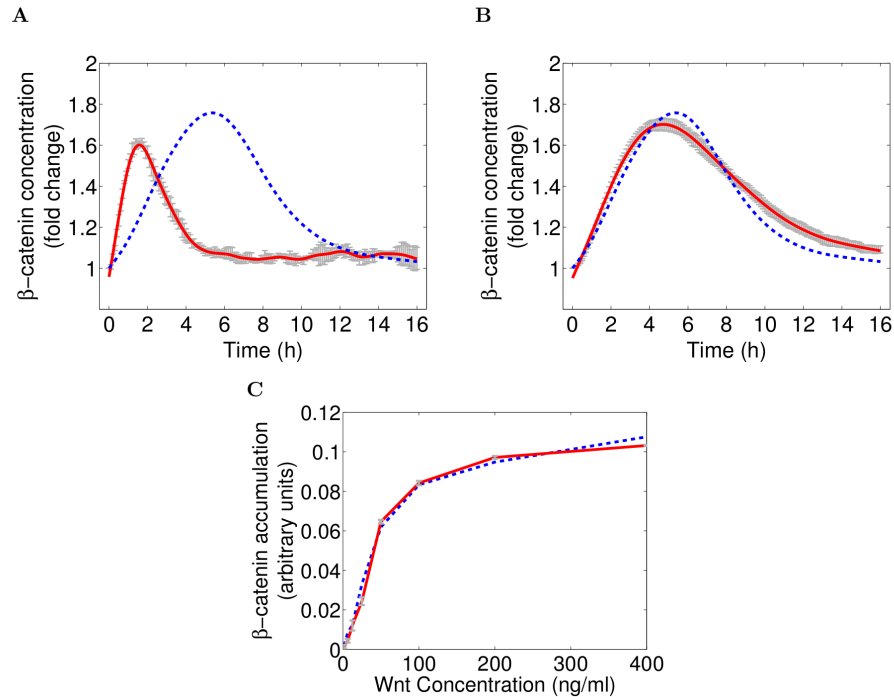


FIGURE 5.6: (A-B) Comparison of simulation results (β -catenin concentration fold change) between the newly derived WNT/ β -catenin signaling model (red line) and the Lee model (blue, dashed line) [116] in response to a transient WNT stimulus. Without adaptation both models expose a similar excitation level, but the temporal scale differs significantly (A). Adopting the temporal scale of our WNT/ β -catenin signaling model yields similar simulation results for both models (B).

(C) β -catenin accumulation after 2 hours of WNT stimulation with varying concentrations, compared between our simulation results (red line) and experimental in-vitro measurements by *Hannoush* (blue line)[76]. Parametrization of the β -catenin model is exactly the same as listed in Table 3.1, despite the WNT production rate (k_1), which has been parameterized in accordance to the varying WNT stimuli applied by *Hannoush*, cf. Table 5.2. The simulation results match almost perfectly with the experimental data for all WNT concentrations applied. Note that the in-silico β -catenin concentration values are scaled by a linear scaling factor to allow a comparison with the experimentally derived values, that measure the β -catenin accumulation based on fluorescence intensities, instead of concentration or fold changes. Simulation results for our model corresponds to mean simulation trajectory (red) with 95% confidence interval (gray error bars).

unknown parameter values were derived by fitting the model to our in vitro measurements of endogenous WNT signaling in ReNcell VM197 cells.

Considering the input parameter values that are required to reproduce our experimental data, it appears that only a model parametrized with an initial amount of WNT molecules ($nWNT = 90$) and a constant WNT synthesis rate ($k_1 = 1.9$) after a certain delay of 90 minutes yields the desired simulation result. The corresponding reaction rule was adapted as follows:

```
// (R5) Wnt production  
Cell[s?] -> Wnt + Cell[s?] @ if (simtime()>k_Wdelay) then k_5 else 0;
```

LISTING 5.1: ML-Rules specification of the delayed Wnt production.

This detail is of great importance, as it suggests that β -catenin accumulation is caused by two different *WNT stimuli* - an initial, transient trigger and a continuous, autocrine signal mechanism. It is the combination of these two WNT stimuli, that allows the cell to first generate an immediate response to the perturbation (removal of growth factor) and in the following to keep the activation on a constant, but moderately incremented level (cf. Fig. 5.7A). With regard to the continuous autocrine signal, our findings are in line with a previous study of our group, where we used a simplified computational model to provide evidence for the self-induced autocrine/paracrine WNT signaling in hNPCs [138]. Thus, our experimental and computational studies underpin our in silico derived hypothesis. In addition, several other studies describe continuous autocrine canonical WNT signaling in the context of neural stem cells [212] and cancer [71, 175].

In contrast, it is not entirely clear where the immediate, transient WNT stimulus might originate from. Possible explanations are that cytosolic vesicles fuse with the membrane in order to spontaneously release a certain amount of WNT molecules [39], and that the initial stimulus is a direct result of crosstalk with growth factor pathways [96].

5.3.5 Discussion

For raft-deficient cells, the simulation trajectory does not show any signal intensity, i.e. the nuclear β -catenin concentration stays at its base line (cf. Fig. 5.7B). This behaviour seems only natural, because in our model the MbCD treatment translates to a complete removal of lipid rafts, which in turn prevents the raft-dependent LRP6 phosphorylation by $CK1\gamma$ in response to a WNT stimulus [173]. Thus WNT molecules may still bind, but the receptor activation and hence the transduction of the extracellular WNT signal is blocked. As a result we would expect a complete inhibition of WNT signaling when disturbing lipid rafts, as predicted by our model.

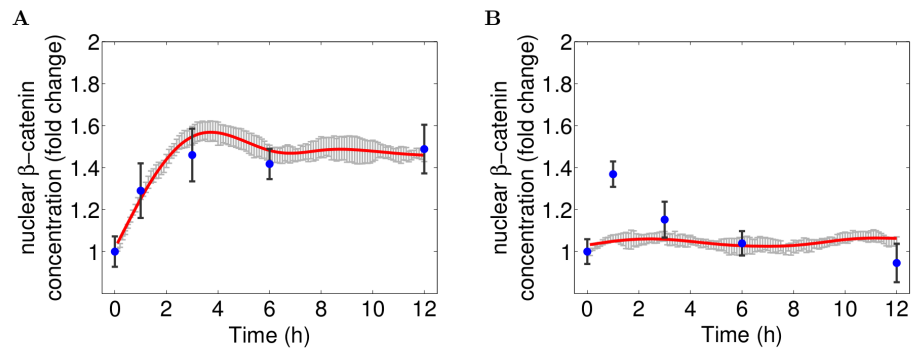


FIGURE 5.7: Nuclear β -catenin concentration fold changes in comparison between experimental data and the validated WNT/ β -catenin model. The simulation result (red) of the WNT/ β -catenin model (cf. Fig. 2, parametrized according to Table 1) matches all experimental values (blue) in untreated control cells (A). Though, in its current state it is not capable of reproducing the immediate early β -catenin activation in raft-deficient cells (B). Simulation results correspond to the mean simulation trajectory (red) with 95% confidence interval (gray error bars).

Though, western blot as well as fluorescence microscopy data indicate a significant increase of nuclear β -catenin at one hour of differentiation for raft deficient cells (see Fig. 5.2C-D). This implies a successful activation of WNT/ β -catenin signaling for this time point, despite lipid rafts disruption. As the deployment of lipid rafts primarily affects membrane-related processes, like the WNT-induced phosphorylation of LRP6, it stands to reason that the activation of β -catenin signaling in raft deficient cells is likely caused by an alternative WNT/LRP6-independent signaling mechanism. Pursuing this line of thought further: What if the early immediate cell response in raft-deficient *and* control cells was triggered by one and the same signaling mechanism, that is completely independent of membrane-related processes and therefore unaffected by raft disruption? In such a scenario, we would find characteristic upstream WNT signaling components already being inactive in untreated control cells with simultaneous (nuclear) β -catenin accumulation. Indeed, earlier studies on the same cell line, provide experimental data, that show these dynamics for the early immediate cell response in untreated ReNcell VM197 cells: p-LRP6 was found to be NOT significantly increased during the early time points (0-3 hours), while β -catenin shows the ascribed transient activation (cf. [137]). At the same time, the positive control confirmed that cells are responsive to WNT stimulation, i.e. transient WNT3a treatment yields a significant increase of p-LRP6 within the membrane. This means in the undisturbed case, β -catenin stabilization is observed, even though upstream WNT signaling components are inactive, but functional. This apparent contradiction clearly underlines our hypothesis of WNT-independent signaling stabilizing and translocating β -catenin into the nucleus. On the one hand, this result corroborates our hypothesis that lipid raft dependent, autocrine WNT signaling induces

the continuous β -catenin activation. On the other hand our results raise the question what mechanism triggers the early immediate cell response at 1 hours?

5.4 Concluding remarks

Here we used the previously derived model of raft-dependent WNT signaling to investigate the mutual influence of lipid rafts on WNT-signaling in the process of cell fate commitment in hNPCs. The model was fitted to experimental data derived from human neural progenitor cells (ReNCell VM 197) and has been extensively validated against in-vitro and in-silico data under a wide range of varying conditions. During our investigations we found that lipid raft disruption by Methyl- β -Cyclodextrin (MbCD) effectively inhibits WNT/ β -catenin signal transduction. This implies that raft disruption serves as an effective inhibitor for WNT/ β -catenin signaling in our cell line.

Surprisingly we found that immediately after the initiation of differentiation, raft-deficient cells still show a transient β -catenin signaling activity. This result has been confirmed by our simulation studies and raises the question what triggers the early immediate response despite the apparent WNT/ β -catenin signaling inhibition? This question will be answered in the following chapter, again based on a combined in vitro and in silico approach.

Chapter 6

Endogenous Reactive Oxygen Species induce early immediate beta-catenin activation in a WNT-independent manner

In the previous chapter we demonstrated, that the combined membrane and axin/ β -catenin model captures relevant processes of canonical WNT signaling and is able to predict the WNT/ β -catenin dynamics in response to arbitrary WNT stimuli of untreated cells with undisturbed lipid rafts. Though, the model is not capable of reproducing the transient activation in raft-deficient cells (see Fig. 5.7 B). To predict this apparently WNT-independent signal, the present WNT/ β -catenin model has to be extended by a presumably intracellular mechanism.

In fact, a recent study with the same cell line uncovered a transient endogenous, WNT-independent activation of WNT/ β -catenin signaling through reactive oxygen species (ROS), that occurs in direct response to the initiation of differentiation through growth-factor removal [166]. Thereby the removal of growth factors induces an increase of intracellular ROS levels, which in turn releases a redox-sensitive binding between NRX and DVL. The sudden increase of unbound DVL promotes a DVL-mediated stimulation of the downstream WNT/ β -catenin signal transduction, which eventually leads to the well known β -catenin accumulation in the nucleus.

Apparently this newly uncovered ROS-mediated beta-catenin pathway could provide a

suitable explanation for the immediate transient beta-catenin activation. In the following we evaluate, whether an interplay between the redox-dependent ROS/- and raft-dependent WNT/ β -catenin pathway is a suitable hypothesis to explain our data. Therefore we extend the current WNT/ β -catenin model by the ROS mediated beta-catenin pathway proposed by [166] and perform further experiments in silico and in vitro.

6.1 Involvement of Reactive Oxygen Species in WNT signaling

While extensive Reactive Oxygen Species (ROS) stimulation may cause oxidative stress and cell damage, it is meanwhile well accepted, that ROS can also act as intracellular messenger inducing redox-sensitive signal transductions when present at physiological concentrations [75]. Apparently this also accounts for canonical WNT signaling. Several experimental studies have demonstrated that ROS can induce a redox-dependent activation of WNT/ β -catenin signaling. *Funato et. al.* reported a robust activation in response to exogenous ROS stimulation in proliferating cells [63], while *Love et. al.* showed that injury-induced ROS is required to activate WNT/ β -catenin pathway in the context of cell regeneration [127].

Redox-dependent activation of beta-catenin through Reactive Oxygen Species

The first to report an involvement of ROS in the regulation of WNT/ β -catenin signaling were *Funato et. al.*. They found that exogenous ROS stimulation yields a robust beta-catenin activation in proliferating cells [63]. According to the data of *Funato et. al.*, a large cytoplasmic pool of DVL is kept inactive due to being [covalently] bound to Nucleoredoxin (NRX), a ubiquitously expressed member of the thioredoxin antioxidant superfamily. ROS treatment leads to a redox-dependent release of DVL from its complex with NRX, which results in the stimulation of downstream WNT/beta-catenin signaling events. The findings of *Funato et. al.* therefore suggest that changes in intracellular ROS levels might positively regulate WNT/ β -catenin signaling by modulating DVL availability in the cytosol.

Related study reveals CA^{2+} -induced ROS production in response to growth factor removal in hNPC

In a recent study with the same cell line, an endogenous, WNT-independent activation of WNT/ β -catenin signaling through reactive oxygen species (ROS) was discovered [166]. Thereby growth factor removal, which induces differentiation in ReNCell VM197, induces an 1,4,5-triphosphate receptor (IP3R)-dependent CA^{2+} -efflux from the Endoplasmatic Reticulum (ER) [33, 206]. Consequently CA^{2+} flood the cytosol and also enter the mitochondria within the first half hour of differentiation [166]. The increase of mitochondrial CA^{2+} levels stimulates the production ROS within the mitochondria. After 30 to 60 minutes the mitochondrial ROS levels significantly increase and ROS start to efflux into the the cytosol, hence changing the cellular redox state. To neutralize the oxidative stress resulting from the ROS influx, redox pathway related proteins, like NADPH oxidase, superoxide dismutase and Catalase are activated [17, 98, 159]. However, ROS are also targeted by a specific member of the thioredoxin-related redox-regulating protein family, termed Nucleoredoxin (NRX). This is particularly noteworthy, because the reduced form of NRX has a strong affinity to DVL, i.e. a large pool of DVL is bound to NRX in a redox-sensitive manner. The cytoplasmic ROS influx thus leads to the oxidation of reduced NRX, therewith releasing the redox-sensitive binding of NRX and DVL [63]. According the concentration of NRX and DVL significantly increases in hNPCs after one hour of differentiation [166]. FRET studies further confirmed that the measured concentration fold change of unbound NRX and DVL occurs concomitantly with the ROS-dependent release of NRX/DVL complex. - In the following cytoplasmic DVL leads to the activation of downstream beta-catenin signal pathway, yielding a transient accumulation of beta-catenin during 1-3 hours of differentiation. The spontaneous release of DVL through ROS apparently mimics an overexpression of DVL, which has been demonstrated to trigger WNT/ β -catenin signaling, bypassing the requirement for WNT ligands [63, 65, 181].

To summarize, an increase of the intracellular ROS level releases the redox-sensitive binding between NRX and DVL, hence promoting a DVL-mediated stimulation of the downstream WNT/ β -catenin signal transduction, which eventually leads to the well known β -catenin accumulation in the nucleus.

6.2 In silico exploration - extending the WNT model

To evaluate, whether an interplay between redox- and lipid raft dependent, autocrine WNT/ β -catenin activation is a suitable hypothesis to explain our data, we extend our model with a redox-dependent/ β -catenin pathway. Since quantitative experimental data is rarely available, we base our model upon the findings of *Funato et. al.* and the recent experimental results of [166].

We refer to the model component, by which the current WNT/beta-catenin model will be extended, as the ROS/DVL model. For the extension of the WNT model we follow a similar approach as for the WNT model. Accordingly we first describe the qualitative structure of the ROS/DVL model (in terms of ML-Rules rule sets) and on what assumptions it is based on. Afterwards the ROS/DVL model is parameterized in order to fit the dynamics determined by *Rharass et. al.* and gradually connected with components of the WNT model while verifying that none of the original dynamics are disrupted. Eventually the ROS/DVL model extension is completely integrated into the existing WNT model allowing further simulation studies to analyze the dynamics of the combined model.

6.2.1 Extending the existing WNT model by endogenous ROS signaling

Model assumptions Due to the limited source of studies analyzing the impact of ROS signaling on the canonical WNT pathway, we primarily base our model assumptions on the work of *Funato et. al.* and *Rharass et. al.*. Since there's almost no quantitative data available for the Ros/DVL pathway described by *Rharass et al*, almost all parameters of the model extension, like initial concentration and reaction rate constants, have to be fitted. Therefore we aim to keep the ROS/DVL model as simple as possible, i.e. reducing the amount of unknown parameter values to the smallest value, while retaining the essential dynamics. In the model we consider three processes that are crucial for the ROS-mediated beta-catenin activation, apparently: 1. The activation/increase of cytoplasmic ROS levels in response to initiation of differentiation; 2. the ROS-mediate release of the NRX-DVL complex; 3. the DVL-induced activation of down-stream WNT/beta-catenin signaling. This means, we particularly omit the detailed molecular mechanisms that lead to the transient increase of mitochondrial ROS production and its subsequent release to the cytosol. Even though being thoroughly studied and described in [166], the numerous processes involved in the CA^{2+} -mediated pathway (as described in the previous section) would largely increase the complexity of the model. Instead the transient increase in cytoplasmic ROS level is represented by a

single first order reaction with a certain delay to account for the time required to pass the CA^{2+} mediated pathway.

Next we consider the redox-dependent binding of NRX to DVL. According to the available experimental data, in particular FRET studies in [166], a rather large pool of DVL molecules is bound by NRX before and shortly after the initiation of differentiation. As soon as the mitochondrial ROS floods the cytoplasm, the NRX/DVL complexes get dissociated, spontaneously releasing the stored pool of cytoplasmic DVL molecules. However, we assume that the oxidation of NRX and its release from DVL are reversible, i.e. after a certain amount of time, NRX returns to its reduced state and rebinds DVL with high affinity.

Finally, a mechanism has to be identified that connects the ROS/DVL model component with the WNT/beta-catenin model. While the clear causal relation between ROS signaling and nuclear beta-catenin accumulation has been demonstrated in vitro [166], the mechanism by which the ROS-mediated increase of cytosolic DVL activates down-stream WNT/beta-catenin signaling is yet unclear. Here we refer to the work of *Schwarz-Romond and Fiedler et. al.* ([60, 180]) who uncovered the ability of DVL molecules to self-accumulate and further compete for the Axin polymerization interface, hence inhibiting its original effector function in the destruction complex (cf. 4.1). Accordingly we assume that unbound, cytosolic DVL molecules accumulate into polymers, and that these activated DVL polymers are capable of binding and inhibiting Axin. As consequence of the DVL/Axin binding, beta-catenin accumulate and shuttles into the nucleus. This process circumvents the need for extracellular WNT molecules and the signalosome formation.

To summarize, in our model we assume that approximately 30 minutes after the induction of differentiation, ROS molecules are (rapidly) released into the cytosole. Cytosolic ROS interfere with the redox-sensitive binding of DVL and NRX, leading to a sudden increase of unbound, cytosolic DVL molecules. The increased local concentration of DVL in turn facilitates the formation of DVL polymers, which then bind and inhibit Axin. This leads to a WNT-independent accumulation of beta-catenin in both cytosole and nucleus.

Molecules and interactions In the following we give a detailed description of the ROS/DVL model, its containing species, their interaction and how the model is integrated in the current WNT/beta-catenin model. Similar to the previous chapters the implementation in ML-Rules will be illustrated in terms of exemplary rule definitions.

ROS production

As motivated in the previous paragraph, the events that lead to the cytoplasmic increase of ROS particles after growth factor removal will be [omitted] in the current implementation. Instead, to initiate ROS/ β -catenin signaling, we introduce a transient ROS signal at the beginning of differentiation [166], which is described by the following rule.

```
// (R25) Release of Ros molecules from Mitochondria
Cell[Mito[ROS]:r] -> Cell[Mito[] + ROS] @
if (simtime() > k_Rdelay) then k_25*#r else 0;
```

LISTING 6.1: Simplified ML-Rules specification for initial ROS activation

In fact, rule 6.1 does not produce, but rather activates a pool of existing, inactive ROS species. Thereby, we can apply a first order reaction, that represents the spontaneous, but transient increase of cytoplasmic ROS, that has been determined in the wet-lab experiments.

Interaction of NRX and DVL

Next, we consider the interaction between NRX and DVL. The most important characteristic of NRX in the context of the ROS/DVL model is its redox state. In the stable (non-active) state, NRX is reduced (attribute values 'n0' vs '0' represent the reduced and non-reduced state of NRX respectively) and may bind to DVL.

```
// (R27) Binding of DVL by NrX
Cell[DVL(a,'f'):d + NrX('n0'):n] -> Cell[DVLNrX] @ k_27*#d*#n;

// (R28) Basal dissociation of DVL from NrX
DVLNrX:dn -> DVL('i','f') + NrX('n0') @ k_28*#dn;
```

LISTING 6.2: Simplified ML-Rules specification for the basal interaction, i.e. binding and unbinding of reduced NRX and DVL

Note, that only reduced NRX has strong affinity to DVL, i.e. may bind to it, which is why rule (R27 6.2) explicitly restricts the binding (reaction) of NRX to DVL to reduced NRX species (NrX('nO')).

The redox state of NRX is modified by ROS through oxidation. The oxidation of NRX can either affect unbound NRX (R26a), or more importantly the NRX-DVL complex (R26). The latter results in the dissociation of the NRX-DVL complex, yielding unbound (inactive) DVL and (oxidized) NRX. After some time NRX returns to its reduced state

(R26b, 6.3) and hence regains the ability of (re-)binding DVL (R27, 6.2).

```
// (R26) Dissociation of DVL from NrX by Ros
Cell[DVLNrX:dn + Ros:r] -> Cell[DVL('i','f') + NrX('0')] @k_26*#dn*#r;

// (R26a) Oxidation of NrX by Ros
Cell[NrX('n0'):n + Ros:r] -> Cell[NrX('0')] @ k_26a*#n*#r;

// (R26b) Reduction of NrX
NrX('0'):n -> NrX('n0') @ k_26b*#n;
```

LISTING 6.3: Simplified ML-Rules specification for the impact of ROS on NRX and its interaction with DVL

DVL activation and interaction with Axin

As mentioned previously, due to the property of DVL to self-associate in a reversible and concentration-dependent manner (R29/R30, 6.4), DVL forms self-assemblies that serve as dynamic recruitment platform for AXIN [60, 181]. However, activated DVL may also be targeted and bound by reduced NRX. This reaction is implicated in rule (R27, 6.2) due to the unspecified attribute of DVL.

```
// (R29) Activation (by e.g. aggregation) of DVL
DVL('i', 'f'):d -> DVL('a','f') @ k_29*#d;

// (R30) Dynamic deactivation of DVL
DVL('a','f'):d -> DVL('i','f') @ k_30*#d;
```

LISTING 6.4: Simplified ML-Rules specification for the activation and inactivation of DVL

Eventually activated DVL binds Axin in a reversible manner (R31/32, 6.5). The binding of DVL and Axin interferes with the regulatory function of Axin. Thereby DVL crucially influences the dynamics of the WNT/ β -catenin model. Thus, rule (R31/R32, 6.5) connects the ROS/DVL model component and the remaining part of the WNT/ β -catenin model.

```
// (R31) Axin binding by activated DVL
Cell[DVL('a','f'):d + Axin(phos,'f','f'):a] ->
Cell[DVL('a', $link) + Axin(phos, 'f', $link)] @k31*#d*#a;

// (R32) Axin DVL unbinding
Cell[DVL('a',bind):da + Axin(phos,'f',bind)] ->
Cell[DVL('a','f') + Axin(phos,'f','f')] @ if (b=='f') then 0 else k32*#da;
```

LISTING 6.5: Simplified ML-Rules specification for interaction of activated DVL and Axin

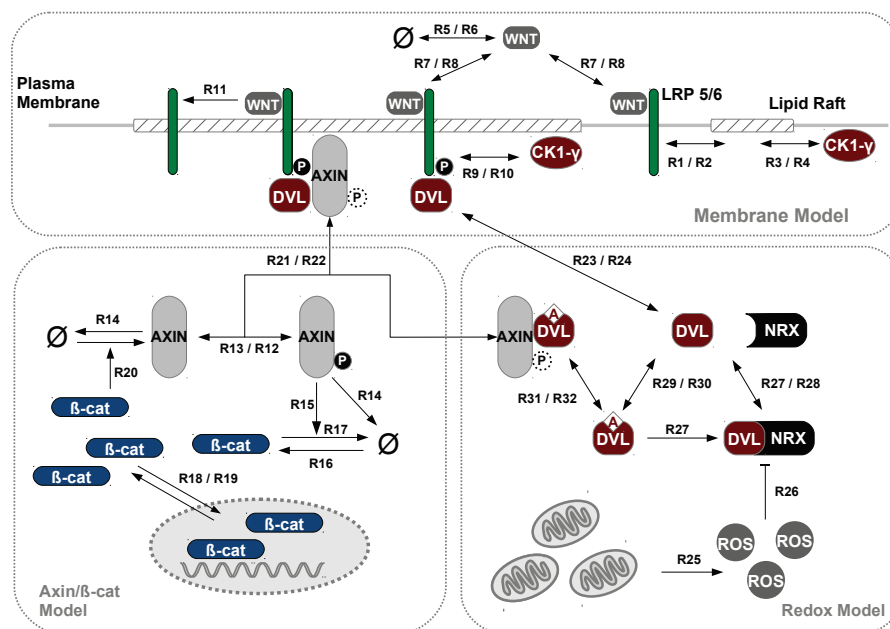


FIGURE 6.1: Schematic view of the extended WNT/ β -catenin model illustrating the potential interplay between WNT/ β -catenin- and DVL-mediated ROS/ β -catenin signaling. In addition to the previous model (cf. Figure 4.6), the newly introduced WNT-independent redox-signaling is depicted in the lower right. Two-sided arrows indicate reversible reactions. Dashed phosphorylation signs indicate that the depicted protein complex (i.e. AXIN/DVL and AXIN/DVL/LRP6) and the corresponding reactions occur independently of the phosphorylation state. The corresponding reaction rate constants are listed in Table 5.1, Table 6.1 and Table 6.2.

The entire model including the extension of the newly derived, redox-dependent model component, is depicted in Fig. 6.1 and the entire model implementation in ML-Rules in Listing 6.7. At this point, we'd like to emphasize another reaction that was additionally introduced when connecting the ROS/DVL with the WNT/ β -catenin model. In the WNT/ β -catenin model the role of DVL involved in the recruitment and binding of Axin to pLRP6 is neglected [11, 152]. However, due to the ROS/DVL extension, DVL has become an explicit and crucial entity in the newly combined model and cannot be disregarded anymore (cf. Fig. 6.1). Therefore we add an additional set of rules that describes the DVL-mediated unspecific, reversible phosphorylation of LRP6 prior to the binding of Axin. In fact, DVL does not *directly* interact with LRP6, but rather provides the binding platform for kinases like GSK3 β and CK1 α . Nevertheless we represent this process as *direct* interaction between DVL and LRP6 for the reason of simplicity.

```
// (R23) Binding of DVL to LRP6/WNT complex
Cell[Membrane[LR(radius, p)[LRP6(diff, ra, 'uP', 'B', bind):1]] + DVL(a, 'f'):d]
-> Cell[Membrane[LR(radius, p)[LRP6(diff, ra, 'dP', 'B', bind)]]] @ k_23*#1*#d;

// (R24) Unbinding of DVL from LRP6/WNT complex
Cell[Membrane[LR(radius, p)[LRP6DVL(diff, ra, 'dP', 'B'):1]] ->
Cell[Membrane[LR(radius, p)[LRP6(diff, ra, 'uP', 'B')]] + DVL('i', 'f')] @ k_24*#1;
```

LISTING 6.6: Simplified ML-Rules specification for unspecific interaction of DVL and LRP6 prior to Axin binding

Note, that the interaction between DVL and LRP6 occurs independently of the activation state of DVL (cf. rule (R23) in 6.6). Moreover, the rule specifying the subsequent binding of Axin has to be adapted as well, as the DVL-mediated phosphorylation of LRP6 is a prerequisite for the binding of Axin. A fact that could be neglected in the WNT/beta-catenin model, because the DVL-mediated phosphorylation of LRP6 is rather unspecific and does not necessarily depend on WNT stimulation [152].

```

// ++++++
// +++++ species definitions (number of attributes) +++++
// ++++++

Cell();
Mito();
Membrane(1);
LR(2);
Wnt(0);
LRP6(5);
CK1y(2);
AXIN(3);
bCat();
Nuc();
Dvl(2);
Nrx(1);
DvlNrx();
Ros(1);

// ++++++
// +++++ initial solution +++++
// ++++++

>>INIT[
  nWnt Wnt +
  nCells Cell[
    (1) Membrane(A)[
      nLR LR(radius, rho) +
      nLRP6 LRP6(1, ra_lrp, 'uP', 'uB', 'f') +
      nCK1y CK1y(1, ra_ck)
    ]
    nAXINU AXIN('u', 'f', 'f') +
    nAXINP AXIN('p', 'f', 'f') +
    nbCat bCat +
    (nDvl) Dvl('i', 'f') +
    (nNrx) Nrx('n0') +
    (nDvlNrx) DvlNrx +
    (1) Nuc[nbCatNuc bCat] +
    (1) Mito[(nRos) Ros] +
  ]
];

// ++++++
// +++++ reaction rules ++++++
// ++++++

// **** Lipid Raft Dynamics ****

// (R1) LRP6 diffusion into lipid rafts
Membrane(A)[LR(radius,p)[s?]:l +LRP6(d,ra,phos,bindW,'f'):r +s_m?] ->
Membrane(A)[LR(radius,p)[LRP6(d*p,ra,phos,bindW,'f') +s?] +s_m?] @ k_1*#l*#r*ra;

// (R2) LRP6 diffusion out of lipid rafts
Membrane(A)[LR(radius,p)[LRP6(d,ra,phos,bindW,'f'):r +s?]:l +s_m?] ->

```

```

Membrane(A)[LR(radius,p)[s?] +LRP6(d/p,ra,phos,bindW,'f') +s_m?] @ k_2*#1*#r;

// (R3) CK1y diffusion into lipid rafts
Membrane(A)[LR(radius,p)[s_lr?]:l +CK1y(d,ra):r +s_m?] ->
Membrane(A)[LR(radius,p)[CK1y(d*p,ra) +s_lr?] +s_m?] @ k_3*#1*#r*ra;

// (R4) CK1y diffusion out of lipid rafts
Membrane(A)[LR(radius,p)[CK1y(d,ra):r +s_lr?]:l +s_m?] ->
Membrane(A)[LR(radius,p)[s_lr?] + CK1y(d/p,ra) +s_m?] @ k_4*#1*#r;

// **** Membrane Signalling ****

// (R5) Wnt production
Cell[s?] -> Wnt + Cell[s?] @ k_5;

// (R6) Wnt degradation
Wnt:w -> @ k_6*#w;

// (R7a) Binding of Wnt to LRP6 (representing Fz,LRP6 receptor complex)
Wnt:w+Cell[Membrane(A)[LRP6(diff,ra,'uP','uB','f'):l +s_m?] +s_c?] ->
Cell[Membrane(A)[LRP6(diff,ra,'uP','B','f') +s_m?] +s_c?] @ k_7a*#w*#1;

// (R7b) Binding of Wnt to raft-associated LRP6
Wnt:w+Cell[Membrane(A)[LR(radius,p)[LRP6(diff,ra,'uP','uB','f'):l +s_lr?]
+s_m?] +s_c?] -> Cell[Membrane(A)[LR(radius,p)[LRP6(diff,ra,'uP','B','f')
+s_lr?] +s_m?] +s_c?] @ k_7b*#w*#1;

// (R8) Dissociation of Wnt from LRP6 (representing Fz, LRP6 receptor complex)
Cell[Membrane(A)[LRP6(diff,ra,'uP','B','f'):l +sm?] +s_c?] ->
Cell[Membrane(A)[LRP6(diff,ra,'uP','uB','f') +sm?] +s_c?]+Wnt @ k_8*#1;

// (R9) Phosphorylation of activated LRP6 in LR
Membrane(A)[LR(radius,p)[CK1y(diff_ck,ra_ck):ck +
LRP6(diff_l,ra_l,'dP','B','f'):l +s_lr?] +s_m?] -> Membrane(A)[LR(radius,p)[
LRP6(diff_l,ra_l,'P','B','f') + CK1y(diff_ck,ra_ck) +s_lr?] +s_m?] @
k_9*#1*#ck / (3.14*radius*radius/A) * p;

// (R10) Dephosphorylation of LRP6
LRP6(diff,ra,'P','B','f'):l -> LRP6(diff,ra,'uP','B','f') + Dvl('i') @ k_10*#1;

// (R11) Recycling of Wnt/LRP6 complex (representing signalosome)
LRP6(diff,ra,'P','B',bind):l -> LRP6(diff,ra,'uP','uB',bind) @
if (bind=='f') then 0 else k_11*#w*#1;

// **** Beta-catenin signalling ****

// (R12) Basal AXIN autophosphorylation
AXIN('u','f','f'):a -> AXIN('p','f','f') @ k_12*#a;

// (R13) Basal AXIN dephosphorylation
AXIN('p','f','f'):a -> AXIN('u','f','f') @ k_13*#a;

// (R14) AXIN degradation
AXIN(phos,'f','f'):a -> @ k_14*#a;

```

```

// (R15) Activated beta-catenin degradation
Cell[AXIN('p','f','f'):a + Bcat:b + s?]:c ->
Cell[AXIN('p','f','f') + s?] @ #c*((k_15*#a*#b));

// (R16) Beta-catenin synthesis
Cell[s?] -> Cell[Bcat + s?] @ #c*k_16;

// (R17) Basal beta-catenin degradation
Bcat:b -> @ k_17*#b;

// (R18) Beta-catenin shuttling into the nucleus
Bcat:b + Nuc[s?] -> Nuc[Bcat + s?] @ k_19*#b;

// (R19) Beta-catenin shuttling out of the nucleus
Nuc[Bcat:b + s?] -> Bcat + Nuc[s?] @ k_12*#b;

// (R20) Beta-catenin driven AXIN synthesis
Nuc[Bcat:b + s?] -> Nuc[Bcat + s?] + AXIN('u','f','f') @ k_20*#b;

// **** AXIN LRP6 signalling ****

// (R21a) AXIN binding by LRP6 in membrane
AXIN(phos,'f',b):a + Membrane(A)[LRP6(diff,ra,'P','B','f'):1] ->
Membrane(A)[AXIN(phos,$link,b) +LRP6(diff,ra,'P','B',$link)] @ ((k_21a*#1*#a));

// (R21b) AXIN binding by LRP6 in lipid rafts
AXIN(phos,'f',b):a + Membrane(A)[LR(radius,p)[LRP6(diff,ra,'P','B','f'):1]]->
Membrane(A)[LR(radius,p)[AXIN(phos,$link,b) + LRP6(diff,ra,'P','B',$link)]] @
((k_21b*#1*#a));

// (R22a) Dissociation of receptor/AXIN complex (signalosome) in membrane
Cell[Membrane(A)[LRP6(diff,ra,'P','B',bind):1a +AXIN(phos,bind,b)]] ->
Cell[Membrane(A)[LRP6(diff,ra,'uP','uB','f')] +AXIN(phos,'f',b) + DVL('i','f')] @
if (bind=='f') then 0 else (k_22a)*#1a;

// (R22b) Dissociation of receptor/AXIN complex (signalosome) in LR
Cell[Membrane(A)[LR(radius,p)[LRP6(diff,ra,'P','B',bind):1a+AXIN(phos,bind,b)]]]->
Cell[Membrane(A)[LR(radius,p)[LRP6(diff,ra,'uP','uB','f')]] +
AXIN(phos,'f',b) + DVL('i','f')] @ if (bind=='f') then 0 else (k_22b)*#1a;

// **** Ros-Dvl Signalling ****

// (R23) Binding of DVL to LRP6/WNT complex
Cell[Membrane[LR(radius,p)[LRP6(diff,ra,'uP','B',bind):1]] + DVL(a,'f'):d]
-> Cell[Membrane[LR(radius,p)[LRP6(diff,ra,'dP','B',bind)]]]@k_23*#1*#d;

// (R24) Unbinding of DVL from LRP6/WNT complex
Cell[Membrane[LR(radius,p)[LRP6(diff,ra,'dP','B'):1]]] ->
Cell[Membrane[LR(radius,p)[LRP6(diff,ra,'uP','B')]] + DVL('i','f')] @ k_24*#1;

// (R25) Release of Ros molecules from Mitochondria
Cell[Mito[ROS]:r] -> Cell[Mito[] + ROS] @
if (simtime() > k_Rdelay) then k_25*#r else 0;

// ( R26 ) Dissociation of DVL from Nrx by Ros

```



```

Cell[DVLNrx:dn + Ros:r] -> Cell[ DVL('i','f') + Nrx('0')] @ k_26*#dn*# r;

// (R26a) Oxidation of Nrx by Ros
Cell [Nrx('n0'):n + Ros:r] -> Cell [Nrx('0')] @ k_26a*#n*# r ;

// (R26b) Reduction of Nrx
Nrx('0'):n -> Nrx('n0') @ k_26b*#n;

// (R27) Binding of DVL by Nrx
Cell[DVL(a,'f'):d + Nrx('n0'):n] -> Cell[DVLNrx] @ k_27*#d*#n;

// (R28) Basal unbinding of DVL from Nrx
DVLNrx:dn -> DVL('i','f') + Nrx('n0') @ k_28*#dn;

// (R29) Activation (by e.g. aggregation) of DVL
DVL('i', 'f'):d -> DVL('a','f') @ k_29*#d;

// (R30) Dynamic deactivation of DVL
DVL('a','f'):d -> DVL('i','f') @ k_30*#d;

// (R31) Axin binding by activated DVL
Cell[DVL('a','f'):d + Axin(phos,'f','f'):a] ->
Cell[DVL('a', $link) + Axin(phos, 'f', $link)] @k31*#d*#a;

// (R32) Axin DVL unbinding
Cell[DVL('a',bind):da + Axin(phos,'f',bind)] ->
Cell[DVL('a','f') + Axin(phos,'f','f')] @ if (bind=='f') then 0 else k32*#da;

```

LISTING 6.7: ML-Rules implementation of the combined Wnt/ β -catenin model including the redox-pathway as depicted in Figure 6.1.

6.2.2 Methods and Parametrization

Again, we perform a number of simulation studies to find a suitable parametrization of the composed model, and - once found - to explore the effects that result from the composition of the ROS/DVL and the WNT/ β -catenin model. Since the model extension is also implemented in ML-Rules, we can apply the same tools for the specification and execution of the simulation experiments as before, i.e. we use SESSL to set up the simulation experiments, like parameter scans and optimization routines and for the individual simulation runs, the approximative τ -leaping simulator is used. For further information regarding the experiment specification and execution we refer to Section 5.3.1.

6.2.3 Parameter Adjustment

In the following we aim to check, whether the composed model is capable of reproducing the beta-catenin dynamics of hNPCs during early differentiation. This means, we look

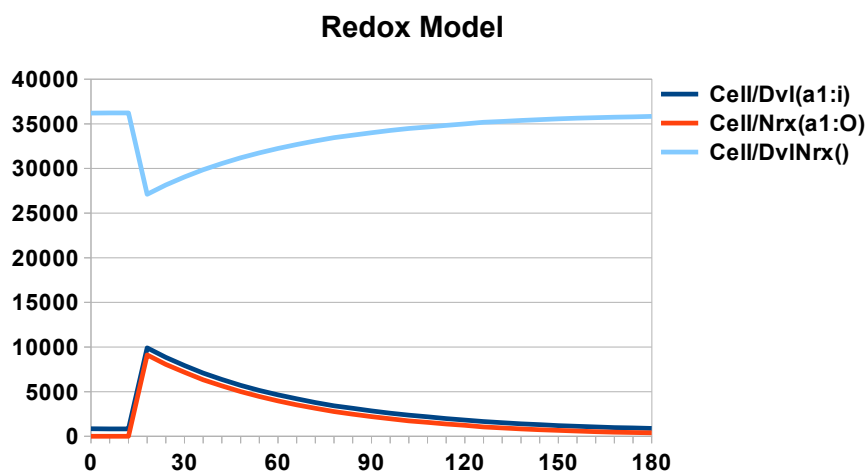


FIGURE 6.2: Simulation result for Redox model,. Representative simulation trajectory demonstrating the dynamics of Dvl and Nucleoredoxin after transient stimulation with ROS

for a parametrization such that the composed model fits the experimental results of [166] as well as our previous simulation and experimental results.

Temporal kinetics of ROS/DVL model

We first calibrate the ROS/DVL model, such that the temporal kinetics of the cytoplasmic increase of ROS and the subsequent release of DVL are in agreement with the experimental data [166]. According to experimental measurements the ROS increase starts between 10 and 20 minutes after the initiation of differentiation. We therefore set the delay for the ROS influx from the mitochondria into the cytosol to 15 minutes (rule 6.1).

The change of the cellular redox state, resulting from the ROS influx, apparently influence the NRX/DVL complex immediately. FRET and Western blot measurements indicate a sustained increase of DVL already after 1 hour of differentiation. However, the amount of unbound DVL diminishes already after 3 hours.

The parameters used to successfully fit the temporal kinetics of the ROS/DVL are listed in table 6.1. As depicted in Fig. 6.2, the initial concentration is restored for the NRX/DVL complex as well as for unbound DVL after three hours of simulation run time.

Parametrization of the composed model

After successfully calibrating the temporal dynamics of the ROS/DVL model we try to fit the composed model to the β -catenin dynamics in untreated cells during early differentiation (cf. Figure 5.2). If our hypothesis, that ROS-mediated DVL/beta-catenin signaling is the source of the immediate early β -catenin activation, is correct, it should be possible to fit the composed model without changing any parameters of the ROS/DVL and WNT/ β -catenin model that have already been validated. Accordingly only input parameters (such as initial WNT/ROS concentrations or delays) and those that connect the ROS/DVL model with the WNT/ β -catenin model (DVL accumulation or the interaction of DVL and Axin), may be modified in the process of fitting.

Intriguingly, there exists a parameter configuration that is indeed capable of reproducing the kinetics in untreated cells and, more importantly the immediate β -catenin activation in raft deficient cells (cf. Fig. 6.3). The parameter values are listed in Table 6.1.

In contrast to the previous model configuration we replaced the initial amount of WNT molecules with a onetime release of ROS molecules ($nRos = 10000$) in response to growth factor removal. Moreover, the parameter values for the delayed (90min) and constant WNT production ($k_5 = 1.9$) are slightly changed, while all other remaining parameter values of our earlier model remain the same. The necessity to include such a delay can be explained by inspecting our results more closely: Note, that the increase of β -catenin concentration during the immediate early response (1h) is not significantly different between control and raft deficient cells. If WNT signaling was directly activated

TABLE 6.1: **Parameter Table of the ROS/DVL model component.**

<i>Molecule Numbers</i>		
Species	Description	Value
ROS	total initial ROS	10000
DVL (cyt)	unbound cytosolic DVL	855
Nrx	unbound cytosolic Nrc	18
DVLNrx	cytosolic DVL bound to Nrx	36200

<i>Reaction Rate Constants</i>		
Rule/Parameter	Description	Value
R26 /k_26	ROS oxidation of Nrx forcing release of DVL	3.2E2
R26a/k_26a (not shown)	ROS oxidation of Nrx	5E2
R26b/k_26b (not shown)	Nrx reduction	2E-2
R27 /k_27	DVL-Nrx Association	22.5
R28 /k_28	DVL-Nrx Dissociation	2.3E-2

Parameter and reference values of the ROS/DVL signaling model.

TABLE 6.2: **Parameter Table of the extended ROS/ β -catenin model component.**

<i>Molecule Numbers</i>		
Species	Description	Value
WNT	total WNT	0

<i>Reaction Rate Constants</i>		
Rule/Parameter	Description	Value
R5/k.5	WNT production	2.2
R6/k.6	WNT degradation	0.27
k_delay	Delay for WNT production	90
R23/k.23	LRP6-DVL association	2.8E4
R24/k.24	LRP6-DVL dissociation	3.5E-4
R29/k.29	Aggregation of DVL	5E-4
R30/k.30	Dissociation of DVL	0.65
R31/k.31	DVL-Axin Association	0.075
R32/k.32	DVL-Axin Dissociation	6.8E-2

Parameter and reference values of the DVL-mediated ROS/ β -catenin signaling model as depicted in Fig. 6.1. The remaining model parameter values listed in Table 5.1 and Table 6.1 are kept fixed.

after induction of differentiation, the signal at 1 hour would add up with the β -catenin activation induced by ROS, hence most likely be significantly higher in control than in raft deficient cells. As this is not the case, we conclude, that the described autocrine, raft-dependent WNT signaling can only be initiated after a certain delay. However, this also implies that the signal after one hour is entirely based upon WNT/LRP6 independent mechanisms like the presented redox-dependent DVL/ β -catenin pathway.

6.2.4 Simulation results and Discussion

The intricate spatio-temporal interplay of redox- and WNT dependent β -catenin signaling becomes even more evident, when considering the localization and binding state of AXIN during signaling (cf. Figure 6.3 C).

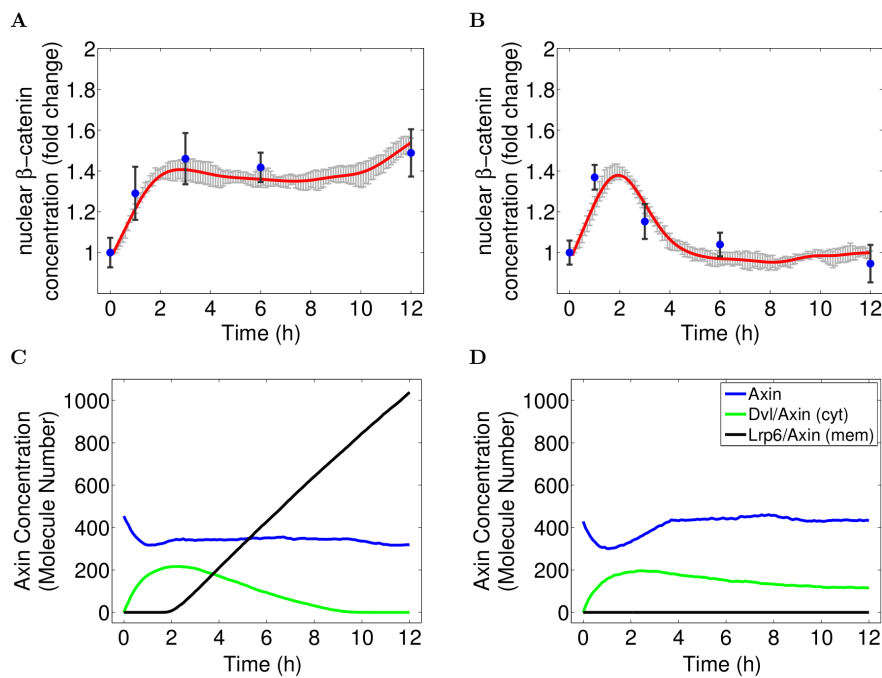


FIGURE 6.3: Experimental vs. Simulation results.

(A-B) Nuclear β -catenin concentration fold changes in comparison between experimental data and the extended WNT/ROS- β -catenin model. The simulation result (red) of the extended WNT/ROS- β -catenin model (cf. Figure 6.1, parametrized according to Table 5.1, Table 6.1 and Table 6.2) match all experimental values (blue) in untreated control (A) and raft deficient cells (B). Simulation results correspond to the mean simulation trajectory (red) with 95% confidence interval (gray error bars).

(C-D) AXIN concentration in comparison between bound (to DVL or LRP6) and unbound state. Simulation mean trajectories of AXIN in its bound and unbound states for untreated (C) and raft deficient cells (D).

Spatio-temporal regulation of AXIN

While unbound AXIN acts as inhibitor of WNT signaling, in place of the complete destruction complex, the (reversible) binding states of AXIN to DVL and membrane-bound LRP6 relate to the two previously described mechanisms for activating β -catenin signaling: During the first two hours, β -catenin activation solely results from DVL/AXIN binding, i.e. the redox-dependent DVL/ β -catenin pathway. Only after that, AXIN starts getting recruited to the membrane and bound by the activated LRP6 receptor complex. This process is driven by the auto-/paracrine WNT signaling, which, in the long run, replaces the transient redox-dependent DVL/ β -catenin pathway, such that AXIN is eventually only bound to LRP6. Note, that due to negative feedback, the elevated concentration of nuclear β -catenin enhances the synthesis of AXIN. As a result, in the long run, the binding of AXIN to LRP6 yields an unrestrained linear increase

of LRP6/AXIN in control cells for late time points. This indicates that additional mechanisms, like endocytosis and recycling, are required to maintain the continuous auto-/paracrine WNT-signaling for a longer period of time.

In summary, our simulation results suggest a two-fold activation mechanism that drives the early differentiation process in human progenitor cells. Accordingly, the cellular response upon differentiation induction through growth-factor removal is characterized by an immediate, transient response through redox-dependent DVL signaling, followed by a constant, auto-or paracrine WNT signaling in a raft-dependent manner.

DVL as a concentration-dependent dual signal transducer

We would like to emphasize the dual role that DVL, a central component of both, canonical and non-canonical WNT signaling, plays in this context [65]. On the one hand, DVL is required for the phosphorylation and accumulation of LRP6 and is thus continuously recruited to the membrane in response to WNT stimulation [11, 181, 183]. On the other hand, DVL itself acts as an independent transducer for β -catenin signaling in a redox dependent manner, independent of WNT molecules. Obviously the function of DVL is characterized by a highly concentration dependent mechanism.

In the inactive state DVL is primarily bound by NRX [63]. The remaining fraction of unbound DVL is too small to initiate self-aggregation, but sufficiently large to support and enhance WNT-induced receptor activation at the membrane. In fact, this process is enhanced by the localization of LRP6 and CK1 γ in lipid rafts, which allows a local, density-dependent activation despite the low concentration of unbound DVL [44].

The redox-sensitive release of DVL from NRX in response to the transient ROS signal, however, results in a spontaneous increase of the cytosolic DVL concentration. As a result DVL immediately gets activated by forming self-aggregates, that provide high affinity binding sites for cytosolic AXIN [181] (cf. Figure 6.3 C&D). The binding of AXIN by aggregated DVL in turn inhibits the destruction complex, hence activating β -catenin signaling. Due to the dynamic nature of DVL aggregates, i.e., their association and disassociation, the β -catenin activation is reversible: as soon as the DVL concentration falls below a certain threshold, e.g. by NRX rebinding, AXIN-DVL binding and thus β -catenin signaling is inhibited again. As a result, the nuclear β -catenin concentration returns to its base-line, as illustrated in Figure 6.3.

To summarize, based on our computational model, we demonstrated, that DVL may either act as amplifier or as direct inducer of canonical WNT signaling. Thereby the state of activity is determined by the concentration and localization of DVL, i.e. low concentrated, membrane-associated DVL amplifies WNT-induced LRP6 receptor activation and signalosome formation, whereas high concentrated DVL directly induces β -catenin

signaling, e.g. in response to a ROS stimulus. This is in line with a number of in vitro studies, that elucidate the role of DVL during WNT/ β -catenin signaling [60, 63, 181].

6.3 In vitro validation

6.3.1 Material and methods

WNT inhibition, fixation and immunostaining ReNcell VM197 cells cultured on coverslips were treated with 50ng/ml Dkk-1 and 0.5 μ g/ml Wif-I. The compounds were added to the differentiation medium, such that the treatment starts simultaneously with the initiation of differentiation through growth factor removal. In the following fixation and immunofluorescence staining was performed as described in the previous chapter 5.2. Accordingly, cells were washed with PBS and fixed with 4% paraformaldehyde for 20 min (Sigma-Aldrich). At first cell membranes were permeabilised with 0.2% Triton X-100 (Sigma-Aldrich). To reduce non-specific binding, cells were treated with 1% gelatin in the following. Afterwards cells were incubated with mouse anti-active- β -catenin (Millipore, dilution 1:250) and subsequently with Alexa Fluor488-conjugated anti-mouse secondary antibody (Invitrogen, dilution 1:300) and Hoechst for nuclei staining (Sigma-Aldrich, dilution 1:1000). Finally, cells were mounted on microscope slides using ProLong Gold antifade reagent (Invitrogen).

Mitochondrial ROS Level For detection of intracellular ROS levels, proliferating cells were incubated with 50nM Mitotracker Red CMXRos (Invitrogen) for 40min. According to [21] the dye strongly accumulates in mitochondria which results in fluorescence quenching. A change in mito-ROS production then induces a dye release leading to a reduction of the quenching with simultaneous rise in the fluorescence. Subsequently, cells were induced to differentiate in the absence or presence of 2 mM cyclodextrine (Sigma-Aldrich). To exclude a ROS-stimulating effect during proliferation, proliferating cells were also treated with 2mM cyclodextrine. The ROS-increasing agent hydrogen peroxide (2mM, Sigma-Aldrich) was used as positive control. Fluorescence was analyzed by confocal microscopy using Nikon A1 confocal imaging system with a 60x/NA 1.4 oil objectives (Nikon, Tokyo, Japan).

Quantification of nuclear beta-catenin fluorescence intensity To analyze the nuclear beta-catenin accumulation we applied a 3D-image quantification approach according to [5]. Accordingly confocal images of randomly chosen areas were acquired. Semi-automatic 3D-reconstruction of Nuclei surfaces based on DNA staining (Hoechst)

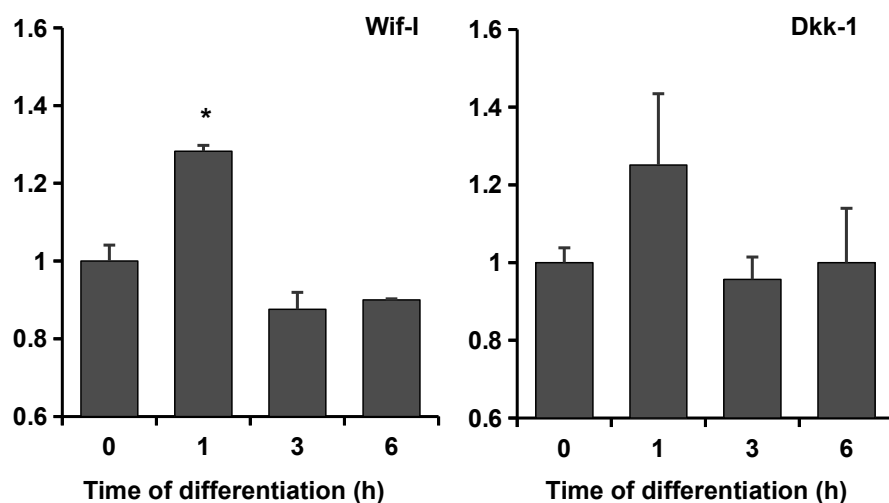


FIGURE 6.4: Upstream β -catenin inhibition with WIF-I (0.5μ g/ml) increases nuclear beta-catenin levels significantly during the early phase of differentiation, i.e. 1 hour after treatment and initiation, but decreases nuclear beta-catenin levels during the later phase of differentiation, i.e. 3-12 hours after treatment and initiation; Treatment with Dickkopf-1 (50 ng/ml Dkk-1) showed a WIF-I-similar response, but beta-catenin levels only decreased to base level; $n = \sim 300$ cells/nuclei per time point, unpaired t-test to control (0h): *, $p \leq 0.05$.

was achieved using the Imaris software platform from Bitplane. Within the 3D-volumes the mean-fluorescence intensity was quantified for beta-catenin staining, resulting in a collection of mean-values that represent the average intra-nuclear protein quantity at the moment of cell fixation. To increase experimental and statistical certainty, at least three randomly chosen fields were selected per coverslip, containing between 80 and 120 cells each. 3D-Images were recorded with identical microscope hardware settings and analyzed with identical software settings. For more details about the quantitative 3D-image cytometry approach, please see ([5] Chapter 3.2).

6.3.2 Experimental results

Early immediate beta-catenin activation is WNT independent In a previous work [5], the impact of common WNT signaling inhibitors like Dickkopf-1 (Dkk-1) and WNT-inhibitory-factor-I (Wif-I) on nuclear beta-catenin levels has been analyzed for the later phase of cell fate commitment (3-12 hours) in ReNcell VM197. Both proteins prevent the activation of WNT/beta-catenin signaling through different mechanisms: Dkk-1 targets LRP6 and triggers its internalization [173], whereas Wif-I unspecifically blocks free WNT-ligands. As shown in the work of [5], both compounds effectively inhibit nuclear beta-catenin accumulation. Apparently WNT ligands as well as LRP6

receptors play a crucial role in the later phase activation of WNT/ β -catenin signaling in ReNcell VM197, suggesting a direct relationship between WNT signaling and the nuclear β -catenin accumulation we observed in our measurements.

However, to analyze the impact of Dkk-1 and Wif-I on nuclear β -catenin accumulation during the initial phase of differentiation (1 hours) in ReNcell VM197 cells, we performed additional experiments as described in the following. We applied the same conditions as in the previous experiments, i.e. cells were treated with 50ng/ml Dkk-1 and 0.5 μ g/ml Wif-I, respectively. The compounds were added to the differentiation medium, such that the treatment starts simultaneously with the initiation of differentiation.

Figure 6.4 shows the nuclear β -catenin levels in Dkk-1 and Wif-1 treated ReNcell VM197 cells during proliferation (0h) and after 1h and 3h (and 6h) of differentiation. In fact, after 1 hour of differentiation, we observe a marked increase of nuclear β -catenin levels in the case of Dkk-1 and a significant increase in the case of Wif-1 treatment, compared to proliferating cells (0h). Whereas at the later phase of differentiation (3 and 6 hours) nuclear β -catenin levels are either decreased or at the base level, which is in agreement with our previous, aforementioned measurements. The β -catenin activation in Dkk-1 and Wif-1 treated cells are also correlate with the dynamics obtained by MbCD treatment, hence corroborating our claim that the nuclear β -catenin accumulation observed in our measurements appropriately reflects the activity of WNT/ β -catenin signaling.

To summarize, we provide experimental measurements of nuclear β -catenin levels in ReNcell VM197 cells during differentiation in response to three different treatments, each targeting different components of the WNT/LRP6 signaling complex, to analyze the same specific hypothesis. Each of these experiments showed the same tendency, i.e. a WNT/LRP6 independent early phase activation and a WNT/LRP6 dependent later phase activation. However, the source of the WNT/LRP6 independent activation of β -catenin signaling remains elusive.

Increased ROS production in response to initiation of differentiation is independent of raft disruption

Our simulation studies confirm that the presented model of combined redox and raft-dependent wnt signaling provides a sustained explanation to our experimental data. However, redox signaling and lipid rafts are closely related to each other, since major components of redox signaling mechanism are found to be raft-associated, like NADPH oxidase, superoxide dismutase and Catalase [17, 98, 159]. Accordingly, we have to re-evaluate our experimental data, as MbCD treatment may have an additional impact on ROS signaling and might even induce the early immediate

response in raft-deficient cells. To test whether the proposed ROS signaling mechanism is independent of the MbCD treatment, we analyzed the mitochondrial ROS (mito-ROS) production in control and raft deficient ReNcell VM197 cells during proliferation and during the early hours of differentiation. To monitor the mito-ROS metabolism we apply MitoTracker Red according to [21]. More details are described in the Material and Methods section.

In proliferating state, control and raft-deficient cells show no detectable changes in the mito-ROS level, whereas H_2O_2 stimulation results in a significant increase (cf. Fig. 6.5). Accordingly ROS metabolism is not induced or promoted by MbCD treatment in proliferating cells. After one hour of differentiation we register a transient, marked increase of mito-ROS production in differentiating cells compared to proliferating cells, that is in accordance with the data reported in [166]. The transient increase of mito-ROS production occurs in untreated control as well as in MbCD treated cells (cf. Fig. 6.5). After three hours, we detect a decrease in the mito-ROS metabolism, that is slightly more pronounced in control than in raft-deficient cells. Apparently MbCD treatment alters the mito-ROS metabolism, but only after three hours of differentiation, whereas the changes in the mitochondrial ROS metabolism in direct response to induction of differentiation occur independent of superoxide dismutase. Consequently, MbCD treatment does not promote the activation of mito-ROS metabolism in response to the induction of differentiation (as described in [166]), but hampers the subsequent elimination of the generated ROS.

However, the increased ROS level at three hours has no apparent effect on β -catenin signaling. While mito-ROS metabolism is still increased after three hours in raft-deficient cells (cf. Fig. 6.5), the nuclear β -catenin concentration is returning to its base-line already (cf. Fig. 5.2). In fact, this insight further corroborates our hypothesis of a biphasic activation pattern, where redox-dependent DVL/ β -catenin signaling is only active during the early immediate response (1h), while the subsequent continuous β -catenin accumulation results from an autocrine/paracrine, raft-dependent WNT/ β -catenin signaling mechanism (3-12h).

6.4 Concluding remarks

In a combined in-vitro and in-silico approach we find strong evidence, that cell fate commitment in human neural progenitor cells is driven by two distinct β -catenin signaling mechanisms. According to our simulation results, only a concisely regulated interplay between redox-dependent and self-induced auto-/paracrine WNT signaling can explain the nuclear β -catenin dynamics observed experimentally during the initial phase of differentiation:

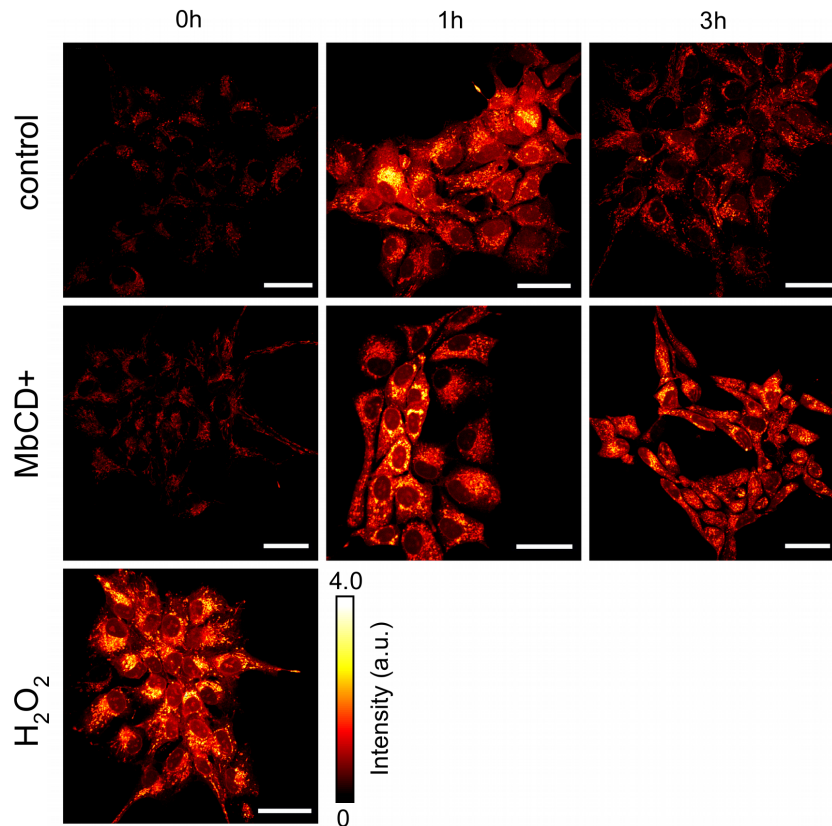


FIGURE 6.5: Confocal microscopy of mito-ROS levels for untreated (control) cells and MbCD-treated cells. Proliferating cells have been treated with H₂O₂ as positive control and MbCD for 1 hour (first column). 1 hour after induction of differentiation cells show a marked increase of mito-ROS levels, and subsequent decrease after 3 hours. Images further confirm that neither proliferating nor differentiating cells are subject to crucial changes in mitochondrial ROS level due to raft disruption through MbCD treatment. Scale bar 20 μm .

In response to growth factor removal, a transient increase of the intracellular ROS level activates DVL in a redox-dependent manner. While DVL is primarily bound by NRX in the inactive state, ROS release the redox-sensitive association between NRX and Dishevelled (DVL). This leads to a spontaneous increase of unbound DVL molecules, which immediately get activated by forming self-aggregates. Activated DVL subsequently stimulates downstream signaling components causing an immediate transient β -catenin signal [63, 181]. After a certain delay, a yet unknown mechanism triggers a continuous production of WNT molecules, which results in a stable activation of WNT/ β -catenin pathway by auto-/paracrine signaling. The resulting continuous WNT signal is raft-dependent, i.e. the disruption of rafts completely inhibits the signal transduction.

However, two additional things are important to consider here. On the one hand, the reversible binding of Axin to activated LRP6, as described in our model, is sufficient to accurately predict and reproduce in-silico and in-vitro measurements under varying

conditions. This means our results indicate that, apparently, endocytosis and recycling processes are not essentially required to maintain the activation level of nuclear β -catenin in response to a constant autocrine Wnt stimulus throughout the initial phase of differentiation (first 12h). On the other hand, in the current model intracellular AXIN levels are continuously increasing during WNT signaling, due to the β -catenin dependent expression of AXIN (negative feedback) (cf. Figure 6.3). This means, β -catenin levels can only be kept on an increased level, as long as enough LRP6 molecules are available to bind AXIN, i.e. WNT signaling is only effective, if the LRP6/AXIN system is not saturated. As a consequence, for longer time scales an additional mechanism, such as the endocytotic cycle, is indeed required to keep WNT signaling running and effective.

Chapter 7

Summary and Concluding Remarks

The results of this thesis demonstrate, that Lipid Rafts are perfectly suited to illustrate

- why the appropriate representation of spatial dynamics in computational modeling is a challenging tasks and
- why spatial dynamics play a crucial role in cellular signal transduction.

In the following we shortly summarize the most important insights drawn from the development of the two lipid rafts models (Chapter 2 and Chapter 4) and the subsequent simulation studies (Chapter 3, Chapter 5 and Chapter 6). A detailed discussion of the individual methodological approaches and biological insights can be found at the end of the respective chapter.

7.1 Methodology / Model development

Here we provided two models of lipid rafts/receptor dynamics, each implemented with a modeling formalism (Cellular Automata, ML-Rules) that is tailored to the scientific question and the corresponding spatial resolution (individual, grid-based, compartmental). Regarding the expressiveness both modeling formalisms (CA and ML-Rules) were able to cope with the modeling features required to represent the dynamics we sought to analyze. However in terms of model complexity and re-usability we found strong distinctions between the two formalisms. Even though the spatial resolution of the CA model was perfectly fitted for the dynamics addressed in this work, it has to be acknowledged

that in terms of expressiveness, CA-formalism was stretched to its limits. In particular the representation of coordinated movement of lipid rafts and the resulting implications for receptor diffusion, i.e. interdependent multilevel processes, were difficult to describe in terms of local transition rules. As a result CA model comprises rather complicated transition rules, which clearly diminishes the re-usability of the model and hampers potential extensions of the model. Instead recent more sophisticated approaches, such as ML-Space [12] or cellular pots models [182] are apparently more suited to describe lipid rafts/receptor dynamics on the membrane.

On the other hand, the ML-Rules formalism used to implement the lipid rafts/WNT model provides sufficient expressiveness to handle all essential modeling features. As a result the ML-Rules model is comparably compact, easy of access and the implementation of potential model extensions is straight-forward. This has been demonstrated has been demonstrated when extending the combined lipid rafts - Wnt/ β -catenin with the intracellular redox signaling (Chapter 6). Another good example for the expressiveness of ML-Rules is the concise description of the endocytotic cycle, where only a pair of rules was sufficient to describe endocytosis of the ternary complex, the dissociation of the complex with subsequent recycling of the LRP6 receptor to the membrane and the simultaneous degradation of the remaining proteins and ligands that were part of the ternary complex (cf. Rule rule:endocytosis).

In summary, the models of lipid rafts dynamics developed here greatly demonstrate that sophisticated modeling approaches are required to describe such complex model features in terms of assessable and (re-)usable models.

7.2 Application / Biological insights

The result of the CA-based simulation studies revealed, that lipid rafts have indeed a significant impact, not only on the accumulation of receptors, as shown in earlier studies, but also on the recruitment and binding of cytosolic proteins by the receptors. Considering the crucial role of protein recruitment and binding for the assembly and activation of receptors, our results thus underline the diverse, but pivotal role of lipid rafts during signal transduction. Generally the impact of lipid rafts on the binding kinetics is limited by the raft concentration within the membrane and its fluidity. Since the raft fluidity is mainly controlled by the cholesterol content of the membrane, our findings are consistent with studies showing that cholesterol depletion alters specific cellular responses in different cells (see [185] for review). However, to retrieve pathway- and cell specific results on binding kinetics that can be incorporated into or combined with other models, a membrane model needs to be specifically parameterized by dissociation and binding rate constants, raft size and coverage distribution, receptor sizes, and raft affinities. Most

often this is not possible due to the experimental limitations.

Unfortunately the lack of experimental data and technical limitations hampered the coupling of the two computational studies performed in this thesis. However, if possible at all, the technical limitations in particular regarding the financial effort and the time required to obtain cell and pathway specific raft characteristics were clearly beyond the scope of this work. This way, the impact of lipid rafts characteristics in the combined lipid raft/WNT model had to be reduced to the essential and fitted to experimental data. Nevertheless, we were able to develop an extended model of the canonical WNT pathway including membrane-related processes and lipid rafts whose predictive ability has been confirmed for various perturbations (e.g. transient and continuous Wnt stimuli) and in particular for lipid raft disruption. Since our model is realized in ML-Rules, a multi-level rule-based language, that facilitates the extension and modification of the model, it serves as a perfect basis for further in-silico investigations. Thus, our results provide both new insights and means to further the understanding of canonical Wnt/ β -catenin signaling and its role in neural differentiation.

Intriguingly, the derived experimental results indicated the involvement of an additional, Wnt-independent control mechanism, which was yet missing in the established signaling network of the canonical Wnt pathway.

The experimental and simulation studies revealed that β -catenin activation during cell fate commitment of human neural progenitor cells (hNPCs) is regulated through a concise spatio-temporal interplay of endogenous ROS and lipid raft dependent canonical Wnt signaling. These findings emphasize the role of ROS as intracellular signaling mediator and further illustrate the elaborate spatio-temporal regulation of Dvl, which may either act as amplifier or as direct inducer of Wnt/ β -catenin signaling, depending on its concentration and localization. Our results are in line with recent studies showing that both WNT- and ROS-induced β -catenin signaling pathways, are essential positive regulators for the neuronal differentiation as the inhibition of either one significantly reduces the neuronal yield [92, 166].

While we were able to explore the general effect that lipid rafts have on WNT signaling during neural differentiation, it also has to be admitted, that the essential mechanism behind this regulatory effect is still unclear, i.e. why lipid rafts are essentially required for the phosphorylation of LRP6. To explore this question, either further experimental data could be performed to find additional regulatory factors, such as e.g. done in [155]; Or a more fine-grained modeling and simulation approach could be used to elucidate whether the regulation of LRP6 and lipid rafts is due to steric, or hydrophobic interaction between the LRP6 receptor and the raft specific lipids.

All in all, on a personal note, in my eyes lipid rafts are still highly underestimated regarding its regulatory function in signal transduction and human physiology. On the one hand lipid rafts have been related to almost all central physiology-related signaling pathways and associated with a continuously growing list of diseases, including immune disorders, degenerative diseases and cancer (cf. Chapter 1, while on the other hand the knowledge about the exact mechanism by which lipid rafts regulate signaling are still unknown for most of the signal transduction pathways they are involved in. This obvious discrepancy needs to be addressed in the near future. Since lipid rafts are difficult to study in vitro and in vivo, insights obtained by computational modeling can give a cutting edge to this problem.

Bibliography

- [1] A. Al-Haddad, M. A. Shonn, B. Redlich, A. Blocker, J. K. Burkhardt, H. Yu, J. A. Hammer, D. G. Weiss, W. Steffen, G. Griffiths, and S. A. Kuznetsov. Myosin va bound to phagosomes binds to f-actin and delays microtubule-dependent motility. *Molecular Biology of the Cell*, 12(9):2742–2755, Sept. 2001. PMID: 11553713 PMCID: PMC59709.
- [2] J. A. Allen, R. A. Halverson-Tamboli, and M. M. Rasenick. Lipid raft microdomains and neurotransmitter signalling. *Nature Reviews Neuroscience*, 8(2):128–140, Feb. 2007.
- [3] S. Amit, A. Hatzubai, Y. Birman, J. S. Andersen, E. Ben-Shushan, M. Mann, Y. Ben-Neriah, and I. Alkalay. Axin-mediated CKI phosphorylation of beta-catenin at Ser 45: a molecular switch for the Wnt pathway. *Genes & Development*, 16(9):1066–1076, May 2002.
- [4] T. Anderson. *An introduction to multivariate statistical analysis*. Wiley series in probability and statistics. Wiley-Interscience, 3rd edition, 2003.
- [5] M. B. Bader. *Spatio-temporal control of Wnt/ β -catenin signaling during fate commitment of human neural progenitor cells*. PhD thesis, University of Rostock, 2010.
- [6] A. Bafico, G. Liu, A. Yaniv, A. Gazit, and S. A. Aaronson. Novel mechanism of wnt signalling inhibition mediated by dickkopf-1 interaction with LRP6/Arrow. *Nature cell biology*, 3(7):683–686, July 2001. PMID: 11433302.
- [7] K. Bartscherer and M. Boutros. Regulation of Wnt protein secretion and its role in gradient formation. *EMBO Reports*, 9(10):977–982, Oct. 2008.
- [8] D. Barua, J. R. Faeder, and J. M. Haugh. A Bipolar Clamp Mechanism for Activation of Jak-Family Protein Tyrosine Kinases. *PLoS Computational Biology*, 5(4), Apr. 2009.

- [9] O. Bernatik, R. S. Ganji, J. P. Dijksterhuis, P. Konik, I. Cervenka, T. Polonio, P. Krejci, G. Schulte, and V. Bryja. Sequential Activation and Inactivation of Dishevelled in the Wnt/ -Catenin Pathway by Casein Kinases. *Journal of Biological Chemistry*, 286(12):10396–10410, Feb. 2011.
- [10] D. C. Berwick and K. Harvey. LRRK2 functions as a Wnt signaling scaffold, bridging cytosolic proteins and membrane-localized LRP6. *Human Molecular Genetics*, 21(22):4966–4979, Nov. 2012.
- [11] J. Bilic, Y.-L. Huang, G. Davidson, T. Zimmermann, C.-M. Cruciat, M. Bienz, and C. Niehrs. Wnt induces lrp6 signalosomes and promotes dishevelled-dependent lrp6 phosphorylation. *Science*, 316(5831):1619–1622, 2007.
- [12] A. T. Bittig, F. Haack, C. Maus, and A. M. Uhrmacher. Adapting rule-based model descriptions for simulating in continuous and hybrid space. In *Proceedings of the 9th International Conference on Computational Methods in Systems Biology, CMSB '11*, pages 161–170, New York, NY, USA, 2011. ACM.
- [13] A. T. Bittig, M. Jeschke, and A. M. Uhrmacher. Towards modelling and simulation of crowded environments in cell biology. *AIP Conference Proceedings*, 1281(1):1326–1329, 2010.
- [14] M. L. Blinov, J. R. Faeder, B. Goldstein, and W. S. Hlavacek. A network model of early events in epidermal growth factor receptor signaling that accounts for combinatorial complexity. *Bio Systems*, 83(2-3):136–151, Mar. 2006.
- [15] J. Blitzer and R. Nusse. A critical role for endocytosis in wnt signaling. *BMC Cell Biology*, 7(1):28, 2006.
- [16] M. Brameshuber, J. Weghuber, V. Ruprecht, I. Gombos, I. Horváth, L. Vigh, P. Eckerstorfer, E. Kiss, H. Stockinger, and G. J. Schütz. Imaging of mobile long-lived nanoplateforms in the live cell plasma membrane. *Journal of Biological Chemistry*, 285(53):41765–41771, Dec. 2010.
- [17] S. Bréchar, S. Plancon, and E. J. Tschirhart. New insights into the regulation of neutrophil NADPH oxidase activity in the phagosome: A focus on the role of lipid and ca^{2+} signaling. *Antioxidants & Redox Signaling*, 18(6):661–676, Feb. 2013.
- [18] K. Brennan, J. M. Gonzalez-Sancho, L. A. Castelo-Soccio, L. R. Howe, and A. M. Brown. Truncated mutants of the putative wnt receptor lrp6/arrow can stabilize [beta]-catenin independently of frizzled proteins. *Oncogene*, 23(28):4873–4884, Apr. 2004.

- [19] D. A. Brown and E. London. Functions of lipid rafts in biological membranes. *Annual Review of Cell and Developmental Biology*, 14(1):111–136, 1998.
- [20] F. J. Bruggeman and H. V. Westerhoff. The nature of systems biology. *Trends in Microbiology*, 15(1):45–50, Jan. 2007.
- [21] J. F. Buckman, H. Hernández, G. J. Kress, T. V. Votyakova, S. Pal, and I. J. Reynolds. MitoTracker labeling in primary neuronal and astrocytic cultures: influence of mitochondrial membrane potential and oxidants. *Journal of Neuroscience Methods*, 104(2):165–176, Jan. 2001.
- [22] J. M. Buick. *Lattice Boltzmann Methods in Interfacial Wave Modelling*. PhD thesis, University of Edinburgh, 1997.
- [23] S. C. Bunnell, D. I. Hong, J. R. Kardon, T. Yamazaki, C. J. McGlade, V. A. Barr, and L. E. Samelson. T cell receptor ligation induces the formation of dynamically regulated signaling assemblies. *The Journal of Cell Biology*, 158(7):1263–1275, Sept. 2002.
- [24] F. C. Boogerd, F. J. Bruggeman, J.-H. S. Hofmeyr, and H. V. Westerhoff. 1 - Towards philosophical foundations of Systems Biology: Introduction. In F. C. Boogerd and F. J. B.-H. S. H. V. Westerhoff, editors, *Systems Biology*, pages 3–19. Elsevier, Amsterdam, 2007.
- [25] G. Campi, R. Varma, and M. L. Dustin. Actin and agonist MHC-peptide complex-dependent T cell receptor microclusters as scaffolds for signaling. *The Journal of Experimental Medicine*, 202(8):1031–1036, Oct. 2005.
- [26] V. Chelliah, N. Juty, I. Ajmera, R. Ali, M. Dumousseau, M. Glont, M. Hucka, G. Jalowicki, S. Keating, V. Knight-Schrijver, A. Lloret-Villas, K. N. Natarajan, J.-B. Pettit, N. Rodriguez, M. Schubert, S. M. Wimalaratne, Y. Zhao, H. Hermjakob, N. Le Novère, and C. Laibe. BioModels: ten-year anniversary. *Nucleic Acids Research*, 43(Database issue):D542–548, Jan. 2015.
- [27] C.-Y. Cheng and Y.-J. Hu. Extracting the abstraction pyramid from complex networks. *BMC bioinformatics*, 11:411, 2010.
- [28] K.-H. Cho, S. Baek, and M.-H. Sung. Wnt pathway mutations selected by optimal beta-catenin signaling for tumorigenesis. *FEBS letters*, 580(15):3665–3670, June 2006.
- [29] W. Cho and R. V. Stahelin. Membrane-protein interactions in cell signaling and membrane trafficking. *Annual Review of Biophysics and Biomolecular Structure*, 34(1):119–151, May 2005.

- [30] B. Chopard and M. Droz. *Cellular Automata Modeling of Physical Systems*. Cambridge University Press, Cambridge, 1998.
- [31] B. Chopard, J.-L. Falcone, R. Razakanirina, A. Hoekstra, and A. Caiazzo. On the Collision-Propagation and Gather-Update Formulations of a Cellular Automata Rule. In H. Umeo, S. Morishita, K. Nishinari, T. Komatsuzaki, and S. Bandini, editors, *Cellular Automata*, number 5191 in Lecture Notes in Computer Science, pages 144–151. Springer Berlin Heidelberg, Jan. 2008.
- [32] T. M. Cioppa and T. W. Lucas. Efficient nearly orthogonal and space-filling latin hypercubes. *Technometrics*, 49(1):45–55, Feb. 2007.
- [33] D. E. Clapham. Calcium Signaling. *Cell*, 131(6):1047–1058, Dec. 2007.
- [34] C. D. Clelland, R. A. Barker, and C. Watts. Cell therapy in huntington disease. *Neurosurgical focus*, 24(3-4):E9, 2008. PMID: 18341412.
- [35] H. Clevers and R. Nusse. Wnt/ β -catenin signaling and disease. *Cell*, 149(6):1192–1205, June 2012.
- [36] F. Cong, L. Schweizer, and H. Varmus. Wnt signals across the plasma membrane to activate the beta-catenin pathway by forming oligomers containing its receptors, frizzled and lrp. *Development*, 131(20):5103–15, 2004.
- [37] M. N. Costa, K. Radhakrishnan, and J. S. Edwards. Monte carlo simulations of plasma membrane corral-induced egfr clustering. *Journal of Biotechnology*, 151(3):261–270, 2011.
- [38] M. N. Costa, K. Radhakrishnan, B. S. Wilson, D. G. Vlachos, and J. S. Edwards. Coupled stochastic spatial and non-spatial simulations of erbb1 signaling pathways demonstrate the importance of spatial organization in signal transduction. *PLoS ONE*, 4(7):e6316, 2009.
- [39] D. Coudreuse and H. C. Korswagen. The making of wnt: new insights into wnt maturation, sorting and secretion. *Development*, 134(1):3–12, Jan. 2007.
- [40] A. A. Cuellar, C. M. Lloyd, P. F. Nielsen, D. P. Bullivant, D. P. Nickerson, and P. J. Hunter. An Overview of CellML 1.1, a Biological Model Description Language. *SIMULATION*, 79(12):740–747, Dec. 2003.
- [41] R. Dajani, E. Fraser, S. M. Roe, M. Yeo, V. M. Good, V. Thompson, T. C. Dale, and L. H. Pearl. Structural basis for recruitment of glycogen synthase kinase 3beta to the axin-APC scaffold complex. *The EMBO journal*, 22(3):494–501, Feb. 2003.

- [42] V. Danos, J. Feret, W. Fontana, R. Harmer, and J. Krivine. Rule-based modelling of cellular signalling. In *CONCUR 2007 - Concurrency Theory, 18th International Conference, CONCUR 2007, Lisbon, Portugal, September 3-8, 2007, Proceedings*, pages 17–41, 2007.
- [43] V. Danos, J. Feret, W. Fontana, R. Harmer, and J. Krivine. Rule-based modelling and model perturbation. *T. Comp. Sys. Biology*, 11:116–137, 2009.
- [44] J. Das, M. Kardar, and A. K. Chakraborty. Positive feedback regulation results in spatial clustering and fast spreading of active signaling molecules on a cell membrane. *The Journal of Chemical Physics*, 130(24):245102–245111, June 2009.
- [45] H. Daub, C. Wallasch, A. Lankenau, A. Herrlich, and A. Ullrich. Signal characteristics of G protein-transactivated EGF receptor. *The EMBO journal*, 16(23):7032–7044, Dec. 1997.
- [46] G. Davidson, W. Wu, J. Shen, J. Bilic, U. Fenger, P. Stannek, A. Glinka, and C. Niehrs. Casein kinase 1 γ couples wnt receptor activation to cytoplasmic signal transduction. *Nature*, 438(7069):867–872, Dec. 2005.
- [47] R. F. M. de Almeida, L. M. S. Loura, A. Fedorov, and M. Prieto. Lipid rafts have different sizes depending on membrane composition: A time-resolved fluorescence resonance energy transfer study. *Journal of Molecular Biology*, 346(4):1109–1120, 2005.
- [48] A. Deutsch and S. Dormann. *Cellular Automaton Modeling of Biological Pattern Formation*. Birkhäuser Boston, 1 edition, Oct. 2005.
- [49] B. Di Ventura, C. Lemerle, K. Michalodimitrakis, and L. Serrano. From in vivo to in silico biology and back. *Nature*, 443(7111):527–533, Oct. 2006.
- [50] V. W. Ding, R. H. Chen, and F. McCormick. Differential regulation of glycogen synthase kinase 3 β by insulin and Wnt signaling. *The Journal of Biological Chemistry*, 275(42):32475–32481, Oct. 2000.
- [51] R. Donato, E. A. Miljan, S. J. Hines, S. Aouabdi, K. Pollock, S. Patel, F. A. Edwards, and J. D. Sinden. Differential development of neuronal physiological responsiveness in two human neural stem cell lines. *BMC neuroscience*, 8:36, 2007. PMID: 17531091 PMCID: PMC1888696.
- [52] C. Eggeling, C. Ringemann, R. Medda, G. Schwarzmann, K. Sandhoff, S. Polyakova, V. N. Belov, B. Hein, C. von Middendorff, A. Schönle, and S. W. Hell. Direct observation of the nanoscale dynamics of membrane lipids in a living cell. *Nature*, 457(7233):1159–1162, Feb. 2009.

- [53] J. Elf and M. Ehrenberg. Spontaneous separation of bi-stable biochemical systems into spatial domains of opposite phases. *Systems biology*, 1(2):230–236, Dec. 2004.
- [54] R. Ewald, J. Himmelspach, M. Jeschke, S. Leye, and A. M. Uhrmacher. Flexible experimentation in the modeling and simulation framework JAMES II—implications for computational systems biology. *Brief Bioinform*, 11(3):290–300, Jan. 2010.
- [55] R. Ewald and A. M. Uhrmacher. SESSL: A domain-specific language for simulation experiments. *ACM Transactions on Modeling and Computer Simulation (TOMACS)*, 24(2):11:1–11:25, Feb. 2014.
- [56] J. R. Faeder, M. L. Blinov, B. Goldstein, and W. S. Hlavacek. Combinatorial complexity and dynamical restriction of network flows in signal transduction. *Systems Biology*, 2(1):5–15, Mar. 2005.
- [57] J. R. Faeder, M. L. Blinov, B. Goldstein, William, and S. Hlavacek. Rule-based modeling of biochemical networks. *Complexity*, 10:22–41, 2005.
- [58] M. Fallahi-Sichani and J. J. Linderman. Lipid raft-mediated regulation of g-protein coupled receptor signaling by ligands which influence receptor dimerization: A computational study. *PLoS ONE*, 4(8):e6604, 2009.
- [59] J. Feret, V. Danos, J. Krivine, R. Harmer, and W. Fontana. Internal coarse-graining of molecular systems. *Proceedings of the National Academy of Sciences*, 106(16):6453–6458, Apr. 2009.
- [60] M. Fiedler, C. Mendoza-Topaz, T. J. Rutherford, J. Mieszczanek, and M. Bienz. Dishevelled interacts with the DIX domain polymerization interface of axin to interfere with its function in down-regulating β -catenin. *Proceedings of the National Academy of Sciences*, 108(5):1937–1942, Feb. 2011. PMID: 21245303.
- [61] L. J. Foster, C. L. d. Hoog, and M. Mann. Unbiased quantitative proteomics of lipid rafts reveals high specificity for signaling factors. *Proceedings of the National Academy of Sciences*, 100(10):5813–5818, May 2003. PMID: 12724530.
- [62] U. Frisch, B. Hasslacher, and Y. Pomeau. Lattice-gas automata for the navier-stokes equation. *Physical Review Letters*, 56(14):1505–1508, Apr 1986.
- [63] Y. Funato, T. Michiue, M. Asashima, and H. Miki. The thioredoxin-related redox-regulating protein nucleoredoxin inhibits wnt- β -catenin signalling through dishevelled. *Nature Cell Biology*, 8(5):501–508, May 2006.
- [64] R. R. Gabdouliline and R. C. Wade. Protein-protein association: investigation of factors influencing association rates by brownian dynamics simulations. *J. Mol. Biol.*, 306(5):1139–1155, Mar. 2001.

- [65] C. Gao and Y.-G. Chen. Dishevelled: The hub of wnt signaling. *Cellular Signalling*, 22(5):717 – 727, 2010.
- [66] D. T. Gillespie. Exact stochastic simulation of coupled chemical reactions. *Journal of Physical Chemistry*, 81(25):2340–2361, 1977.
- [67] F. M. Goni. Non-permanent proteins in membranes: when proteins come as visitors (review). *Molecular Membrane Biology*, 19(4):237–245, 2002.
- [68] J. M. González-Sancho, Y. E. Greer, C. L. Abrahams, Y. Takigawa, B. Baljinnyam, K. H. Lee, K. S. Lee, J. S. Rubin, and A. M. C. Brown. Functional Consequences of Wnt-induced Dishevelled 2 Phosphorylation in Canonical and Noncanonical Wnt Signaling. *Journal of Biological Chemistry*, 288(13):9428–9437, Mar. 2013.
- [69] J. E. Goose and M. S. P. Sansom. Reduced Lateral Mobility of Lipids and Proteins in Crowded Membranes. *PLoS Comput Biol*, 9(4):e1003033, Apr. 2013.
- [70] D. Goswami, K. Gowrishankar, S. Bilgrami, S. Ghosh, R. Raghupathy, R. Chadda, R. Vishwakarma, M. Rao, and S. Mayor. Nanoclusters of GPI-anchored proteins are formed by cortical actin-driven activity. *Cell*, 135(6):1085–1097, Dec. 2008.
- [71] J. L. Green, J. La, K. W. Yum, P. Desai, L.-W. Rodewald, X. Zhang, M. Leblanc, R. Nusse, M. T. Lewis, and G. M. Wahl. Paracrine wnt signaling both promotes and inhibits human breast tumor growth. *Proceedings of the National Academy of Sciences*, 110(17):6991–6996, Apr. 2013.
- [72] N.-C. Ha, T. Tonzuka, J. L. Stamos, H.-J. Choi, and W. I. Weis. Mechanism of phosphorylation-dependent binding of APC to beta-catenin and its role in beta-catenin degradation. *Molecular Cell*, 15(4):511–521, Aug. 2004.
- [73] F. Haack, K. Burrage, R. Redmer, and A. M. Uhrmacher. Studying the role of lipid rafts on protein receptor bindings with cellular automata. *IEEE/ACM transactions on computational biology and bioinformatics*, 10(3):760–770, June 2013. PMID: 24091408.
- [74] J. F. Hancock. Lipid rafts: contentious only from simplistic standpoints. *Nat Rev Mol Cell Biol*, 7(6):456–462, June 2006.
- [75] D. E. Handy and J. Loscalzo. Redox regulation of mitochondrial function. *Antioxidants & redox signaling*, 16(11):1323–1367, June 2012. PMID: 22146081 PMCID: PMC3324814.
- [76] R. N. Hannoush. Kinetics of wnt-driven beta-catenin stabilization revealed by quantitative and temporal imaging. *PLoS ONE*, 3(10):e3498, 2008.

- [77] J. Hardy, Y. Pomeau, and O. d. Pazzis. Time evolution of a two-dimensional model system. invariant states and time correlation functions. *Journal of Mathematical Physics*, 14(12):1746–1759, Dec 1973.
- [78] L. Harris, J. Hogg, and J. Faeder. Compartmental rule-based modeling of biochemical systems. In *Simulation Conference (WSC), Proceedings of the 2009 Winter*, pages 908–919, Dec. 2009.
- [79] L. H. Hartwell, J. J. Hopfield, S. Leibler, and A. W. Murray. From molecular to modular cell biology. *Nature*, 402(6761 Suppl):C47–52, Dec. 1999.
- [80] H. Hatzikirou, K. Böttger, and A. Deutsch. Model-based Comparison of Cell Density-dependent Cell Migration Strategies. *Mathematical Modelling of Natural Phenomena*, 10(1):94–107, 2015.
- [81] H. Hatzikirou, L. Brusch, C. Schaller, M. Simon, and A. Deutsch. Prediction of traveling front behavior in a lattice-gas cellular automaton model for tumor invasion. *Computers & Mathematics with Applications*, 59(7):2326–2339, Apr 2010.
- [82] R. Heinrich, B. G. Neel, and T. A. Rapoport. Mathematical models of protein kinase signal transduction. *Molecular Cell*, 9(5):957–970, May 2002.
- [83] T. Helms, M. Luboschik, H. Schumann, and A. Uhrmacher. An approximate execution of rule-based multi-level models. In A. Gupta and T. Henzinger, editors, *Lecture Notes in Computer Science*, volume 8130, pages 19–32. Springer Berlin Heidelberg, 2013.
- [84] K. Hibino, T. Shibata, T. Yanagida, and Y. Sako. Activation Kinetics of RAF Protein in the Ternary Complex of RAF, RAS-GTP, and Kinase on the Plasma Membrane of Living Cells: SINGLE-MOLECULE IMAGING ANALYSIS. *Journal of Biological Chemistry*, 286(42):36460–36468, Oct. 2011.
- [85] J. Himmelspach and A. M. Uhrmacher. Plug’n simulate. In *Proc. of the 40th Annual Simulation Symposium*, pages 137–143. IEEE CS, 2007.
- [86] Y. Hirabayashi, Y. Itoh, H. Tabata, K. Nakajima, T. Akiyama, N. Masuyama, and Y. Gotoh. The wnt/ β -catenin pathway directs neuronal differentiation of cortical neural precursor cells. *Development*, 131(12):2791–2801, June 2004. PMID: 15142975.
- [87] W. S. Hlavacek, J. R. Faeder, M. L. Blinov, A. S. Perelson, and B. Goldstein. The complexity of complexes in signal transduction. *Biotechnology and Bioengineering*, 84(7):783–794, Dec. 2003.

- [88] A. G. Hoekstra, A. Caiazzo, E. Lorenz, J.-L. Falcone, and B. Chopard. Complex automata: Multi-scale modeling with coupled cellular automata. In J. Kroc, P. M. A. Sloot, and A. G. Hoekstra, editors, *Simulating Complex Systems by Cellular Automata*, Understanding Complex Systems, pages 29–57. Springer Berlin Heidelberg, Jan 2010.
- [89] R. Hoffrogge, S. Mikkat, C. Scharf, S. Beyer, H. Christoph, J. Pahnke, E. Mix, M. Berth, A. Uhrmacher, I. Z. Zubrzycki, E. Miljan, U. Völker, and A. Rolfs. 2-DE proteome analysis of a proliferating and differentiating human neuronal stem cell line (ReNcell VM). *Proteomics*, 6(6):1833–1847, Mar. 2006. PMID: 16475233.
- [90] M.-y. Hsieh, S. Yang, M. Raymond-Stinz, J. Edwards, and B. Wilson. Spatio-temporal modeling of signaling protein recruitment to egfr. *BMC Systems Biology*, 4(1):57, 2010.
- [91] W. Hsu, L. Zeng, and F. Costantini. Identification of a domain of Axin that binds to the serine/threonine protein phosphatase 2a and a self-binding domain. *The Journal of Biological Chemistry*, 274(6):3439–3445, Feb. 1999.
- [92] R. Hübner, A.-C. Schmöle, A. Liedmann, M. J. Frech, A. Rolfs, and J. Luo. Differentiation of human neural progenitor cells regulated by wnt-3a. *Biochemical and Biophysical Research Communications*, 400(3):358–362, Sept. 2010.
- [93] M. Hucka, A. Finney, H. M. Sauro, H. Bolouri, J. C. Doyle, H. Kitano, A. P. Arkin, B. J. Bornstein, D. Bray, A. Cornish-Bowden, A. A. Cuellar, S. Dronov, E. D. Gilles, M. Ginkel, V. Gor, I. I. Goryanin, W. J. Hedley, T. C. Hodgman, J.-H. Hofmeyr, P. J. Hunter, N. S. Juty, J. L. Kasberger, A. Kremling, U. Kummer, N. Le Novère, L. M. Loew, D. Lucio, P. Mendes, E. Minch, E. D. Mjolsness, Y. Nakayama, M. R. Nelson, P. F. Nielsen, T. Sakurada, J. C. Schaff, B. E. Shapiro, T. S. Shimizu, H. D. Spence, J. Stelling, K. Takahashi, M. Tomita, J. Wagner, J. Wang, and SBML Forum. The systems biology markup language (SBML): a medium for representation and exchange of biochemical network models. *Bioinformatics (Oxford, England)*, 19(4):524–531, Mar. 2003.
- [94] J. H. Hurley and T. Meyer. Subcellular targeting by membrane lipids. *Current Opinion in Cell Biology*, 13(2):146–152, Apr. 2001.
- [95] S. Ikeda, S. Kishida, H. Yamamoto, H. Murai, S. Koyama, and A. Kikuchi. Axin, a negative regulator of the Wnt signaling pathway, forms a complex with GSK-3 β and β -catenin and promotes GSK-3 β dependent phosphorylation of β -catenin. *The EMBO Journal*, 17(5):1371–1384, Mar. 1998.

- [96] N. Israsena, M. Hu, W. Fu, L. Kan, and J. A. Kessler. The presence of FGF2 signaling determines whether beta-catenin exerts effects on proliferation or neuronal differentiation of neural stem cells. *Developmental Biology*, 268(1):220–231, Apr. 2004.
- [97] P. W. Janes, S. C. Ley, A. I. Magee, and P. S. Kabouridis. The role of lipid rafts in T cell antigen receptor (TCR) signalling. *Seminars in Immunology*, 12(1):23–34, Feb. 2000.
- [98] S. Jin, F. Zhou, F. Katirai, and P.-L. Li. Lipid raft redox signaling: Molecular mechanisms in health and disease. *Antioxidants & Redox Signaling*, 15(4):1043–1083, Aug. 2011.
- [99] M. John, C. Lhoussaine, J. Niehren, and C. Versari. Biochemical reaction rules with constraints. In G. Barthe, editor, *Programming Languages and Systems*, number 6602 in Lecture Notes in Computer Science, pages 338–357. Springer Berlin Heidelberg, Jan. 2011.
- [100] N. Juty, R. Ali, M. Glont, S. Keating, N. Rodriguez, M. Swat, S. Wimalaratne, H. Hermjakob, N. Le Novère, C. Laibe, and V. Chelliah. BioModels: Content, Features, Functionality, and Use. *CPT: Pharmacometrics & Systems Pharmacology*, 4(2):55–68, Feb. 2015.
- [101] B. Kagermeier-Schenk, D. Wehner, G. Özhan-Kizil, H. Yamamoto, J. Li, K. Kirchner, C. Hoffmann, P. Stern, A. Kikuchi, A. Schambony, and G. Weidinger. Waif1/5t4 Inhibits Wnt/ β -Catenin Signaling and Activates Noncanonical Wnt Pathways by Modifying LRP6 Subcellular Localization. *Developmental Cell*, 21(6):1129–1143, Dec. 2011.
- [102] J. R. Karr, J. C. Sanghvi, D. N. Macklin, M. V. Gutschow, J. M. Jacobs, B. Bolival, N. Assad-Garcia, J. I. Glass, and M. W. Covert. A whole-cell computational model predicts phenotype from genotype. *Cell*, 150(2):389–401, July 2012.
- [103] B. N. Kholodenko. Negative feedback and ultrasensitivity can bring about oscillations in the mitogen-activated protein kinase cascades. *European journal of biochemistry / FEBS*, 267(6):1583–1588, Mar. 2000.
- [104] S. Kishida, H. Yamamoto, S. Hino, S. Ikeda, M. Kishida, and A. Kikuchi. DIX domains of Dvl and axin are necessary for protein interactions and their ability to regulate beta-catenin stability. *Molecular and Cellular Biology*, 19(6):4414–4422, June 1999.

- [105] E. Klipp, R. Herwig, A. Kowald, C. Wierling, and H. Lehrach. *Systems Biology in Practice: Concepts, Implementation and Application*. Wiley-VCH, Weinheim, 2005.
- [106] E. Klipp, B. Nordlander, R. Krüger, P. Gennemark, and S. Hohmann. Integrative model of the response of yeast to osmotic shock. *Nature Biotechnology*, 23(8):975–982, Aug. 2005.
- [107] B. Kofahl and J. Wolf. Mathematical modelling of Wnt/ β -catenin signalling. *Biochemical Society transactions*, 38(5):1281–1285, Oct. 2010.
- [108] Y. Kogan, K. E. Halevi-Tobias, G. Hochman, A. K. Baczmanska, L. Leyns, and Z. Agur. A new validated mathematical model of the wnt signalling pathway predicts effective combinational therapy by sFRP and dkk. *Biochemical Journal*, 444(1):115–125, May 2012.
- [109] K. J. Krager, M. Sarkar, E. C. Twait, N. L. Lill, and J. G. Koland. A novel biotinylated lipid raft reporter for electron microscopic imaging of plasma membrane microdomains. *Journal of Lipid Research*, 53(10):2214–2225, Oct. 2012.
- [110] E. Kriehoff, J. Behrens, and B. Mayr. Nucleo-cytoplasmic distribution of β -catenin is regulated by retention. *Journal of Cell Science*, 119(7):1453–1463, Apr. 2006. PMID: 16554443.
- [111] R. Krüger and R. Heinrich. Model reduction and analysis of robustness for the Wnt/ β -catenin signal transduction pathway. *Genome Informatics. International Conference on Genome Informatics*, 15(1):138–148, 2004.
- [112] A. Kusumi, I. Koyama-Honda, and K. Suzuki. Molecular Dynamics and Interactions for Creation of Stimulation-Induced Stabilized Rafts from Small Unstable Steady-State Rafts. *Traffic*, 5(4):213–230, Apr. 2004.
- [113] C. Lange, E. Mix, J. Frahm, A. Glass, J. Müller, O. Schmitt, A.-C. Schmöle, K. Klemm, S. Ortinau, R. Hübner, M. J. Frech, A. Wree, and A. Rolfs. Small molecule gsk-3 inhibitors increase neurogenesis of human neural progenitor cells. *Neuroscience Letters*, 488(1):36–40, Jan. 2011.
- [114] D. A. Lauffenburger and J. J. Linderman. *Receptors: models for binding, trafficking, and signaling*. Oxford University Press, New York, 1996.
- [115] A. D. Lean, J. M. Stadel, and R. J. Lefkowitz. A ternary complex model explains the agonist-specific binding properties of the adenylate cyclase-coupled beta-adrenergic receptor. *Journal of Biological Chemistry*, 255(15):7108–7117, Aug. 1980.

- [116] E. Lee, A. Salic, R. Krüger, R. Heinrich, and M. W. Kirschner. The roles of apc and axin derived from experimental and theoretical analysis of the wnt pathway. *PLoS Biol*, 1(1):e10, 2003.
- [117] R. J. Lefkowitz, S. Cotecchia, P. Samama, and T. Costa. Constitutive activity of receptors coupled to guanine nucleotide regulatory proteins. *Trends in Pharmacological Sciences*, 14(8):303–307, Aug. 1993.
- [118] H. Lemcke and S. A. Kuznetsov. Involvement of connexin43 in the EGF/EGFR signalling during self-renewal and differentiation of neural progenitor cells. *Cellular Signalling*, 25(12):2676–2684, Dec. 2013.
- [119] H. Lemcke, M.-L. Nittel, D. G. Weiss, and S. A. Kuznetsov. Neuronal differentiation requires a biphasic modulation of gap junctional intercellular communication caused by dynamic changes of connexin43 expression. *European Journal of Neuroscience*, 38(2):2218 – 2228, 2013.
- [120] P.-F. Lenne, L. Wawrezinieck, F. Conchonaud, O. Wurtz, A. Boned, X.-J. Guo, H. Rigneault, H.-T. He, and D. Marguet. Dynamic molecular confinement in the plasma membrane by microdomains and the cytoskeleton meshwork. *The EMBO Journal*, 25(14):3245–3256, July 2006.
- [121] O. Lindvall, Z. Kokaia, and A. Martinez-Serrano. Stem cell therapy for human neurodegenerative disorders: how to make it work. *Nature Medicine*, 10:S42–S50, July 2004.
- [122] D. Lingwood and K. Simons. Lipid rafts as a membrane-organizing principle. *Science*, 327(5961):46–50, Jan. 2010.
- [123] C. Liu, Y. Li, M. Semenov, C. Han, G. H. Baeg, Y. Tan, Z. Zhang, X. Lin, and X. He. Control of beta-catenin phosphorylation/degradation by a dual-kinase mechanism. *Cell*, 108(6):837–847, Mar. 2002.
- [124] C.-C. Liu, J. Prior, D. Piwnica-Worms, and G. Bu. LRP6 overexpression defines a class of breast cancer subtype and is a target for therapy. *Proceedings of the National Academy of Sciences*, 107(11):5136–5141, Mar. 2010.
- [125] B. Lloyd-Lewis, A. G. Fletcher, T. C. Dale, and H. M. Byrne. Toward a quantitative understanding of the wnt/ β -catenin pathway through simulation and experiment. *Wiley Interdisciplinary Reviews: Systems Biology and Medicine*, 5(4):391–407, July 2013.
- [126] C. Y. Logan and R. Nusse. The wnt signaling pathway in development and disease. *Annual Review of Cell and Developmental Biology*, 20(1):781–810, 2004. PMID: 15473860.

- [127] N. R. Love, Y. Chen, S. Ishibashi, P. Kritsiligkou, R. Lea, Y. Koh, J. L. Gallop, K. Dorey, and E. Amaya. Amputation-induced reactive oxygen species are required for successful xenopus tadpole tail regeneration. *Nature Cell Biology*, 15(2):222–228, Feb. 2013.
- [128] M. Luboschik, C. Tominski, A. Bittig, A. Uhrmacher, and H. Schumann. Towards interactive visual analysis of microscopic-level simulation data. In *Proceedings of SIGRAD 2012 – Interactive Visual Analysis of Data*, pages –, Växjö, Sweden, Nov. 2012.
- [129] M. Lukaszewicz, M. Glass, F. Reimann, and J. Teich. Opt4J: a modular framework for meta-heuristic optimization. In *Proceedings of the 13th Annual Conference on Genetic and Evolutionary Computation, GECCO '11*, pages 1723–1730. ACM, 2011.
- [130] W. Luo, H. Zou, L. Jin, S. Lin, Q. Li, Z. Ye, H. Rui, and S.-C. Lin. Axin contains three separable domains that confer intramolecular, homodimeric, and heterodimeric interactions involved in distinct functions. *The Journal of Biological Chemistry*, 280(6):5054–5060, Feb. 2005.
- [131] D. Machado, R. Costa, M. Rocha, E. Ferreira, B. Tidor, and I. Rocha. Modeling formalisms in Systems Biology. *AMB Express*, 1(1):45–45, 2011.
- [132] S. Mahammad and I. Parmryd. Cholesterol depletion using methyl- β -cyclodextrin. *Methods in Molecular Biology (Clifton, N.J.)*, 1232:91–102, 2015.
- [133] A. F. Marée and P. Hogeweg. How amoeboids self-organize into a fruiting body: multicellular coordination in *Dictyostelium discoideum*. *Proceedings of the National Academy of Sciences of the United States of America*, 98(7):3879–3883, Mar. 2001.
- [134] S. Margarit, H. Sondermann, B. E. Hall, B. Nagar, A. Hoelz, M. Pirruccello, D. Bar-Sagi, and J. Kuriyan. Structural evidence for feedback activation by ras-gtp of the ras-specific nucleotide exchange factor sos. *Cell*, 112(5):685–695, Mar. 2003.
- [135] S. Marino, I. B. Hogue, C. J. Ray, and D. E. Kirschner. A methodology for performing global uncertainty and sensitivity analysis in systems biology. *Journal of Theoretical Biology*, 254(1):178–196, Sept. 2008.
- [136] C. Maus, S. Rybacki, and A. M. Uhrmacher. Rule-based multi-level modeling of cell biological systems. *BMC Systems Biology*, 5(1):166, 2011.

- [137] O. Mazemondet, R. Hubner, J. Frahm, D. Koczan, B. Bader, D. Weiss, A. Uhrmacher, M. Frech, A. Rolfs, and J. Luo. Quantitative and kinetic profile of wnt/ β -catenin signaling components during human neural progenitor cell differentiation. *Cellular & Molecular Biology Letters*, 16(4):515–538, 2011.
- [138] O. Mazemondet, M. John, S. Leye, A. Rolfs, and A. M. Uhrmacher. Elucidating the sources of β -catenin dynamics in human neural progenitor cell. *Plos One*, 7(8):e42792, 2012.
- [139] T. J. McIntosh and S. A. Simon. Roles of bilayer material properties in function and distribution of membrane proteins. *Annual Review Of Biophysics And Biomolecular Structure*, 35:177–198, 2006.
- [140] M. Mehrbod and M. R. K. Mofrad. Localized Lipid Packing of Transmembrane Domains Impedes Integrin Clustering. *PLoS Comput Biol*, 9(3):e1002948, Mar. 2013.
- [141] C. Metcalfe and M. Bienz. Inhibition of gsk3 by wnt signalling - two contrasting models. *Journal of Cell Science*, 124(21):3537–3544, Nov. 2011.
- [142] C. Metcalfe, C. Mendoza-Topaz, J. Mieszczynek, and M. Bienz. Stability elements in the lrp6 cytoplasmic tail confer efficient signalling upon dix-dependent polymerization. *Journal of Cell Science*, 123(9):1588–1599, 2010.
- [143] G. R. Mirams, H. M. Byrne, and J. R. King. A multiple timescale analysis of a mathematical model of the wnt/beta-catenin signalling pathway. *Journal of mathematical biology*, 60(1):131–160, Jan. 2010. PMID: 19288106.
- [144] A. Monteagudo and J. Santos. Treatment Analysis in a Cancer Stem Cell Context Using a Tumor Growth Model Based on Cellular Automata. *PloS One*, 10(7):e0132306, 2015.
- [145] R. T. Moon, A. D. Kohn, G. V. D. Ferrari, and A. Kaykas. Wnt and β -catenin signalling: diseases and therapies. *Nature Reviews Genetics*, 5(9):691–701, Sept. 2004.
- [146] M. J. Morelli and P. R. ten Wolde. Reaction Brownian dynamics and the effect of spatial fluctuations on the gain of a push-pull network. *The Journal of Chemical Physics*, 129(5):054112, Aug. 2008.
- [147] M. Morimatsu, H. Takagi, K. G. Ota, R. Iwamoto, T. Yanagida, and Y. Sako. Multiple-state reactions between the epidermal growth factor receptor and grb2 as observed by using single-molecule analysis. *Proceedings of the National Academy of Sciences*, 104(46):18013–18018, Nov. 2007.

- [148] A. Mugler, A. G. Bailey, K. Takahashi, and P. Rein ten Wolde. Membrane Clustering and the Role of Rebinding in Biochemical Signaling. *Biophysical Journal*, 102(5):1069–1078, Mar. 2012.
- [149] S. Munro. Lipid Rafts. *Cell*, 115(4):377–388, Nov. 2003.
- [150] D. V. Nicolau, K. Burrage, R. G. Parton, and J. F. Hancock. Identifying optimal lipid raft characteristics required to promote nanoscale Protein-Protein interactions on the plasma membrane. *Mol. Cell. Biol.*, 26(1):313–323, Jan. 2006.
- [151] D. V. Nicolau, J. F. Hancock, and K. Burrage. Sources of anomalous diffusion on cell membranes: A monte carlo study. *Biophysical journal*, 92(6):1975–1987, mar 2007.
- [152] C. Niehrs and J. Shen. Regulation of lrp6 phosphorylation. *Cellular and Molecular Life Sciences*, 67:2551–2562, 2010. 10.1007/s00018-010-0329-3.
- [153] P. S. Niemelä, S. Ollila, M. T. Hyvönen, M. Karttunen, and I. Vattulainen. Assessing the nature of lipid raft membranes. *PLoS Comput Biol*, 3(2):e34, Feb. 2007.
- [154] M. Odersky, L. Spoon, and B. Venners. *Programming in Scala*. Artima, 2nd edition, Jan. 2011.
- [155] G. Özhan, E. Sezgin, D. Wehner, A. S. Pfister, S. J. Köhl, B. Kagermeier-Schenk, M. Köhl, P. Schwille, and G. Weidinger. Lypd6 enhances wnt/ β -catenin signaling by promoting lrp6 phosphorylation in raft plasma membrane domains. *Developmental cell*, 26(4):331–345, Aug. 2013. PMID: 23987510.
- [156] J. A. Papin and B. O. Palsson. Topological analysis of mass-balanced signaling networks: a framework to obtain network properties including crosstalk. *Journal of Theoretical Biology*, 227(2):283–297, Mar. 2004.
- [157] D. L. Parton, A. Tek, M. Baaden, and M. S. P. Sansom. Formation of Raft-Like Assemblies within Clusters of Influenza Hemagglutinin Observed by MD Simulations. *PLoS Comput Biol*, 9(4):e1003034, Apr. 2013.
- [158] A. A. Patel, E. T. Gawlinski, S. K. Lemieux, and R. A. Gatenby. A cellular automaton model of early tumor growth and invasion. *Journal of Theoretical Biology*, 213(3):315–331, Dec. 2001.
- [159] H. H. Patel and P. A. Insel. Lipid rafts and caveolae and their role in compartmentation of redox signaling. *Antioxidants & redox signaling*, 11(6):1357–1372, 2009.

- [160] D. Peng, R. Ewald, and A. M. Uhrmacher. Towards Semantic Model Composition via Experiments. In *Proceedings of the 2Nd ACM SIGSIM Conference on Principles of Advanced Discrete Simulation*, SIGSIM PADS '14, pages 151–162, New York, NY, USA, 2014. ACM.
- [161] I. I. Pottosin, G. Valencia-Cruz, E. Bonales-Alatorre, S. N. Shabala, and O. R. Dobrovinskaya. Methyl-cyclodextrin reversibly alters the gating of lipid raft-associated kv1.3 channels in jurkat t lymphocytes. *Pflugers Arch - Eur J Physiol*, 454(2):235–244, May 2007.
- [162] A. Pralle, P. Keller, E.-L. Florin, K. Simons, and J. K. H. Hörber. Sphingolipid-cholesterol rafts diffuse as small entities in the plasma membrane of mammalian cells. *The Journal of Cell Biology*, 148(5):997–1008, Mar. 2000. PMID: 10704449.
- [163] I. A. Prior, C. Muncke, R. G. Parton, and J. F. Hancock. Direct visualization of Ras proteins in spatially distinct cell surface microdomains. *The Journal of Cell Biology*, 160(2):165–170, Jan. 2003.
- [164] K. Radhakrishnan, A. Halász, D. Vlachos, and J. S. Edwards. Quantitative understanding of cell signaling: the importance of membrane organization. *Current Opinion in Biotechnology*, 21(5):677–682, 2010.
- [165] E. Ravasz, A. L. Somera, D. A. Mongru, Z. N. Oltvai, and A. L. Barabási. Hierarchical organization of modularity in metabolic networks. *Science (New York, N. Y.)*, 297(5586):1551–1555, Aug. 2002.
- [166] T. Rharass, H. Lemcke, M. Lantow, S. A. Kuznetsov, D. G. Weiss, and D. Panáková. Ca²⁺-mediated mitochondrial reactive oxygen species metabolism augments wnt/ β -catenin pathway activation to facilitate cell differentiation. *Journal of Biological Chemistry*, 289(40):27937–27951, Oct. 2014.
- [167] D. M. Roberts, M. I. Pronobis, J. S. Poulton, E. G. Kane, and M. Peifer. Regulation of Wnt signaling by the tumor suppressor adenomatous polyposis coli does not require the ability to enter the nucleus or a particular cytoplasmic localization. *Molecular Biology of the Cell*, 23(11):2041–2056, June 2012.
- [168] U. Rothbächer, M. N. Laurent, M. A. Deardorff, P. S. Klein, K. W. Cho, and S. E. Fraser. Dishevelled phosphorylation, subcellular localization and multimerization regulate its role in early embryogenesis. *The EMBO journal*, 19(5):1010–1022, Mar. 2000.
- [169] B. Rubinfeld, D. A. Tice, and P. Polakis. Axin-dependent phosphorylation of the adenomatous polyposis coli protein mediated by casein kinase 1epsilon. *The Journal of Biological Chemistry*, 276(42):39037–39045, Oct. 2001.

- [170] P. G. Saffman and M. Delbrück. Brownian motion in biological membranes. *Proceedings of the National Academy of Sciences*, 72(8):3111–3113, Aug. 1975.
- [171] T. Saitou, K. Kajiwara, C. Oneyama, T. Suzuki, and M. Okada. Roles of Raft-Anchored Adaptor Cbp/PAG1 in Spatial Regulation of c-Src Kinase. *PLoS ONE*, 9(3):e93470, Mar. 2014.
- [172] C. Sakanaka and L. T. Williams. Functional domains of axin. Importance of the C terminus as an oligomerization domain. *The Journal of Biological Chemistry*, 274(20):14090–14093, May 1999.
- [173] H. Sakane, H. Yamamoto, and A. Kikuchi. Lrp6 is internalized by dkk1 to suppress its phosphorylation in the lipid raft and is recycled for reuse. *Journal of Cell Science*, 123:360–368, 2010.
- [174] S. Sanchez. Better than a petaflop: The power of efficient experimental design. In *Simulation Conference, 2008. WSC 2008. Winter*, pages 73–84, 2008.
- [175] T. Schlange, Y. Matsuda, S. Lienhard, A. Huber, and N. E. Hynes. Autocrine WNT signaling contributes to breast cancer cell proliferation via the canonical WNT pathway and EGFR transactivation. *Breast cancer research*, 9(5):R63, 2007.
- [176] Y. Schmitz, K. Rateitschak, and O. Wolkenhauer. Analysing the impact of nucleocytoplasmic shuttling of β -catenin and its antagonists APC, Axin and GSK3 on Wnt/ β -catenin signalling. *Cellular Signalling*, 25(11):2210–2221, Nov. 2013.
- [177] Y. Schmitz, O. Wolkenhauer, and K. Rateitschak. Nucleo-cytoplasmic shuttling of APC can maximize β -catenin/TCF concentration. *Journal of Theoretical Biology*, 279(1):132–142, June 2011.
- [178] M. Schulz, E. Klipp, and W. Liebermeister. Propagating semantic information in biochemical network models. *BMC Bioinformatics*, 13(1):18, 2012.
- [179] M. Schulz, F. Krause, N. Le Novere, E. Klipp, and W. Liebermeister. Retrieval, alignment, and clustering of computational models based on semantic annotations. *Molecular Systems Biology*, 7(1):512–512, Apr. 2014.
- [180] T. Schwarz-Romond, M. Fiedler, N. Shibata, P. J. G. Butler, A. Kikuchi, Y. Higuchi, and M. Bienz. The DIX domain of Dishevelled confers Wnt signaling by dynamic polymerization. *Nature Structural & Molecular Biology*, 14(6):484–492, June 2007.
- [181] T. Schwarz-Romond, C. Metcalfe, and M. Bienz. Dynamic recruitment of axin by dishevelled protein assemblies. *Journal of Cell Science*, 120(14):2402–2412, July 2007.

- [182] M. Scianna and L. Preziosi. *Cellular Potts Models: Multiscale Extensions and Biological Applications*. CRC Press, Mar. 2013.
- [183] P. Shahi, D. Park, A. C. Pond, M. Seethammagari, S.-H. Chiou, K. Cho, J. L. Carstens, W. K. Decker, P. D. McCrea, M. M. Ittmann, J. M. Rosen, and D. M. Spencer. Activation of wnt signaling by chemically induced dimerization of LRP5 disrupts cellular homeostasis. *PLoS One*, 7(1):e30814, Jan. 2012. PMID: 22303459 PMCID: PMC3267738.
- [184] P. Sharma, R. Varma, R. C. Sarasij, Ira, K. Gousset, G. Krishnamoorthy, M. Rao, and S. Mayor. Nanoscale organization of multiple gpi-anchored proteins in living cell membranes. *Cell*, 116(4):577–589, Feb. 2004.
- [185] K. Simons and R. Ehehalt. Cholesterol, lipid rafts, and disease. *J Clin Invest*, 110(5):597–603, Sept. 2002.
- [186] K. Simons and D. Toomre. Lipid rafts and signal transduction. *Nat Rev Mol Cell Biol*, 1(1):31–39, Oct. 2000.
- [187] S. Singer and G. L. Nicolson. The fluid mosaic model of the structure of cell membranes. *Science*, 175(4023):720–31, 1972.
- [188] M. J. Smalley, E. Sara, H. Paterson, S. Naylor, D. Cook, H. Jayatilake, L. G. Fryer, L. Hutchinson, M. J. Fry, and T. C. Dale. Interaction of axin and Dvl-2 proteins regulates Dvl-2-stimulated TCF-dependent transcription. *The EMBO journal*, 18(10):2823–2835, May 1999.
- [189] M. W. Sneddon, J. R. Faeder, and T. Emonet. Efficient modeling, simulation and coarse-graining of biological complexity with NFsim. *Nature Methods*, 8(2):177–183, Feb. 2011.
- [190] P. Sobrado, A. Jedlicki, V. H. Bustos, C. C. Allende, and J. E. Allende. Basic region of residues 228-231 of protein kinase CK1alpha is involved in its interaction with axin: binding to axin does not affect the kinase activity. *Journal of Cellular Biochemistry*, 94(2):217–224, Feb. 2005.
- [191] O. Sorokina, A. Sorokin, J. Douglas Armstrong, and V. Danos. A simulator for spatially extended kappa models. *Bioinformatics (Oxford, England)*, 29(23):3105–3106, Dec. 2013.
- [192] A. Spaar, D. Flock, and V. Helms. Association of cytochrome c with membrane-bound cytochrome c oxidase proceeds parallel to the membrane rather than in bulk solution. *Biophys J*, 96(5):1721–1732, Mar. 2009.

- [193] J. L. Stamos and W. I. Weis. The β -Catenin Destruction Complex. *Cold Spring Harbor Perspectives in Biology*, 5(1):a007898, Jan 2013.
- [194] T. Suzuki. Lipid rafts at postsynaptic sites: distribution, function and linkage to postsynaptic density. *Neuroscience Research*, 44(1):1–9, Sept. 2002.
- [195] T. Suzuki, J. Ito, H. Takagi, F. Saitoh, H. Nawa, and H. Shimizu. Biochemical evidence for localization of AMPA-type glutamate receptor subunits in the dendritic raft. *Brain Research. Molecular Brain Research*, 89(1-2):20–28, Apr. 2001.
- [196] V. F. Taelman, R. Dobrowolski, J.-l. Plouhinec, L. C. Fuentealba, P. P. Vorwald, I. Gumper, D. D. Sabatini, and E. M. D. Robertis. Wnt signaling requires sequestration of glycogen synthase kinase 3 inside multivesicular endosomes. *Cell*, 143(7):1136–1148, 2010.
- [197] K. Takahashi, S. Arjunan, and M. Tomita. Space in systems biology of signaling pathways – towards intracellular molecular crowding in silico. *FEBS Letters*, 579(8):1783–1788, Mar. 2005.
- [198] K. Takahashi, S. Tanase-Nicola, and P. R. ten Wolde. Spatio-temporal correlations can drastically change the response of a MAPK pathway. *Proceedings of the National Academy of Sciences of the United States of America*, 107(6):2473–2478, Feb. 2010.
- [199] C. W. Tan, B. S. Gardiner, Y. Hirokawa, M. J. Layton, D. W. Smith, and A. W. Burgess. Wnt signalling pathway parameters for mammalian cells. *PLoS ONE*, 7(2):e31882, Feb. 2012.
- [200] C. W. Tan, B. S. Gardiner, Y. Hirokawa, D. W. Smith, and A. W. Burgess. Analysis of Wnt signaling β -catenin spatial dynamics in HEK293t cells. *BMC systems biology*, 8:44, 2014.
- [201] T. M. Thomson, K. R. Benjamin, A. Bush, T. Love, D. Pincus, O. Resnekov, R. C. Yu, A. Gordon, A. Colman-Lerner, D. Endy, and R. Brent. Scaffold number in yeast signaling system sets tradeoff between system output and dynamic range. *Proceedings of the National Academy of Sciences*, 108(50):20265–20270, Dec. 2011.
- [202] T. Tian, A. Harding, K. Inder, S. Plowman, R. G. Parton, and J. F. Hancock. Plasma membrane nanoswitches generate high-fidelity ras signal transduction. *Nat Cell Biol*, 9(8):905–914, Aug. 2007.
- [203] N. S. Tolwinski, M. Wehrli, A. Rives, N. Erdeniz, S. DiNardo, and E. Wieschaus. Wg/Wnt signal can be transmitted through arrow/LRP5,6 and axin independently

- of Zw3/Gsk3beta activity. *Developmental cell*, 4(3):407–418, Mar. 2003. PMID: 12636921.
- [204] I. Tremmel, H. Kirchhoff, E. Weis, and G. Farquhar. Dependence of plastoquinol diffusion on the shape, size, and density of integral thylakoid proteins. *Biochimica et Biophysica Acta (BBA) - Bioenergetics*, 1607(2-3):97–109, Dec. 2003.
- [205] M. S. Turner, P. Sens, and N. D. Socci. Nonequilibrium raftlike membrane domains under continuous recycling. *Phys. Rev. Lett.*, 95(16):168301–1 – 168301–4, Oct. 2005.
- [206] N. Ueda and S. V. Shah. Role of intracellular calcium in hydrogen peroxide-induced renal tubular cell injury. *The American Journal of Physiology*, 263(2 Pt 2):F214–221, Aug. 1992.
- [207] G. Vereb, J. Szöllösi, J. Matkó, P. Nagy, T. Farkas, L. Víg, L. Mátyus, T. A. Waldmann, and S. Damjanovich. Dynamic, yet structured: The cell membrane three decades after the singer-nicolson model. *Proceedings of the National Academy of Sciences*, 100(14):8053–8058, July 2003.
- [208] M. von Smoluchowski. Zur kinetischen Theorie der Brownschen Molekularbewegung und der Suspensionen. *Annalen der Physik*, 326(14):756–780, Jan. 1906.
- [209] D. Waltemath, R. Adams, F. T. Bergmann, M. Hucka, F. Kolpakov, A. K. Miller, I. I. Moraru, D. Nickerson, S. Sahle, J. L. Snoep, and N. Le Novère. Reproducible computational biology experiments with SED-ML—the Simulation Experiment Description Markup Language. *BMC systems biology*, 5:198, 2011.
- [210] T. Warnke, T. Helms, and A. M. Uhrmacher. Syntax and Semantics of a Multi-Level Modeling Language. In *Proceedings of the 2015 ACM SIGSIM Conference on Principles of Advanced Discrete Simulation*, SIGSIM-PADS '15, pages 133–144, New York, NY, USA, 2015. ACM.
- [211] C. Wawra, M. Köhl, and H. A. Kestler. Extended analyses of the Wnt/ β -catenin pathway: Robustness and oscillatory behaviour. *FEBS Letters*, 581(21):4043–4048, Aug. 2007.
- [212] E. M. Wexler, A. Paucer, H. I. Kornblum, T. D. Palmer, T. D. Plamer, and D. H. Geschwind. Endogenous wnt signaling maintains neural progenitor cell potency. *Stem Cells*, 27(5):1130–1141, May 2009.
- [213] K. Willert, J. D. Brown, E. Danenberg, A. W. Duncan, I. L. Weissman, T. Reya, J. R. Yates, and R. Nusse. Wnt proteins are lipid-modified and can act as stem cell growth factors. *Nature*, 423(6938):448–452, May 2003.

- [214] H. Yamamoto, S. Kishida, M. Kishida, S. Ikeda, S. Takada, and A. Kikuchi. Phosphorylation of axin, a Wnt signal negative regulator, by glycogen synthase kinase-3beta regulates its stability. *The Journal of Biological Chemistry*, 274(16):10681–10684, Apr. 1999.
- [215] H. Yamamoto, H. Komekado, and A. Kikuchi. Caveolin is necessary for wnt-3a-dependent internalization of lrp6 and accumulation of b-catenin. *Developmental Cell*, 11(2):213–223, 2006.
- [216] S. Yanagawa, F. van Leeuwen, A. Wodarz, J. Klingensmith, and R. Nusse. The dishevelled protein is modified by wingless signaling in Drosophila. *Genes & Development*, 9(9):1087–1097, May 1995.
- [217] J. Yang-Snyder, J. R. Miller, J. D. Brown, C. J. Lai, and R. T. Moon. A frizzled homolog functions in a vertebrate Wnt signaling pathway. *Current biology: CB*, 6(10):1302–1306, Oct. 1996.
- [218] X. Zeng, H. Huang, K. Tamai, X. Zhang, Y. Harada, C. Yokota, K. Almeida, J. Wang, B. Doble, J. Woodgett, A. Wynshaw-Boris, J.-C. Hsieh, and X. He. Initiation of wnt signaling: control of wnt coreceptor lrp6 phosphorylation/activation via frizzled, dishevelled and axin functions. *Development*, 135(2):367–375, 2008.
- [219] X. Zeng, K. Tamai, B. Doble, S. Li, H. Huang, R. Habas, H. Okamura, J. Woodgett, and X. He. A dual-kinase mechanism for wnt co-receptor phosphorylation and activation. *Nature*, 438(7069):873–877, Dec. 2005.
- [220] H.-X. Zhou. Crowding effects of membrane proteins. *The Journal of Physical Chemistry B*, 113(23):7995–8005, Mar. 2009.

Erklärung

Ich, Fiete Haack erkläre, dass ich die vorgelegte Dissertationsschrift mit dem Thema: Exploring the spatio-temporal dynamics of lipid rafts and their role in signal transduction selbst verfasst und keine anderen als die angegebenen Quellen und Hilfsmittel benutzt, ohne die (zulässige) Hilfe Dritter verfasst und auch in Teilen keine Kopien anderer Arbeiten dargestellt habe.

Datum:

Unterschrift:
